Institute of Physics, Polish Academy of Sciences

Structural and magnetic properties of Co thin and ultra-thin films - ^{59}Co NMR study

PhD Thesis in Physics prepared at the Institute of Physics of the Polish Academy of Sciences (IP PAS) by

Przemysław Nawrocki

PhD Supervisor:

dr hab. Marek Wójcik

Submission date: 2022

Warsaw 2022

Abstract

Magnetic and structural properties of an ultrathin Co layer strongly depend on the type of the upper and lower interface. Therefore, it is crucial to have an insight about different interface effects and their influence on magnetic properties of Co thin films. Due to the fact, that different systems containing Co thin films are nowadays an important elements of spintronic devices it is pivotal to study their magnetic and structural properties in different interface configurations. Therefore, ^{59}Co NMR (nuclear magnetic resonance) technique was used for this purpose in the case of several series of samples containing thin Co layers as the main component.

The influence of the upper and lower surfaces on the structural and magnetic properties of the Co layer was investigated, depending on the nature (crystal structure and interaction force between the two components) of the metal forming the second layer. The Co with Au and Mo metals were selected as the most common for spintronic devices. The research was conducted on the Co layers in all possible combinations of Au and Mo buffers/cappings.

Another of the studied series were Co ultra-thin films grown by molecular beam epitaxy (MBE) on an Au(111) buffer in which Co layer thickness d_{Co} is varied from 1,5 nm to 10 nm. Samples were investigated due to a crucial role of Co/Au interface in defining the perpendicular magnetic anisotropy (PMA) in this system. It was shown that Co layers with $d_{Co} < 3$ nm make atomically sharp interface to Au(111) substrate in significant part of the Co/Au interface area. Co atoms located inside a bulk of the layer reveal a higher resonance frequency than that reported for a bulk hcp Co sample with in-plane magnetization which reveals a distorted/not fully continuous hexagonal structure in the thin film samples with $d_{Co} < 3$ nm. For thicker layers with $d_{Co} \geq 3$ nm a structural transition to a uniform hexagonal structure takes place in the entire volume of the Co film evidenced by a downshift of the resonance frequency to the value characteristic for bulk hcp. There were also additionally measured ^{59}Co NMR restoring fields of the samples at 4.2 K temperature which have revealed a significantly lower magnetic stiffness in samples where Co makes a continuous layer than in samples with discontinuous Co layer.

Last of the series of studied samples were polycrystalline Au/Co(30nm)/Au layers implanted (with 40 keV energy) with different doses of oxygen ions (from $3x10^{16}$ ions/cm^2 to $35x10^{16}$ ions/cm^2). Oxygen ion implantation is a new and efficient method of inducing exchange bias effect (EB) in the entire volume of the Co film. NMR research has shown that while the as-deposited sample consists of a mixture of fcc Co (face centred cubic) and hcp Co (hexagonal close packed) phases and stacking faults, implanted samples exhibit different structural features. Although there is no observed allotropic fcc › hcp phase transformation, the metallic Co undergoes a significant loss of crystalline order. For high fluence implantation, traces of CoO can be envisaged from a new ^{59}Co NMR line present at frequency around 490 MHz. ^{59}Co NMR restoring fields indicate a large increase of magnetic stiffness at 4.2 K temperature due to the exchange anisotropy introduced by the presence of antiferromagnetic CoO (i.e. exchange bias effect). Moreover, ^{59}Co NMR study from annealed (573 K) samples have shown radical structural changes indicating a migration of implanted oxygen from the inner part of the Co film due to thermal activation. This process leads to a partial recrystallization of the Co layer.

Preface

This thesis is the result of experimental research performed at the Institut of Physics of the Polish Academy of Sciences in Poland and Instituut voor Kern- en Stralingsfysica of the Katholieke Universiteit Leuven in Belgium and University of Bialystok. All of the presented results are gathered from papers either published or in preparation for publication in international peer-reviewed journals. The thesis itself situates this research within the field of nanomagnetism, introduces the necessary physical concepts and applied experimental methods, and comprehensively summarizes the different results in a broad discussion. Finally, a general conclusion and an outlook for further research on the topic is given. This thesis is based on the following publications:

1) E. Menéndez, J. Demeter, J. Van Eyken, **P. Nawrocki**, E. Jędryka, M. Wójcik, J. F. Lopez-Barbera, J. Nogués, A. Vantomme, and K. Temst - *Improving the Magnetic Properties of Co−CoO Systems by Designed Oxygen Implantation Profiles* – ACS Applied Materials & Interfaces Vol. 5 (10), p. 4320-4327 (2013), 3/10

2) A. Wawro, Z. Kurant, M. Tekielak, **P. Nawrocki**, E. Milińska, A. Pietruczik, M. Wójcik, P. Mazalski, , J. Kanak , K. Ollefs, F. Wilhelm, A. Rogalev and A. Maziewski - *Engineering the magnetic anisotropy of an ultrathin Co layer sandwiched between films of Mo or Au* - Journal of Physics D: Applied Physics, Vol. 50 (21), p. 215004 (2017)

3) **P. Nawrocki**, J. Kanak, A. Petruczik, A. Wawro and M. Wojcik - *Epitaxial $Co_{1-x}Mo_x$ thin film alloys studied by ^{59}Co NMR* – Journal of Alloys and Compounds, Vol. 788 (5), p. 559-564 (2019)

4) **P. Nawrocki**, L. Gładczuk and M. Wójcik - *Structural changes of Co thin films on Au buffer with the increasing Co thickness – ^{59}Co NMR studies* – in preparation

5) **P. Nawrocki**, M. Wójcik, E. Jędryka, E. Menéndez, J. Nogués, A. Vantomme, K. Temst - *Influence of O^+ ion implantation on structural and magnetic properties of Co thin films studied by ^{59}Co NMR technique* - in preparation

Acknowledgements:

First of all, I would like to thank to my supervisor, dr. hab. Marek Wójcik, prof. IP PAS, for supporting me during these past years.

I would like to thank my friends who share with me not only their work and ideas but also enjoyable things in life.

I will forever be thankful to my family who always support me spiritually throughout my life.

Last but not least, I want to thank staff of Institute of Physics of the Polish Academy of Sciences in Warsaw who supported me a lot during my PhD study.

Table of contents:

Warsaw 2022

Warsaw 2022

1

Introduction

1.1 Properties of Co and the aim of the work

The device miniaturization alongside with traditional electronics (which is based on electrons as a source of information) slowly reaches its technological limits. Addition of another degree of freedom to the electron into conventional electronics appears to be a promising solution of this problem, which can revolutionize future IT industry. This new electronic is called spintronics and it is an emerging field of nanoelectronics which involves the detection and manipulation of electron spin which can have one of two possible orientations (known as down and up) resulting in an additional two binary states. Carrying information in both the charge and spin of an electron potentially offers devices with a greater diversity of functionality, increased memory density, greater processing power, higher data transfer speed and increased storage capacity.

The aim of this dissertation is the presentation of the results from the ^{59}Co nuclear magnetic resonance study of structural and magnetic properties of thin and ultra-thin cobalt films. Thin metallic magnetic films showing uniaxial magnetic anisotropy perpendicular to the plane of the film along with multilayers showing tailorable coupling between successive magnetic layers are of great interest in magneto-optical and spintronic applications. In the case of such systems an important and active role in the defining of the layer properties play the interface areas which may strongly influence the properties of the thin film comparing to the bulk materials. The interfaces between the magnetic layer and the non-magnetic buffer/inter-/capping layer play a

decisive role in determining the interactions and couplings that affect the magnetization [SCH99] hence they can be designed to exhibit the desired properties in a several ways. For example: by post-growth temperature treatment; by selecting materials of suitable properties that determine the growth mode (such as crystallographic structure, alloying potential); or even by ion beam irradiation, including implantation process.

The need to know the influence of interface on the properties of Co thin films, which are widely used as an element of spintronic devices, motivated me to take on this subject. Because of the fact that Co is a ferromagnetic metal with relatively high spin polarity of valence electrons and which has got a very high Curie temperature reaching 1388 K for bulk Co (however it may be adjusted by reducing dimensionality and growing it on different substrates) [CRA55],[SCH90] it represents a high potential for innovative spin-based devices. For example, sufficiently thin hexagonal Co films with perpendicular magnetic anisotropy (PMA) can be used as a source of highly polarized spin current in magnetic random access memories (MRAM) with magnetic tunnel junctions (MTJ's) which significantly increases the information storage density in mentioned systems [CAR90]. Such films are currently of great interest in relation to high-density magnetic recording. Also Co thin films with induced exchange bias effect (EB) are widely studied in spintronics because of the fact that this effect is used in devices such as MRAM's or magnetic readback heads in computer hard disks drives and due to this, they play an important role in modern computer technology.

Hcp-Co is the most common form of cobalt single crystal under ambient conditions. It is commonly known that at equilibrium conditions this phase structure transforms into fcc-Co when heated above 689 K [HAN58]. Coexistence of both structural phases is frequently observed for systems far from equilibrium. In the case of thin films, selecting the appropriate substrate on which Co is grown, growth parameters or layer thickness may lead to growth of Co as fcc (for example, Co tends to grow as fcc on Cu(100) substrate [WEB96]) or the appearance of a mixture of fcc and hcp Co (like in the case of Co/Au multilayers [JOM00], [KEH00] or polycrystalline Au/Co/Au thin films [MEN13]) - despite the fact that in most cases Co tends to grow as hcp on Au(111) substrate. Figure 1.1.1 shows the cobalt phase diagram an fig. 1.1.2 shows schematic illustration of fcc and hcp phase.

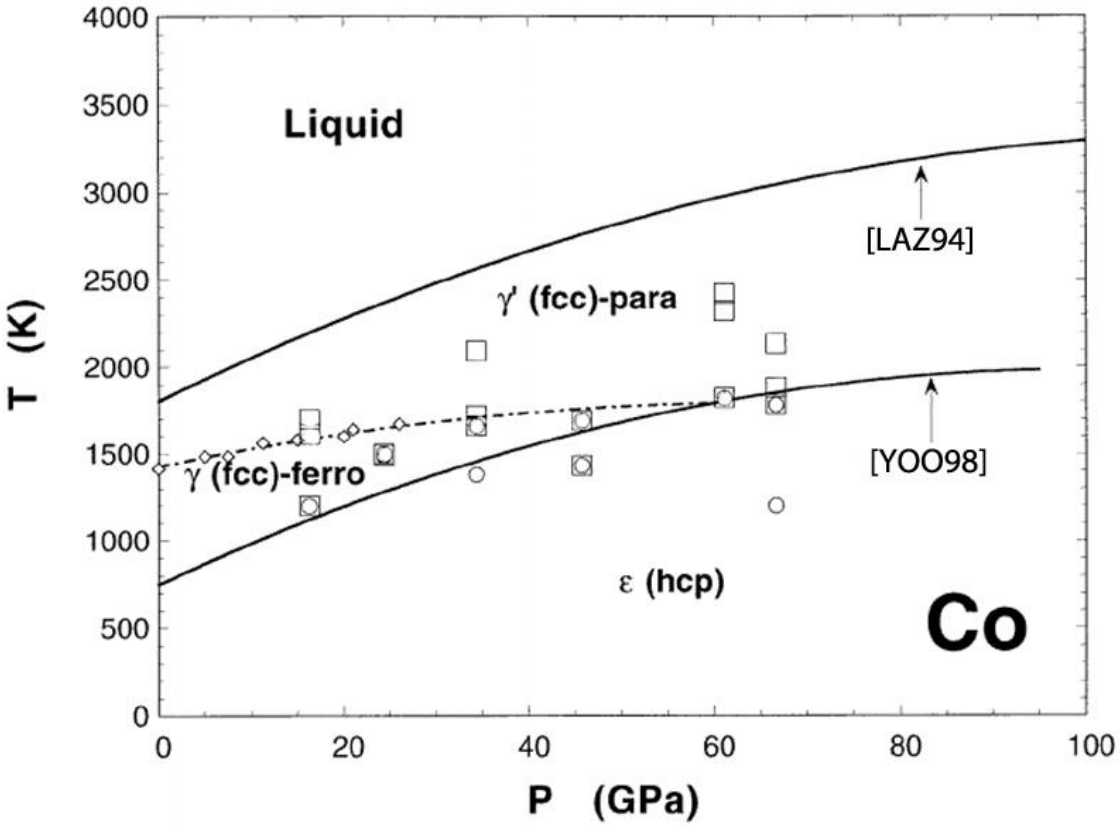

Fig. 1.1.1 The phase diagram of cobalt taken from [YOO98]. The symbols represent the phases of cobalt which were determined by means of *in situ* x-ray diffraction at high pressure and temperature; γ-Co (open squares), ε-Co (open circles), melting curve and the magnetic transition temperatures (open diamonds [LAZ94]). The ε/γ -phase line is drawn below the stability field of γ-Co and is constrained by the transition temperature at ambient pressure [NIS83].

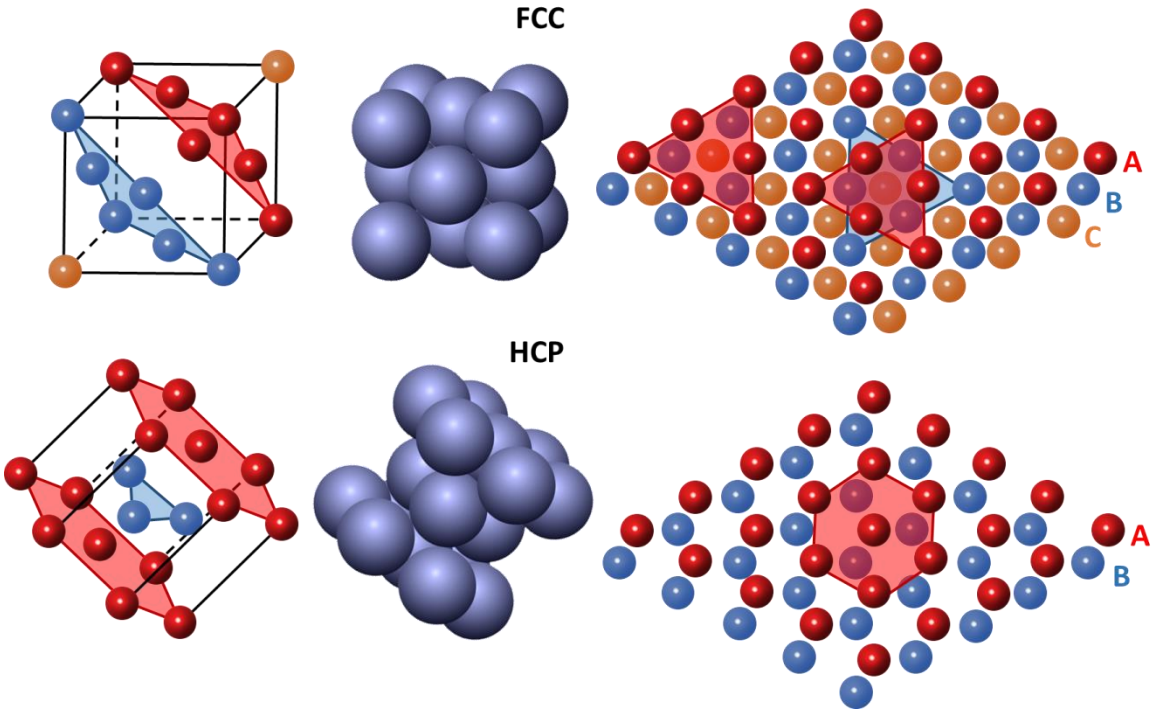

Fig. 1.1.2 Schematic illustration of fcc and hcp phase. The crystal structure of Co consists of regularly arranged planes of densely packed Co atoms. Depending on the order in which the successive layers are stacked, one of the two crystal structures will be formed: face centered cubic for ABCABC stacking or a hexagonal closed packed structure for ABABAB stacking. In both structures the cobalt atom has twelve nearest neighbors (NN).

The magnetic properties of nanometric Co depend on its structure, which in turn is sensitive to the underlying microstructure [CHE01]. Therefore, it is crucial to control the growth of the structure and all parameters that have a high influence on it such as surface morphology and its roughness in particular. Therefore, there is a need to check the quality and structural properties of the eventual layer (and thus the correctness of the selected growth parameters). For this, it would be adequate to use a structural technique such as ^{59}Co NMR.

Three types of systems were investigated in which the main element was a thin Co layer:

- Epitaxial Co thin films with different types of buffer and capping layer (Mo and Au) were investigated in order to acquire the knowledge about the actual impact

of the upper and lower interface on the structural and magnetic properties of the Co layer, depending on the nature (crystal structure and interaction force between the two components) of the metal forming the second layer. The Co with Au and Mo metals were selected as the most common for spintronic devices. The research was conducted on the Co layers in all possible combinations of Au and Mo interiors [ch. 3.2, p. 46].

- Thin Au/Co/Au films were studied because of the important role of Co/Au interface in defining of the perpendicular magnetic anisotropy (which significantly increases the density of information in Magnetic Random Access Memories - MRAM). In this system, lattice mismatch reaches 14% and its role is investigated in Au/Co(t)/Au thin film epitaxial layers as a Co layer thickness in the range ($1 < t < 10$ nm). Layers were made in IFPAN by the MBE method. Sufficiently thin magnetic films which exhibit perpendicular magnetic anisotropy are an example of very interesting materials which can be used in spintronics. PMA greatly increases the density of information which can be stored which may be used in MRAM's with magnetic tunnel junctions. Au/Co/Au heterostructures are considered to be adequate materials for this purpose and are interesting due to interface effects which may have a significant influence on the PMA of the layer [ch. 3.3, p. 50].

- Epitaxial and polycrystalline Au/Co(30nm)/Au thin films implanted with oxygen ions studied as a function of the oxygen ion dose ranging from $3x10^{16}$ ions/cm^2 to $35x10^{16}$ ions/cm^2. The studies were performed in order to investigate the effects of oxygen implantation on the Co layer structure and to find a correlation between changes in the structure and the occurrence of the exchange bias effect (EB). The hypothesis about the allotropic transformation of fcc / hcp Co as a possible effect of implantation was also verified. Thin films with induced exchange EB effect are widely studied due to their wide technological applications. It is generally accepted that exchange bias originates from the interfacial exchange interaction between a ferromagnetic (FM) and antiferromagnetic (AFM) material (uncompensated spins at the interface) which results in a preferential direction for the ferromagnetic spins. It typically

manifests itself by a shift and a broadening of a hysteresis loop of the FM. EB effect is used in spintronic devices, such as magnetic read heads of hard disk drives or magneto-resistive memories (MRAM) and due to this fact it plays an important role in modern computer technology. One of the best known EB systems consists of FM cobalt and AFM cobalt oxide, created through Co surface oxidation. In this dissertation, the main focus will be placed on observation, understanding and explanation of the influence which has implantation on the structural and magnetic properties of studied systems. Previous studies suggest that implanted oxygen ions strongly modify primarily grain boundary regions [DEM11, MEN13]. However, the actual impact of the implantation on the samples structure remains still unclear. The second important issue is the actual effect of annealing treatment on already implanted systems. Oxygen ion implantation is a recently introduced method of inducing EB effect in Co material which is being far more effective than already used and well known surface oxidation. Since it is a self-limiting process it results in an oxide thickness of only a few nm, which forms a single interface between Co and CoO. Oxygen ion implantation however, allows for the formation of Co/CoO interfaces spread throughout the whole volume of the Co film resulting in a creation of multiple FM/AFM interfaces (more effective way of inducing strong EB effect). Recent measurements suggest that EB properties of Co-CoO systems prepared by ion implantation can be tuned by controllably modifying the local microstructure through annealing treatment. This could give the opportunity to tailor magnetic properties of such system which increases eventual potential of this system [ch. 3.4, p. 68].

However, in the first step, in order to better understand the impact of Au or Mo alien nearest neighbors (NNs) on local ^{59}Co hyperfine field distribution, two series of $Co_{1-x}Mo_x$ and $Co_{1-x}Au_x$ thin film alloys co-deposited on V or Au buffer were prepared (ch. 3.1, p. 28). Conclusions obtained on the basis of research on these alloys, in turn, made an important contribution to the determination of the structure of interfaces in Co thin layers described in the latter part of this dissertation. Observed modifications of the ^{59}Co hyperfine field are being interpreted as a function of:

a) Co layer thickness (from 10 nm to 30 nm) and increasing concentration of an Au dopant ($0 \leq x \leq 0{,}05$) in case of $Co_{1-x}Au_x$ alloys,
b) increasing concentration of Mo dopant in case of the $Co_{1-x}Mo_x$ alloy ($0 \leq x \leq 0{,}1$)

To achieve goals taken at the beginning of the PhD studies, a ^{59}Co nuclear magnetic resonance technique (^{59}Co NMR) was chosen as the main research tool. NMR often proved to be very useful as a probe of the short-range chemical and topological order, especially to study the nanostructure of non-homogeneous magnetic materials such as magnetic thin films, multilayers or granular alloys containing magnetic and non-magnetic components where the interfaces between magnetic and nonmagnetic elements exist. These type of materials are extensively studied because of its potential technological applications (in data storage/recording, field detectors, magnetic tunnel junctions) or for its fundamental purposes (surface/interface magnetic anisotropy, exchange bias effect, spin dependent scattering and tunnel magnetoresistance). The structural complexity of those systems allows their properties to be tailored by selecting the proper components, structure and mixture. Therefore, it is obvious that understanding the interactions at the interfaces alongside with its structure is crucial, and NMR technique allows to determine the nature of interface in such systems, whether it is sharp or diffused. In the case of thin films long-range surface or near-surface research methods like atomic force microscopy, x-ray diffraction or Rutherford backscattering spectrometry often give insufficient information about the crystallographic structure of the whole film, especially at the interface areas [VAZ08]. However, characteristic feature of the NMR method is that it gives unique short-range information about structural and magnetic properties of the studied thin film and allows in particular to discriminate between the interface and bulk areas of the sample [PAN97], [MEN93].

Physical basics of NMR and its uniqueness in gaining short-range information regarding the structural and magnetic properties of Co thin films are being described in detail in chapter 2.

2

NMR technique

This chapter is devoted to a detailed description of the used NMR technique. Firstly, the physical basics of the technique will be discussed in terms of the principles of quantum mechanics. Next, the NMR research methodology will be discussed in which terms important for NMR technique such as enhancement factor or restoring field will be explained. In addition, the apparatus used for the measurements will be briefly described and the influence of the nearest neighbor atoms on the NMR spectrum will be explained.

2.1 Physical basics of the NMR technique

The spin of the nucleus is determined by its quantum spin number *I*. If the spin quantum number *I* of a given nucleus is different from zero, then the nucleus can be treated as a magnetic dipole having a magnetic moment μ. The magnitude of the nuclear magnetic moment μ is directly related to the nuclear spin *I* with expression [ABR61, TUR69, STA05, SZE12]:

$$\mu = \boldsymbol{\gamma I} = \frac{\boldsymbol{g_n \mu_n}}{\hbar} \boldsymbol{I} \qquad \textbf{(2.1.1)}$$

where $\boldsymbol{\gamma = g_n \frac{e}{2m_p}}$ is a gyromagnetic ratio, which adopts characteristic values for various atomic nuclei, μ_n is a nuclear magneton and $\boldsymbol{h = \frac{\hbar}{2\pi}}$ is a reduced Planck constant. Hamiltonian E_{Zee}, which assumes Zeeman interaction between the nuclear magnetic moment μ and the applied external magnetic field $\boldsymbol{\vec{H}_0 = (0, 0, H_0)}$ can be expressed as:

$$\boldsymbol{E_{Zee} = -\mu \cdot H_0 = -\gamma I_z H_0} \qquad \textbf{(2.1.2)}$$

The external magnetic field $\boldsymbol{\vec{H}_0}$ removes a degeneracy of nuclear spin levels due to the magnetic quantum number $\boldsymbol{m}$, which determines the eigenvalues of the operator $\boldsymbol{I_z}$ assuming the values of $\boldsymbol{m = -I, -I+1, \ldots, I-1,\ I}$ as illustrated in Fig. 2.1.1.

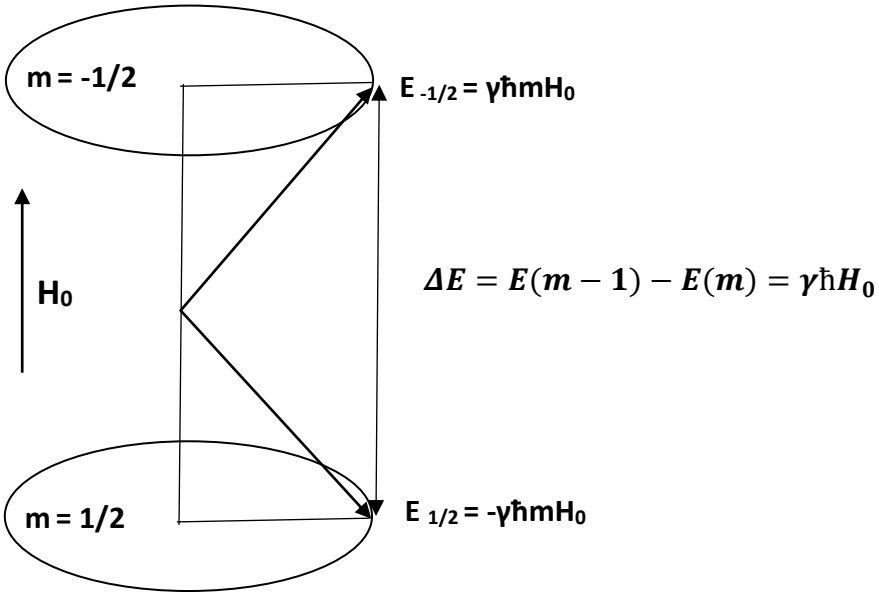

Fig. 2.1.1 2I + 1 energy of the Zeeman levels of the atomic nucleus with a spin I = 1/2. In the external H_0 magnetic field, the degeneracy of energy levels is removed and splitting into 2I + 1 equidistant Zeeman levels occurs.

As a result, the energy level of nuclear spin is split into 2I + 1 energy levels with energies that are Hamilton's eigenstates E_{Zee}:

$$E_m = -m\gamma\hbar H_0 \quad (2.1.3)$$

Selection rules for dipole transitions only allow transitions between levels meeting the condition Δm = ± 1. The energy difference between adjacent nuclear spin energy levels is:

$$\Delta E = E(m-1) - E(m) = \gamma\hbar H_0 \quad (2.1.4)$$

Transitions between adjacent levels can be induced by applying a variable magnetic field H_{app} at Larmor frequency (ω_L), which defines the phenomenon of nuclear magnetic resonance (NMR) [TUR69], [FUK81]:

$$\omega_L = \gamma H_{app} \quad (2.1.5)$$

In the magnetically ordered material, a strong magnetic field is present in the area of the nucleus, which is mainly the result of hyperfine interactions. In this case, the Zeeman Hamiltonian H_{Zee} is dependent on the effective magnetic field acting on the nucleus and takes the form:

$$H_{Zee} = -\mu \cdot H_{eff} = -\gamma\hbar I H_{eff} \quad (2.1.6)$$

where H_{eff} is the effective magnetic field in the atomic nucleus including the following components [RAD65]:

$$\vec{H}_{eff} = \vec{H}_0 + \vec{H}_{dem} + \vec{H}_{HF} \quad (2.1.7)$$

where $\vec{H}_0$ is the external magnetic field, $\vec{H}_{dem}$ is the demagnetizing field, while $\vec{H}_{HF}$ is the hyperfine field ($\vec{H}_{HF}$ is the dominant contribution to the effective field for atoms with magnetically active 3d shell , e.g. cobalt). The demagnetization field is the result of long-range dipole interaction and is closely related to the shape of the sample. For thin

magnetic layers, the demagnetization field depends on the angle between magnetization and normal to the surface.

The hyperfine field $\vec{H}_{HF}$ is the main contribution to the effective field on the nucleus in ferromagnetic materials and its source is the hyperfine interaction between the nucleus and the electron shell of self atom and the electrons of neighborig atoms. The hyperfine field $\vec{H}_{HF}$ can be represented as the sum of three elements [WAT61, TUR69]:

$$\vec{H}_{HF} = \left(\vec{H}_{HF,orb} + \vec{H}_{HF,dip} + \vec{H}_{HF,Fc}\right) \sim \left(\frac{\vec{l}}{r^3} + \left(\frac{-\vec{s}}{r^3} + 3\frac{\vec{r}(\vec{s}\cdot\vec{r})}{r^5}\right) + \frac{8\pi}{3}\vec{s}\delta(\vec{r})\right) \tag{2.1.8}$$

The first component is the orbital hyperfine field $\vec{H}_{HF,orb} = \hat{A}_{orb}\vec{\mu}_{loc}^{l}$ and it results from the non-suppressed orbital moment of magnetically active electrons from not completely filled 3d shell. The components of the hyperfine interaction tensor $\hat{A}_{orb}$ are positive, which indicates the parallelism of the orbital contribution and the orbital magnetic moment. The second component $\vec{H}_{HF,dip}$ is a dipole field which is due to the spin density of the unfilled 3d orbital of the considered atom and can be written as: $\vec{H}_{HF,dip} = \hat{A}_{dip}\vec{\mu}_{loc}^{s}$. The size and direction of this contribution depends on the symmetry of the 3d electron orbitals. The third component $\vec{H}_{HF,Fc}$ is called the Fermi contact term, which is particularly important in metals with unfilled 3d orbital and can be expressed as: $\vec{H}_{HF,Fc} = \hat{A}_{core}\vec{\mu}_{loc}^{s}$. For the atoms of the iron group, the magnetic field around the nucleus originates mainly from the Fermi contact term. However, in order for the magnetic field to be induced by the Fermi term, the electronic spin density at the nucleus must be non zero:

$$|\Psi_{s\uparrow}(0)|^2 - |\Psi_{s\downarrow}(0)|^2 \neq 0 \tag{2.1.9}$$

The above condition denotes the spin polarization of the inner shell s electrons and it is caused by the exchange interactions of the inner shell electrons with the electrons of the unfilled d orbital. [TUR69]

2.2 Methodology of NMR research

Contribution to the NMR spectrum on the given frequency ω originates from all magnetic atoms for which local magnetic field H_0 on the nucleus fulfills the condition 2.1.5. And that is why NMR gives an information on a distribution of local properties of all resonating nuclei in the sample which makes NMR complementary to the long-range methods. In a nutshell - the field which is experienced by a nuclei of an examined ferromagnetic atom consists of magnetic field due to magnetic moment of the whole atom and of magnetic field transferred by neighboring atoms. Therefore any change in the local symmetry, occurrence of defects, other phases, grain boundaries, stacking faults (which may be defined as arrangement alterations from the ideal fcc or hcp Co stacking sequence [MIC01] [MEN94]), strains or incorporation of alien (magnetic or nonmagnetic) atoms in the nearest neighborhood modifies local hyperfine field (and thus resonance frequency) which results in a so-called satellite structure of the NMR spectra which is different for various atomic arrangements and chemical configurations. In other words NMR spectrum reflects the distribution of the hyperfine fields in the sample, which are very sensitive to the local atomic arrangement, thus it also reflects a variety of chemical and topological configurations around the probed nuclei which makes this technique a very suitable instrument for the structural examination of ferromagnetic thin films on the nanoscopic scale [CER01, JED04, SOR03].

In order to acquire a structural information about the interface of ultra-thin film, NMR spectra can be compared to those which would result from various structural models of interfaces (from a quasi-perfect sharp interface to sharp interfaces containing monoatomic steps, defects, granular interfaces or strongly interdiffused interfaces). The shape of the interface and the type of mixing can be inferred from spectral simulations. Concentration profiles of incorporated impurities, amount of stacking faults or size of grains can be evaluated, so characterization of the interface is possible at the atomic scale. NMR probes primarily H_{HF} around the observed nuclei which in turn determines the position of the NMR lines and which depends on the local structure and chemical environment. Structural examination carried out by the help of NMR need a prior knowledge (acquired by other investigations) of the quantitative relationship between the H_{HF} and the local crystallographic and chemical structure before any information

and conclusions can be drawn out of the experiment. Moreover using NMR technique a local magnetic stiffness of the studied material can be investigated by studying a NMR restoring field distribution (NMR H_{rest} - discussed on the next page).

^{59}Co NMR experiments were carried out at low temperature (4.2 K), after zero-field cooling from room temperature, using an automated and phase sensitive spin-echo spectrometer. All spectra were taken in the 150–240 MHz frequency range with 1 MHz step at several values of the r.f. field amplitude. Due to the heterogenic character of the enhancement factor in the examined samples, all of the NMR spectra were corrected for the NMR enhancement factor characteristic to the examined sample following the Panissod protocol [PAN01n] in order to ensure that resulting NMR spectra reflect the actual number of nuclei resonating at a given frequency.

2.2.1 NMR in magnetic materials – enhancement factor and restoring field

In magnetic materials the applied alternating magnetic field H_{app} is only indirectly a source of resonance transitions between nuclear spin energy levels [TUR69]. This happens due to the magnetic state of the studied material. In ferromagnets, H_{app} field that is applied to excite the resonance transition at the frequency ω interacts also with the electronic magnetization, located in a certain magnetic field H_{rest} determining magnetization equilibrium. The H_{rest} can be considered as a kind of a virtual internal magnetic field, which is a manifestation of all factors affecting the magnetic stiffness of the sample (like magnetocrystalline anisotropy, coercive field or exchange coupling between the magnetic layers). During NMR measurement, in order to induce nuclear resonance, H_{rest} needs to be overcome by an applied magnetic field [MAL99], [PAN01n]. The external r.f. field H_{app} causes oscillations of magnetization around the equilibrium direction set by $H_{rest,}$ which in turn translates into the oscillations of the hyperfine field vector on the nucleus (H_{HF}). This causes the appearance of an oscillating transverse component of H_{HF}:

$$\boldsymbol{H_{\perp} = H_{HF}(\frac{H_{app}}{H_{rest}})} \qquad \textbf{(2.2.1.1)}$$

which is much stronger than the H_{app} and this is the field directly responsible for the nuclear transitions. The ratio:

$$\boldsymbol{\frac{H_{\perp}}{H_{app}} = \frac{H_{HF}}{H_{rest}} = \eta} \qquad \textbf{(2.2.1.2)}$$

is called the NMR enhancement factor and its value depends on the type of the material but typical value of the enhancement factor is in the order of 100-10000.

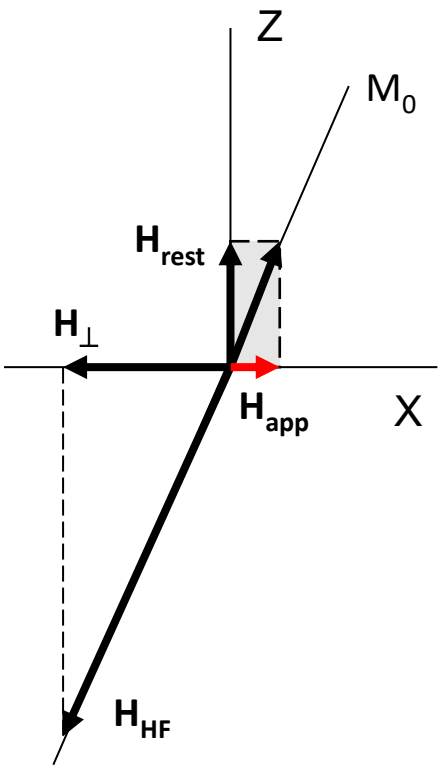

Fig. 2.2.1.1 The relationship between the magnetization M_0 and the hyperfine field H_{HF}, and the perpendicular component $H_\perp$ of the hyperfine field responsible for resonance transitions.

In many cases there can be a dispersion of the enhancement factor value within the same material which is a result of the distribution of magnetization orientation, demagnetizing field, etc. [STE67]. The true distribution of enhancement factors is the convolution product of these distributions and tends to a log-normal distribution. Therefore, the spin-echo intensity signal $\boldsymbol{S(H_{app}, \omega)}$ at each frequency ω can be expressed as a function of the amplitude of the excitation field H_{app} with the following formula [MAL99, PAN01n]:

$$\boldsymbol{S(H_{app}, \omega) = \eta(\omega) I_0(\omega) exp[-\frac{log^2\left(\frac{H_{app}}{H_{app\ opt}}\right)}{2\sigma^2}]} \qquad \textbf{(2.2.1.3)}$$

where $I_0(\omega)$ is the actual signal intensity proportional to the number of nuclei having the resonance at ω, σ is the width of the Gaussian distribution in $\log(H_{app})$ (experimentally $0{,}7 \leq \sigma \leq 1{,}2$ for single-phase materials), $H_{app\ opt}$ is the experimentally determined optimal r. f. field strength value for which the amplitude of the NMR signal is maximal and η is an macroscopic average enhancement factor. The spin-echo theory predicts that the maximum of NMR signal intensity is acquired when the nuclear spins are subjected to the effective r. f. field strength such that the nuclear magnetization rotates 90^o from its equilibrium position along H_{HF}. This condition is met when $H_{\perp}$ reaches the value of $\boldsymbol{H_{app,opt}}$ such that:

$$\frac{\pi}{2} = \gamma \boldsymbol{H_{app,opt}} \tau \qquad \textbf{(2.2.1.4)}$$

where γ is the nuclear gyromagnetic ratio and τ is the pulse length used in the experiment. Consequently the $\boldsymbol{H_{rest}}$ value, can be directly inferred from eq. (2.2.1.1):

$$\boldsymbol{H_{rest}} = \boldsymbol{H_{app\ opt}} \left(\frac{\boldsymbol{H_{HF}}}{\boldsymbol{H_{opt}}}\right) = \boldsymbol{\beta H_{app\ opt}} \qquad \textbf{(2.2.1.5)}$$

Describing the magnetic stiffness of the sample is much easier and more intuitive when using H_{rest} (also because it adopts values comparable to the coercive field) than when we use the optimum excitation field. By knowing the H_{rest} one can acquire the information about the magnetic stiffness of the sample. Enlarged value of H_{rest} indicates, that the nuclear spin precession, which gives rise to the NMR signal, is harder to excite (requires stronger magnetic field) and thus it can indicate an enhancement of the magnetic anisotropy is the system [CHA88] [PAN97].

2.2.2 NMR spectrometer used in research

All ^{59}Co NMR studies presented in this dissertation were performed using a pulsed, broadband, coherent and phase-sensitive spin echo spectrometer [Fig. 2.2.2.1] which was designed and built in the NMR laboratory in the Department of Physics of Magnetism IP PAS.

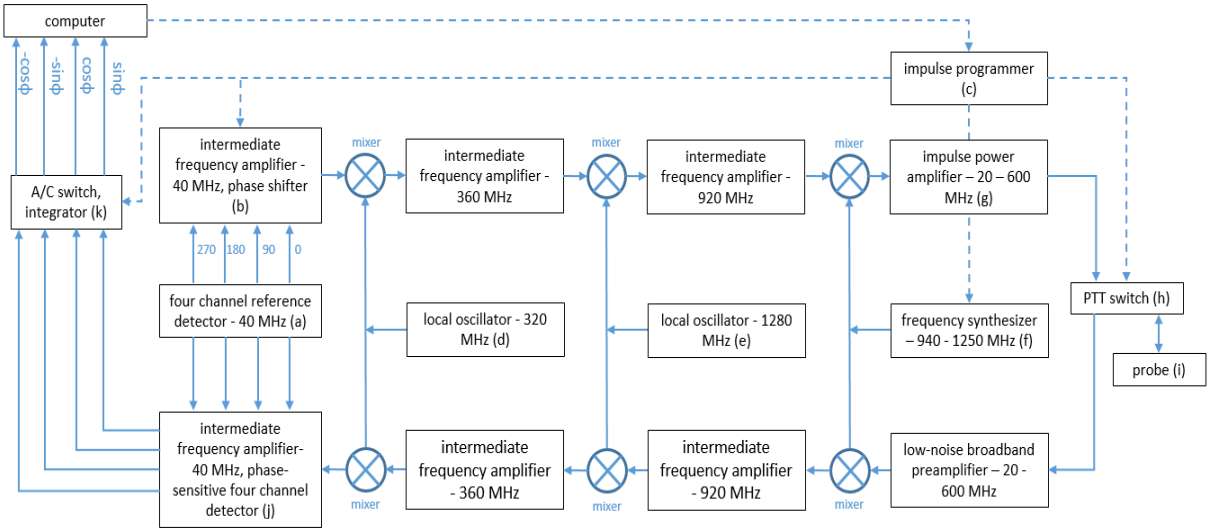

Fig. 2.2.2.1 Block diagram of nuclear magnetic resonance spectrometer used in ^{59}Co NMR thin film studies.

The detailed design of this spectrometer has been described in several works [NAD95, NAD03, MEN94]. The radio frequency reference generator (a) provides a continuous, constant 40 MHz signal. This generator has four output channels, on which the signal is phase shifted by 90 degrees in comparison to the previous channel. These four channels can be assigned four directions of the alternating magnetic field H_{app} in a rotating coordinate system: x (0°), y (90°), -x (180°), -y (270°). Subsequently, in the phase shifter (b) controlled by the pulse programmer (c), electromagnetic wave pulses are formed, and each with specified phases and duration. Phase shifter allows to independently control the phase of the pulses. Sixteen combinations of two-pulse sequences with phases shifted by 0, 90, 180 or 270 degrees from each other can be generated. This makes it possible to encode the sign and phase of the spin echo

[HAH50] signal to separate it from false signals, such as the free induction decay appearing after the second pulse. The spectrometer has a triple frequency conversion. Due to this fact, the desired operating frequency is obtained in three stages: 1) formation of first intermediate frequency 360 MHz, resulting from mixing a 40 MHz signal with a 320 MHz signal generated in the oscillator d), 2) formation of second intermediate frequency 920 MHz, resulting from mixing with a 1280 MHz signal generated in the oscillator e), 3) the 920 MHz signal obtained as a result of this transformation is then mixed with a variable frequency signal from the synthesizer (f) which operates in the 940-1520 MHz range. This process ensures spectrometer operation in the range of 20 to 600 MHz. The amplitude of the excitation field H_{app} at a given operating frequency of spectrometer is then determined by a pulse amplifier which provides an output signal amplified to 200 W (g). The desired amplitude of the signal in a given experiment is selected by setting the appropriate attenuation of the output power by the decibel attenuator situated at the output of the amplifier. The amplified impulses are directed through the transceiver switch (h) to the coil located in the probe (i), in which the studied sample is placed. The coil acts as a transceiver. The received spin echo signal is then transformed in the receiving chain to a 40 MHz signal using the reverse procedure to the one used in the transmission chain. This triple frequency conversion allows the rejection of false signals of harmonic frequencies relative to the base resonance frequency. The spin echo signal with a carrier frequency of 40 MHz then goes to the phase-sensitive detector (j), where in each of the four channels it is compared with the 40 MHz reference signal from the reference generator (a). Multiplication of the spin echo signal by a reference signal and then cutting off the variable component by a filter ensures a constant phase difference of both signals, provided that the phase stability of the reference signal is ensured - and this means that the spectrometer is coherent. The analog-to-digital converter (k), operating at 10 MHz frequency, is responsible for the conversion of the analog signal in the form of dependence of coil voltage versus time into a series of digits specifying the amplitude of the spin echo signal sampled with a resolution of 10 samples per microsecond. Each of the signals received in four orthogonal receiving channels can be treated as projections of the nuclear magnetization vector on the axes in a rotating coordinate system. The use of those channels is required to recover the amplitude of the signal independent of the phase shift which occurs during frequency scanning. The accumulation of the signal is performed in two steps -

short accumulation at fixed frequency followed by accumulation of full spectra. Echo signals from detectors with a phase corresponding to the directions 0 and 180 and 90 and 270 degrees are subtracted in pairs and divided by two to obtain the average components of the spin echo signal S_x and S_y. Finally, the amplitude of the nuclear magnetic resonance signal S [MAL99] at a given frequency is determined by the formula

$$\boldsymbol{S(H_{app}, \omega) = \sqrt{S_s^2 + S_y^2}} \qquad \textbf{(2.2.2.1)}$$

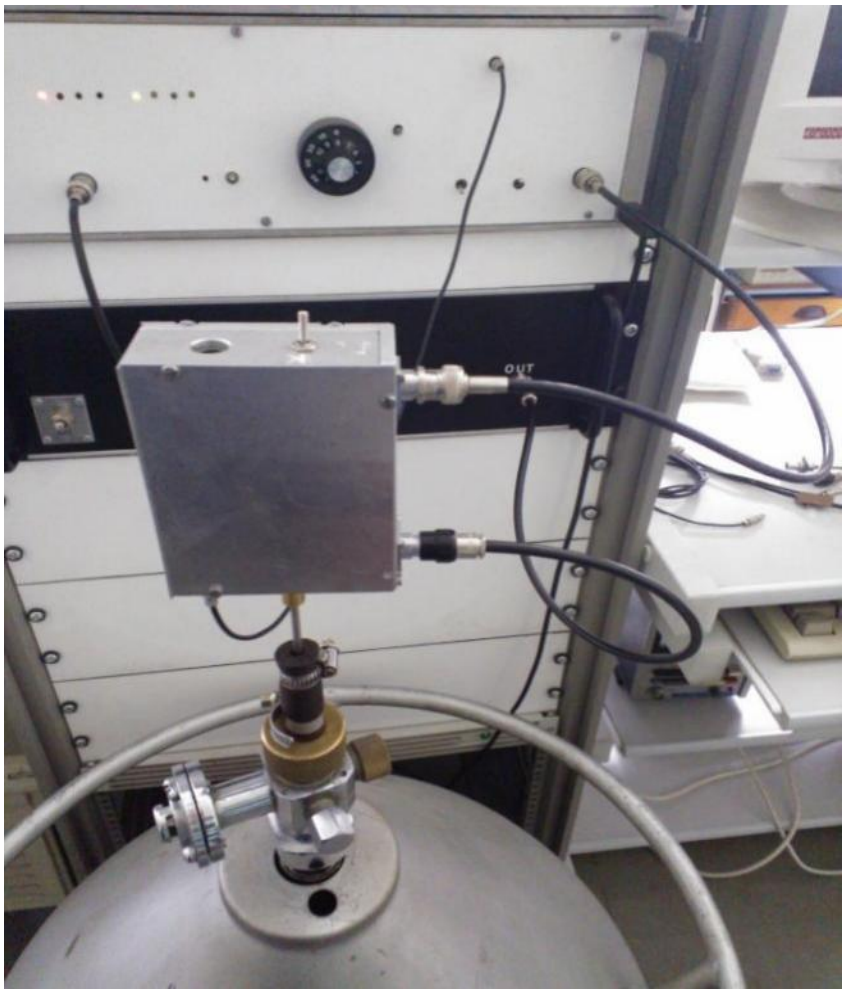

Fig. 2.2.2.2 Picture showing the apparatus used in the experiments performed for this dissertation.

2.2.3 Influence of the nearest neighborhood on the hyperfine field

In the case of Co material, the resonant frequency of the central Co atom is determined mainly by the twelve Co nearest neighbors located in three adjacent densely packed atomic planes. Depending on the order of the atomic planes stacking (ABAB or ABCABC) the symmetry of arrangement of Co atoms and distances of the nearest neighbors from the core are different and the central Co atom shows the response at frequencies characteristic for the individual phase (either hcp, fcc or stacking faults in both phases [MEN93], fig. 2.2.3.1).

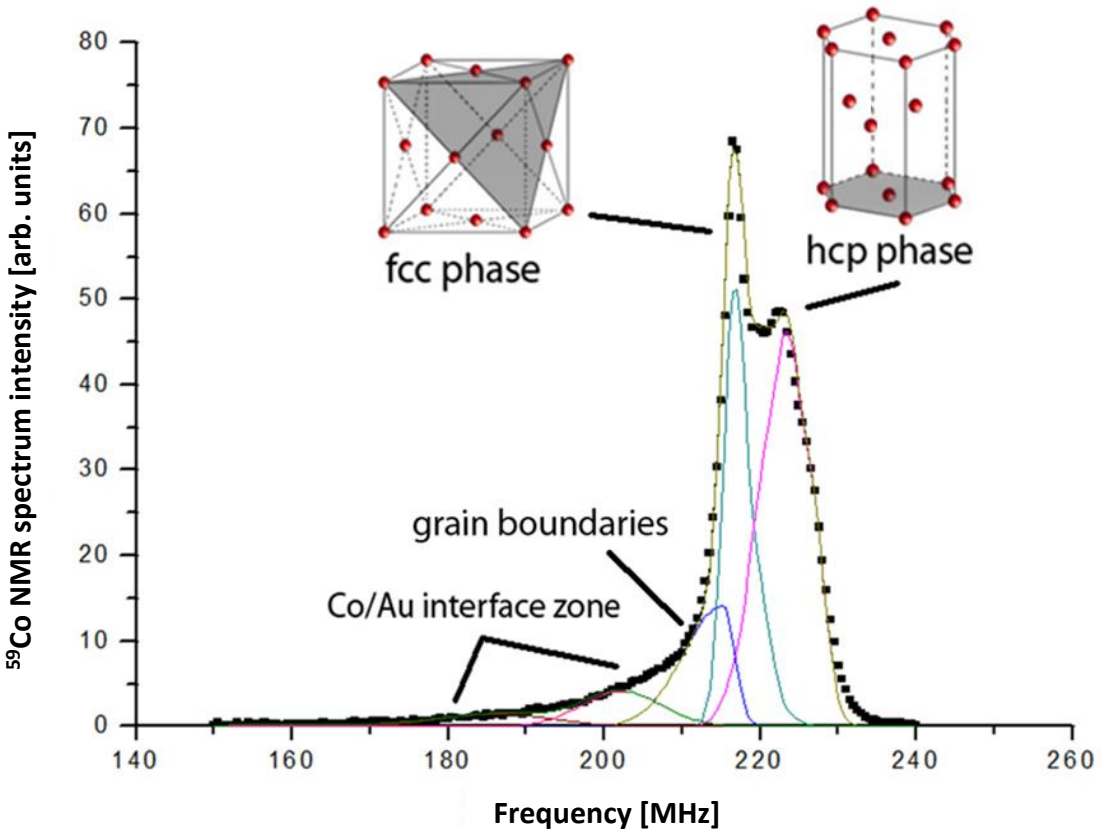

Fig. 2.2.3.1 The figure shows an exemplary ^{59}Co NMR spectrum from a <111> textured thin Au/Co/Au layer decomposed into subspectra representing the fcc and hcp phase (217-223 MHz) and grain boundaries (~210 MHz) using a fitting procedure described in

more detail in [MIC01]. The model takes into account five lines. Two main lines, green and magenta, reflect the ABCABC and ABABAB stacking respectively. Next two lines representing stacking faults are not visible independently in the fit. Due to a certain degree of structural heterogeneity these lines (220 MHz corresponding to one hcp fault in the fcc structure and, at the same time, two fcc faults in the hcp stacking; 223 MHz corresponding to two hcp faults in the fcc stacking or one fcc fault in the hcp structure) are not separable from the fcc an hcp lines. In the fit, parameters corresponding to the amount of hcp and fcc stacking faults are broadening the peaks related to fcc and hcp phases towards higher (fcc) or lower (hcp) resonance frequencies. This model also assumes a random distribution of stacking faults of which content in each crystallographic phase is characterized by the binomial law. The last fifth line in the model (blue) reflects the signal originating from Co atoms located at the grain boundaries.
Additionally, signal originating from the Co/Au interfaces (low frequency „tail" < 210 MHz) was fitted by a sum of three Gauss lines.

In bulk Co, where the environment has ideal symmetry, the fcc-Co frequency is located around 217 MHz [POR61] and for hcp Co between 222 - 229 MHz (hyperfine field in hexagonal Co is anisotropic - when the magnetization is along the hexagonal c axis the NMR frequency is 220-222 MHz, when it is in hexagonal c plane the resonance frequency is 225-228 MHz) [PAN96]. However, because of the distortions of the closest environment around Co due to stacking faults, strains, grain boundaries, etc., the fcc/hcp-Co resonance frequencies in examined samples may differ. In a pure bulk metal sample with magnetization oriented in a specific direction (state corresponding to a single domain) the NMR spectrum has a single line originating from nuclei that are all in the same crystallographic configuration. However, incorporation of alien atoms into the crystal lattice in the vicinity of the nucleus locally modifies the electronic structure leading to a change in the magnitude of the surrounding magnetic moments and to the reduction of the s-electron polarization which directly alternates the hyperfine field H_{HF} on this nucleus (see [RIE68], [KAW76], [SHA79], [MEN93]). This, in a consequence, will manifest itself as the new lines, called the satellite lines, in the NMR spectrum shifted away from the main line [PAN01n, MAL98]. It has been shown that dominant contribution to H_{HF} comes from the first coordination shell [KOB66], [NAS74].

Influence of consecutive neighboring shells decreases significantly with increasing distance and usually contributes to the broadening of the NN satellite lines. Therefore, in a system where Co is mixed with another element, the Co resonance frequency depends on chemical composition of its NN composition. Replacement of a NN Co atom by an alien or nonmagnetic atom results in a shift of H_{HF}. In many systems this effect is (almost) additive (i.e. the shift due to n Co neighbors replaced by n alien atoms is a multiple of the shift caused by a single admixture atom) and satellite lines for configurations corresponding to 1, 2, 3… alien NN are nearly equally spaced. For this reason a spectrum from alloy-like materials consists in successive satellites to the main bulk line [MEN93]. Furthermore, H_{HF} depends not only on the type on NN atoms, but also on an atomic distance (as can be deduced from pressure experiments and theoretical calculations [JON60]) and on the local symmetry. Therefore, the shift of a spectrum can be also linked to the atomic volume or to the lattice strains.

Phenomenologically hyperfine field H_{HF} in ferromagnetic metals can be represented as a sum of three components:

$$\boldsymbol{H_{HF} = A_{core}\mu_l + A_{cond}\mu_l + A_{tran}\sum n_i\mu_i} \qquad \textbf{(2.2.3.1)}$$

where A values are hyperfine coupling coefficients ([KOB66], [PAN82], [YAS71]).

The first component determines the polarization of the core electrons as a result of the exchange interaction between the magnetic moment of the 3d valence electrons and 1s electrons. The second component is associated with the spin polarization of conductivity electrons as a result of interaction with its own magnetic moment. In addition, the third component originates from polarized valence s electrons hybridized with the d orbital of directly adjacent magnetic atoms. In general, the first two terms in equation 2.2.3.1 are proportional to the atom's own magnetic moment $\boldsymbol{\mu_l}$. However, the third component depends on the number of adjacent magnetic atoms $\boldsymbol{n_i}$ and the magnitude of their magnetic moments $\boldsymbol{\mu_i}$. This explains why the hyperfine field also depends on neighboring magnetic atoms and why changes in the hyperfine field are mainly caused by changes in the closest neighborhood.

2.2.4 Preparation of the samples

[Regarding the epitaxial Co thin film alloys described in chapter 3.1] Samples were fabricated using a MBE system under UHV conditions (10^{-10} Torr) [WAW17, NAW19]. Sapphire wafers $(11\bar{2}0)$ oriented were used as the substrates. The Co layers were deposited on two buffer types: V(110) 2.5 nm thick or Au(111) 20 nm thick (Au buffer was deposited on Mo(110) film coating the sapphire substrate). Different buffers affected the structure of grown Co(111) layer (thickness range from 10 to 30 nm). Doping of the Co layers was obtained in co-evaporation process. Required concentration was assured by the proper rate ratio of depositing materials (Au: 1-5%; Mo: 1-10%). The materials were evaporated from the effusion cells or electron guns. The deposition rate was controlled and stabilized by mass spectroscopy detector and quartz monitor. Samples were prepared at the Institute of Physics of the Polish Academy of Sciences, Warsaw.

[Regarding the epitaxial thin Co (3nm) films grown on various type of buffer (Au or Mo) and capping layer (Au or Mo) described in chapter 3.2] Investigated samples were fabricated in a MBE (molecular beam epitaxy) system under UHV conditions (10^{-10} Torr). A buffer Mo(110) 20 nm thick was deposited from an electron gun on a $(11\bar{2}0)$ sapphire substrate kept at ca. 1000 °C. An Au buffer in the reference samples was fabricated by evaporation of an Au 20 nm thick layer from an effusion cell on the earlier grown Mo film. Deposition at room temperature was followed by 30 min annealing at 200 °C to smooth out the surface. The Co layer (3nm) was grown both on the Mo and Au buffers at room temperature. The 5 nm thick Au or Mo cap layers were deposited at room temperature. In addition, the Mo cap layer was covered with the 5 nm thick Au layer. In this way, four sandwich sample configurations were grown: Mo/Co/Mo, Mo/Co/Au, Au/Co/Mo, and Au/Co/Au [WAW17]. Samples were prepared at the Institute of Physics of the Polish Academy of Sciences, Warsaw.

[Regarding the epitaxial Au/Co(1,5-10nm)/Au heterostructures described in chapter 3.3] Heterostructures of Mo/Au/Co/Au with varying Co layer thickness were grown on sapphire, oriented normal to the $(11\bar{2}0)$ surface, using the molecular beam epitaxy (Ribber EVE 32) at a base pressure of $1x10^{-10}$ Torr (more detailed description of sample preparation and crystallographic characterization can be found in [GLA09],

[GLA13]). Molybdenum and cobalt were deposited by an electron-gun vapor source, and gold was thermally evaporated from a standard Knudsen cell. Initially, a 20 nm thick Mo seed layer was deposited on Al_2O_3 substrate, heated up to 950 °C, and after cooling down an Au buffer layer (20 nm) was grown. Subsequently, the structures were annealed (30 min at 200 °C), and the Co (1,5 – 10nm) magnetic film followed by Au layer of the 10 nm thickness were deposited at room temperature. Samples were prepared at the Institute of Physics of the Polish Academy of Sciences, Warsaw.

[Regarding the oxygen implanted polycrystalline Co(30nm) thin films described in chapter 3.4] Polycrystalline Au(10nm)/Co(30nm)/Au(15 or 30nm) tri-layers were grown by a MBE system [MEN13]. Subsequently they have undergone an oxygen implantation process at fluences of 3×10^{16}, 5×10^{16}, 10×10^{16}, 15×10^{16}, 20×10^{16} and 35×10^{16} ions/cm^2 at the energy of 40 keV. Performed earlier TRIM simulations have shown [MEN13] that these conditions give rise to a relatively uniform distribution of oxygen ions in the Co layer with 5%, 8%, 15%, 26%, 34%, and 44% concentration respectively. All layers were grown at room temperature at a pressure of just about 3×10^{-10} mbar. Subsequently, the samples have undergone an annealing treatment with the aim to verify the thermal stability of the exchange-biased FM/AFM system [MEN14]. The samples were annealed in vacuum ($<1\cdot10^{-6}$mbar) at 300 ^{o}C for 1h.

Additionally a similar series of polycrystalline samples was grown which were implanted with similar doses of oxygen ions/cm^2 at the same implantation energy which were surface-oxidized prior to implantation. Polycrystalline Au(10nm)/Co(30nm)/Au(15 or 30nm) sandwiches were grown by a MBE technique and then implanted using oxygen ions, with an energy of 50 keV, at fluences of 5.5×10^{16}, 8.5×10^{16}, 17.5×10^{16}, 25×10^{16} and 35×10^{16} ions/cm^2. Those samples were grown in order to verify the eventual role of the Au capping overlayer during the implantation process.

Moreover, in order to demonstrate a crucial influence of the amount of grain boundaries in the process of creation of Co/CoO interfaces after oxygen implantation, a serie of three textured Si(100)[substrate]/Cu(100nm)Co(100nm)/Co(100nm)/Au(5nm) samples was made by MBE. Two of the samples have undergone an oxygen implantation process at fluences of 3.3×10^{16}, 15×10^{16} ions/cm^2 with the energy of 60 keV. Samples were prepared at the Instituut voor Kern- en Stralingsfysica, KU Leuven.

3

NMR results and discussion

3.1 Epitaxial Co thin film alloys

For the correct analysis and interpretation of the NMR spectrum allowing to obtain the desired information about the unknown type of interface it is obligatory to examine a known referential system in which hyperfine fields (short range order) are altered in a controlled manner. One way to do this is to put the alien element in a matrix with a well-known crystal structure and magnetic properties [JAY96], [WOJ97], [THO00], [PAN97]. This allows to relate the structural and chemical short range order modification and the corresponding changes in the local hyperfine field $H_{HF.}$ The information obtained by this procedure can be in turn used in the final analysis of an experiment performed in a system of unknown short range order (in the interfaces particularly).

An influence of Mo and Au dopant on ^{59}Co local hyperfine field H_{HF} in ferromagnetic metallic Co of known crystallographic structure has never been studied intentionally despite the fact that Co thin films in various combinations with Au and Mo buffer or capping layers make many studied artificial materials showing new properties ([KUH94], [OIK03], [MOR12], [WAW18]). In this chapter ^{59}Co NMR technique was used to examine the structural properties in a series of $Co_{1-x}Au_x$ and $Co_{1-x}Mo_x$ epitaxial thin film alloys. This study was performed especially with the aim to verify the actual impact of Au or Mo alien atoms on the structural properties of Co and to establish the relation between the hyperfine field at ^{59}Co nuclei H_{HF} and the structural/magnetic character of the local environment enriched with the Au or Mo dopant. This knowledge

will be used as reference in following chapters of this dissertation containing ^{59}Co NMR analysis of series of Co thin and ultra-thin samples with Au interfaces. However, in the case of Co layers in which buffer is of different type of material than the capping layer, it is not possible to clearly distinguish the effect on the ^{59}Co NMR spectrum resulting from two different interfaces.

3.1.1 $Co_{1-x}Au_x$ thin films

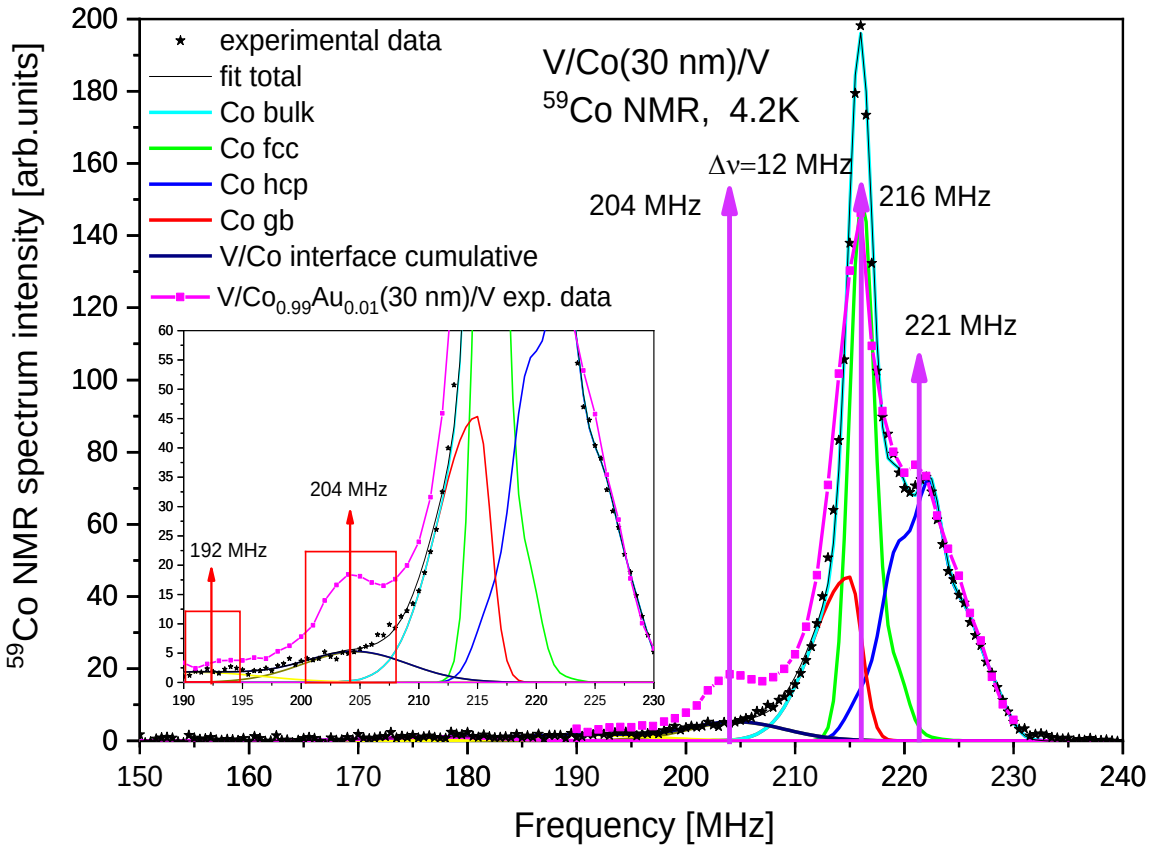

Fig. 3.1.1.1 ^{59}Co NMR in V/Co(30nm)/V thin film registered at 4.2 K. The decomposition shows Co bulk part with fcc-Co phase (green line), hcp-Co phase (blue line), grain boundary contribution (red line) and V/Co interface contribution (dark blue line). Magenta points are experimental data acquired from the $V/Co_{0.99}Au_{0.01}/V$ thin film.

Fig. 3.1.1.1 presents the decomposed ^{59}Co NMR spectrum taken from V/Co(30nm)/V sample (black stars). To illustrate the changes introduced by the Au admixture the ^{59}Co NMR spectrum recorded from V/$Co_{0.99}Au_{0.01}$/V thin film was added to the graph (magenta line+squares). It is clearly visible that the structure of the undoped V/Co(30nm)/V film is multiphase and consists of a mixture of fcc-Co and hcp-Co phases. NMR line which corresponds to a crystalline fcc-Co is situated at 216 MHz which is a lower frequency than that reported for the bulk Co (217,6 MHz) which shows a strain introduced because of the growth of Co on V buffer. V adopts bcc crystalline structure and grows in [110] direction with lattice constant a = 0,303 nm [WEB]. Due to different symmetries of the V and Co and lattice mismatch at the Co/V interface Co grows anisotropically strained [WAW17] which is visible in the shift of the resonance frequency from bulk literature 217,6 MHz to 216 MHz. The low frequency „tail" of the ^{59}Co NMR spectrum, extending down from 210 MHz to around 160 MHz, originates from a modified/distorted parts of the Co layer (Co atoms located in grain boundaries of the epitaxial film (~210 MHz), where a structural disorder due to grain misorientation lowers the H_{HF} acting on ^{59}Co nuclear spins; Co from Co/V interfaces - the spectrum part in the 160-210 MHz range which is in agreement with the analysis of Co NMR spectra in [Co(x nm)/V(1.5nm)]n multilayers [THO00]).

The ^{59}Co NMR spectrum from the V/$Co_{0.99}Au_{0.01}$/V alloy (fig. 3.1.1.1. magenta squares) is very similar to the one from V/Co(30nm)/V thin film with one difference, which is a visible satellite structure (fig. 3.1.1.1. inset - red square mark) that provides the evidence for the presence of Co atoms with one or more nearest neighbors (NN) replaced by a non-magnetic Au atoms in the first coordination shell. Such chemical configurations are characterized by a reduced ^{59}Co hyperfine field H_{HF} and thus the resonance frequency is correspondingly smaller.

The NMR spectrum from $Co_{0.99}Au_{0.01}$ alloy also clearly shows that discussed layer isn't a single phase material, thus it is not easy to conclude which of the Co phases, whether hcp or fcc, is a host for the Au dopant. However, a deeper spectrum analysis allows the observation that the frequency spacing between the first satellite (204 MHz) corresponding to a single Au nearest neighbor, and the second satellite line (192 MHz) corresponding to two Au nearest neighbors is similar as between the first satellite and the line representing the Co fcc phase, which lead to the conclusion, that that the satellite structure is caused by the presence of Au in the fcc Co phase. However, it

cannot be ruled out that a small fraction of Au is also in hcp Co but the corresponding satellite structure is not visible because it overlaps with the line from fcc-Co. In any case, if Au is present in the hcp Co phase, its effect must be similar to that caused by Au in the fcc phase. And in fact, this similarity has been shown in the chapter 3.3.1 devoted to the experimental results from epitaxial Au/Co(1,5-10 nm)/Au heterostructures ^{59}Co NMR study.

As illustrated in fig. 3.1.1.1, the frequency spacing ($\Delta\nu$) between the main Co line in V/$Co_{0.99}Au_{0.01}$/V NMR spectrum and the first satellite equals around 12 MHz. It is significantly smaller than $\Delta\nu$ due to the V admixture to Co that equals around 30 MHz [THO00] and therefore, V/Co interfacial effects can be omitted as the source of the satellite structure in the NMR spectrum of V/$Co_{0.99}Au_{0.01}$/V. The value by which one Au NN reduces the H_{HF} around probed ^{59}Co nuclei can be obtained from the relation $2\pi\upsilon = \gamma H_{HF}$ ($\gamma/2\pi$ = 10,054 MHz/T) [ALP94], therefore $\Delta H_{HF} = \Delta\nu/\gamma$ = 12MHz/10,054(MHz/T) = 1,19 T.

The inferred possibility of the tendency for the selective presence of Au admixture in the fcc-Co phase areas in the multiphase Co layer grown on V buffer layer (in which the fcc Co phase accounts for about 50% of the volume in the undoped layer) need to be verified in case of the Co layer grown on Au since it is known that the epitaxial growth of Co on Au(111) leads to the hcp structure of Co with the epitaxial relation Au[111]//Co[0001]. ^{59}Co NMR experiment has been carried out in the reference Co layers Au/Co(t)/Au, with t = 30, 10 nm and in Co layers of the nominal composition: Au/$Co_{0.99}Au_{0.01}$(30nm)/Au, Au/$Co_{0.99}Au_{0.01}$(20nm)/Au, Au/$Co_{1-x}Au_x$(10nm)/Au (x=0.01, 0.02 and 0.05). The ^{59}Co NMR spectra recorded for the above-mentioned samples are presented in fig. Fig. 3.1.1.2.

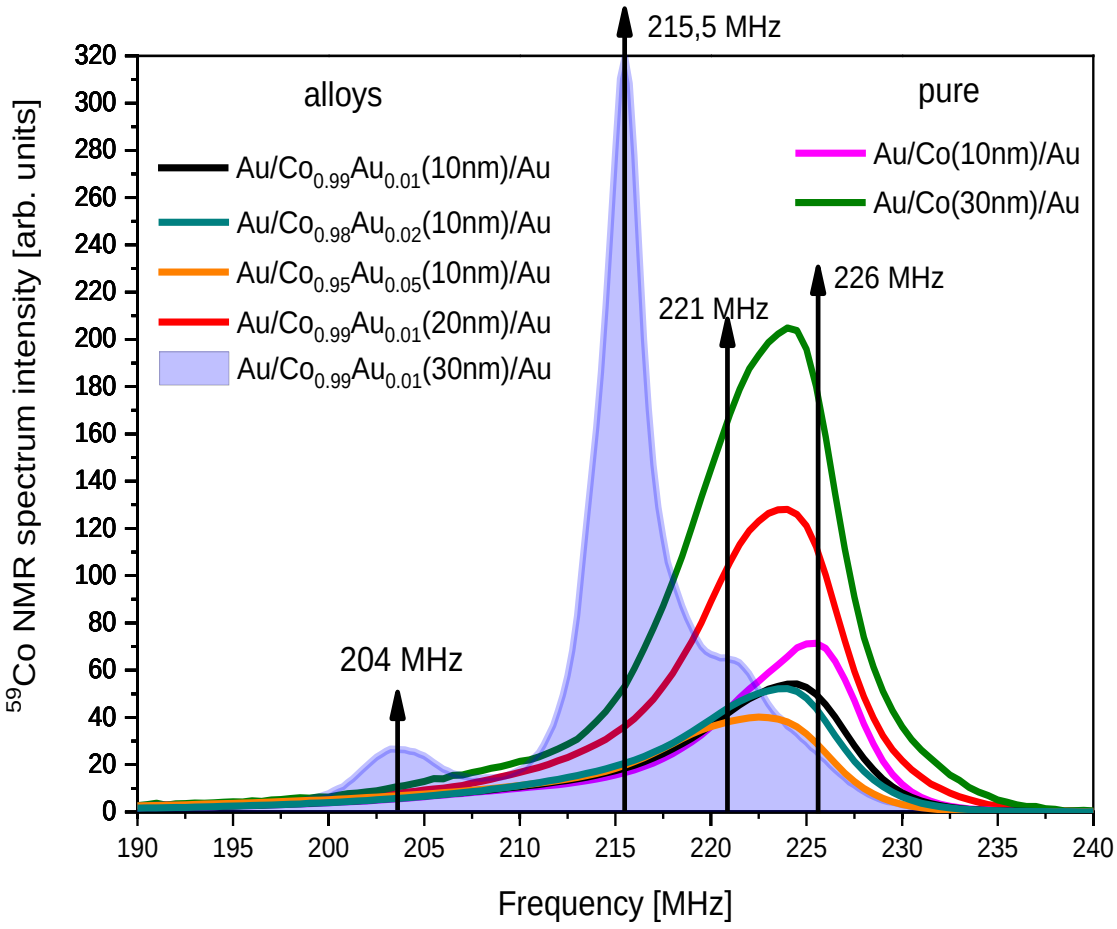

Fig. 3.1.1.2 ^{59}Co NMR spectra recorded for all Au/$Co_{1-x}Au_x$/Au thin films.

^{59}Co NMR spectra recorded in the reference layers Au/Co(t)/Au (t = 10, 30 nm) (Fig. 3.1.1.2) show that the Co layer for both studied thicknesses gives rise to a single ^{59}Co NMR line located near 226 MHz (the frequency of hcp-Co phase with magnetization aligned in the hexagonal c plane) as expected for Co layer in this thickness range. The resonance frequency is slightly shifted towards lower value for a thicker layer (10 nm – 225,5 MHz, 30 nm – 224,5 MHz) which gives the first indication of some kind of degradation of the layer structure but without the evidence of eventual phase separation into a mixture of fcc and hcp phases. Simultaneously the discussed ^{59}Co NMR lines have characteristic asymmetric tails extending towards lower frequencies (down to 180 MHz). This feature unambiguously reveals the presence of structurally or compositionally modified Co environments. Spectrum intensity in these low-frequency tails increases with the growing layer thickness meaning that the

population of such deformed Co environments increases as the layer becomes thicker. Moreover, the low-frequency parts of the discussed spectrum show an intensity bump around 208 MHz, which suggests that some certain type of modified Co environments is preferentially populated (fig. 3.1.1.2).

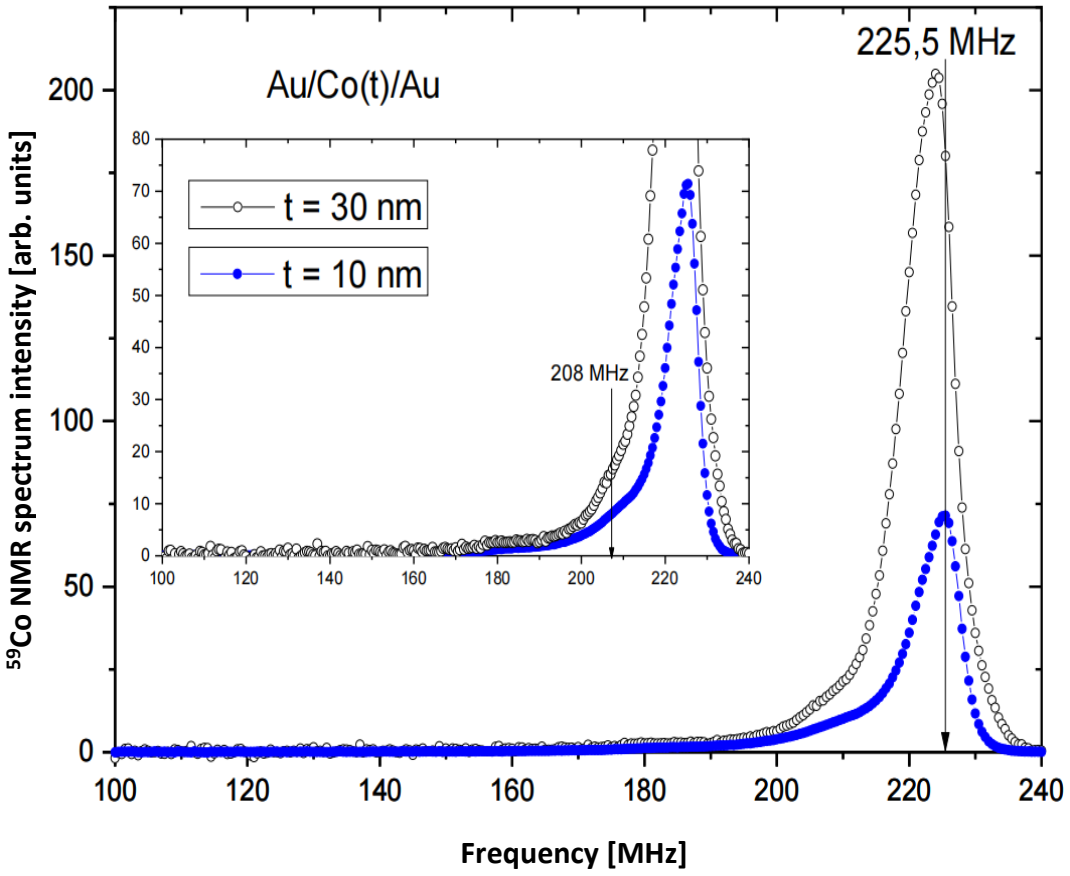

Fig. 3.1.1.2 ^{59}Co NMR spectra recorded for the 30 and 10 nm thick Co layers, grown on Au buffer and covered with Au capping layer. Arrows indicate the characteristic frequencies corresponding to Co in pure hcp (~226 MHz) and modified hcp (~208 MHz) local environments as discussed in the text.

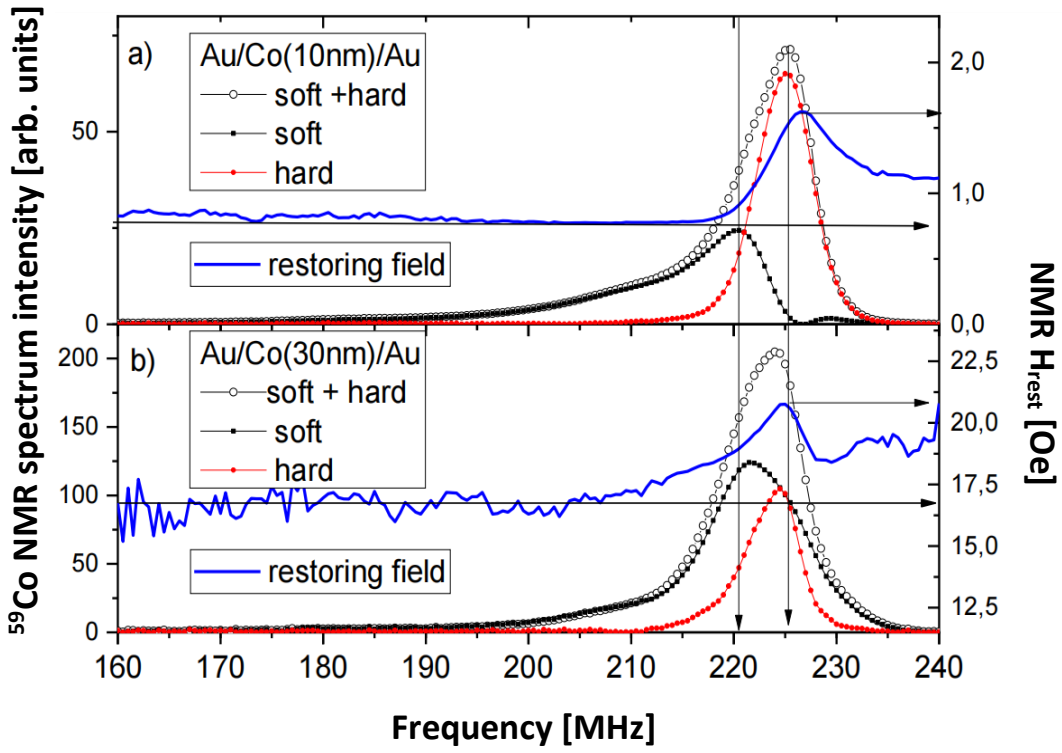

Fig. 3.1.1.3 ^{59}Co NMR spectra from Au/Co(t)/Au, t = 10, 30 nm samples decomposed into "soft" (black dots) and "hard" (red dots) components. The spectra are compared with the restoring fields (right side scale) characteristic for each sample (blue lines).

A non-uniform character of the r.f. field amplitude ($H_{app\ opt}$), which is required to induce the maximum intensity of NMR signal in studied layers allows to relate the structural inhomogeneity of the material to the magnetic one. Following the broad description in [PAN01n], the spin echo NMR intensity has been analysed as a function of H_{app} for each frequency in the studied samples, to separate the spectra corresponding to different soft and hard magnetic components of the Co layers corresponding to different $H_{app\ opt}$. As shown in the Fig. 3.1.1.3 (a, b) (right side, vertical scale) the $H_{app\ opt}$, which is expressed as NMR restoring field: $\boldsymbol{H_{rest} = H_{app\ opt}\left(\frac{H_{HF}}{H_{opt}}\right) = \beta H_{app\ opt}}$ **(2.2.1.5)**, demonstrates a rapid increase in the frequency range corresponding to the main Co line located around 226 MHz. The spectra obtained from 30 nm and 10 nm thick layers, decomposed using the above procedure, are presented in Fig. 3.1.1.3 (a, b) (left side, vertical scale) and on those spectra are superimposed H_{rest} values (presented in

(Fig. 3.1.1.3 (a, b), right side, vertical scale). The course of the H_{rest} values significantly changes with the increasing frequency. The difference in the H_{rest} values alongside the corresponding ^{59}Co NMR spectrum frequency range and the spectrum shape implies the conclusion that the discussed layers are magnetically inhomogeneous, which is a result of a structural irregularity. In all layers exist structurally homogeneous regions, where Co exhibits regular hcp order represented in the ^{59}Co NMR spectrum by a single narrow line around 226 MHz with higher restoring field, as well as the regions that are structurally distorted and magnetically softer represented by the line with maximum intensity near 220 MHz asymmetrically broadened down to 180 MHz. In further discussion in this chapter these two components are called "hard component", representing the regular well-defined hcp-Co structure, and "soft component", representing heavily distorted hcp-Co structure (in terms of arrangement, distances, strains and possible composition) and grain boundaries.

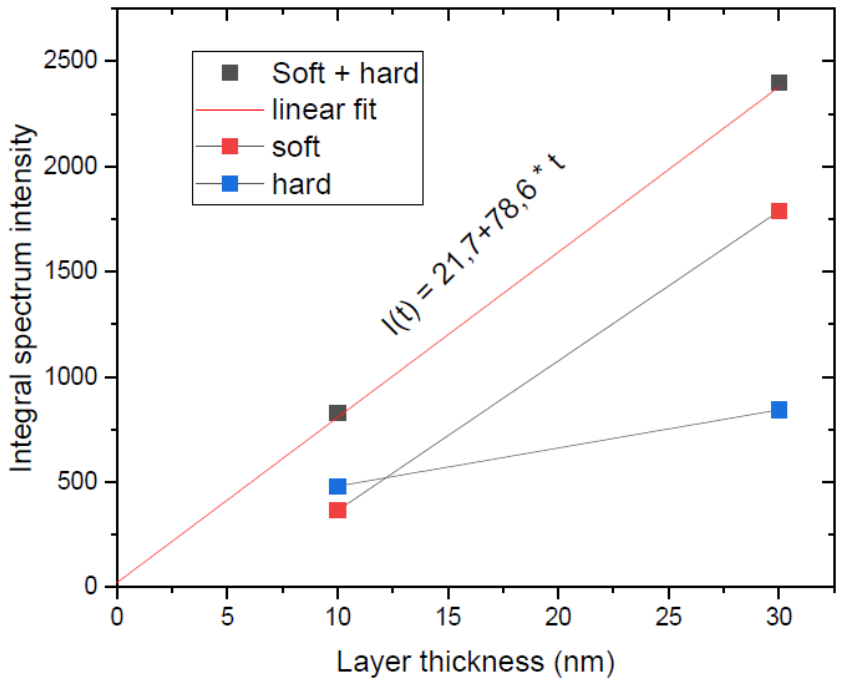

Fig. 3.1.1.4 Integrated ^{59}Co NMR spectrum intensities of Au/Co(t)/Au (t = 10, 30 nm) samples (black squares) compared with the intensities of "soft" (red squares) and "hard" (blue squares) spectrum components as a function of the Co layer thickness.

The above analysis clearly points to a very fast increase of the distorted „soft" regions in the films with respect to the regular well-defined "hard" hcp-Co regions with the rising thickness of the Co layer up to 30 nm. As shown in fig. 3.1.1.4, the integral fraction of the regular hcp regions in 10 nm thick layer is definitely dominating over the distorted „soft" component whereas in thicker sample the situation is quite opposite, which suggests that the structure of the Co layer grown above the thickness of 10 nm becomes heavily deteriorated.

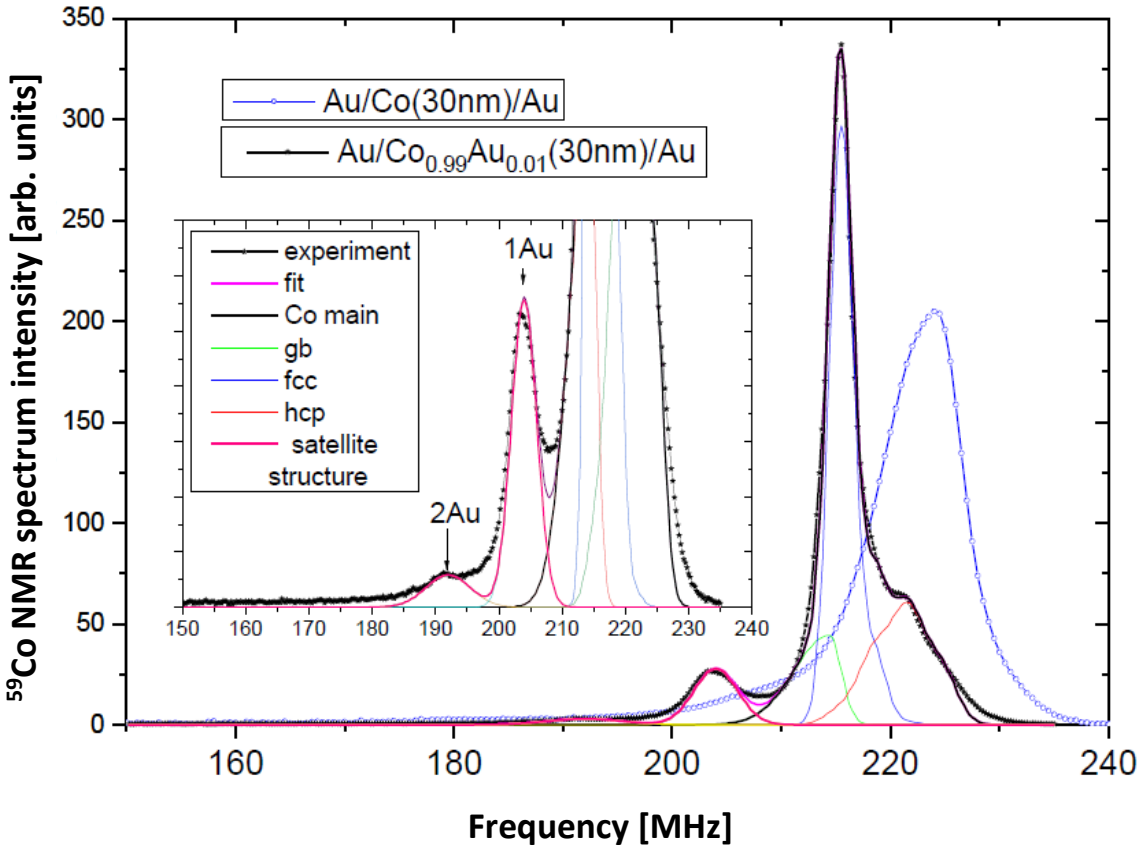

Fig. 3.1.1.5 ^{59}Co NMR spectra registered for Au/$Co_{0.99}Au_{0.01}$(30 nm)/Au layer (black line and points) and for the referential Au/Co(30 nm)/Au layer (blue line/empty points). The inset pictures the satellite structure in the Au/$Co_{0.99}Au_{0.01}$(30 nm)/Au layer.

^{59}Co NMR spectrum registered for Au/$Co_{0.99}Au_{0.01}$(30 nm)/Au sample is shown in fig. 3.1.1.5 and compared with the spectrum from the reference Au/Co(30 nm)/Au layer. This comparison shows distinctly the structural difference between the two films. The

layer that is the single hcp-Co phase material in case of the pure Co film becomes a multiphase when an Au is added. This can be clearly seen in the spectrum by the presence of lines at 215,5 MHz and around 221 MHz, representing fcc-Co phase and hcp-Co phase with numerous fcc stacking faults, respectively. Moreover, the spectrum reveals the satellite structure similar to that present in case of the V/$Co_{0.99}Au_{0.01}$(30 nm)/V layer. The frequency position of the satellites is the same for both systems and equals 204 MHz for the first satellite line and 192 MHz for the second.

If spectra of Au/$Co_{0.99}Au_{0.01}$(30 nm)/Au and V/$Co_{0.99}Au_{0.01}$(30 nm)/V thin films are compared, which are similar to each other at first glance, it can be seen that the satellite linewidth is visibly smaller in the case of Au/$Co_{0.99}Au_{0.01}$(30 nm)/Au layer. The satellite structure in the spectrum is better separated from the main Co lines than in case of V/$Co_{0.99}Au_{0.01}$/V layer, which in turn allows to conclude, that if in the spectrum from Au/$Co_{0.99}Au_{0.01}$(30 nm)/Au there is another satellite line that could be associated with Au atoms in hcp-Co, its intensity is comparably low. This observation is in agreement with the previous result obtained for V/$Co_{0.99}Au_{0.01}$/V film and both show that despite the fact that Co and Au make the non-soluble system [OKA85], a small amount of Au can be alloyed with fcc-Co when grown as a thin film.

^{59}Co NMR spectra obtained for the Au/$Co_{1-x}Au_x$ (10 nm)/Au (x = 0.01, 0.02, 0.05) and Au/$Co_{0.99}Au_{0.01}$(20nm)/Au samples show significantly different structural properties of Co layer than those observed in case of Au/$Co_{0.99}Au_{0.01}$(30 nm)/Au thick film. These layers retain hcp structure without any clearly visible trace of transformation to a mixture of defected hcp and fcc phases. However, in the range characteristic for fcc-Co there is present a signal intensity which could be associated not only for strongly defected hcp-Co phase but also for a origin of an eventual residual fcc-Co phase (not distinguishable due to huge predominance of hcp phase and overall highly defected crystalline structure, which leads to a broadening and loss of detail in the NMR spectrum). In the frequency range characteristic for the satellite structure in 30 nm thick layer, the spectra shape in 20 nm and 10 nm $Co_{1-x}Au_x$ layers remains essentially the same as in the spectrum corresponding to the pure Co layers and does not show any trace of new satellites.

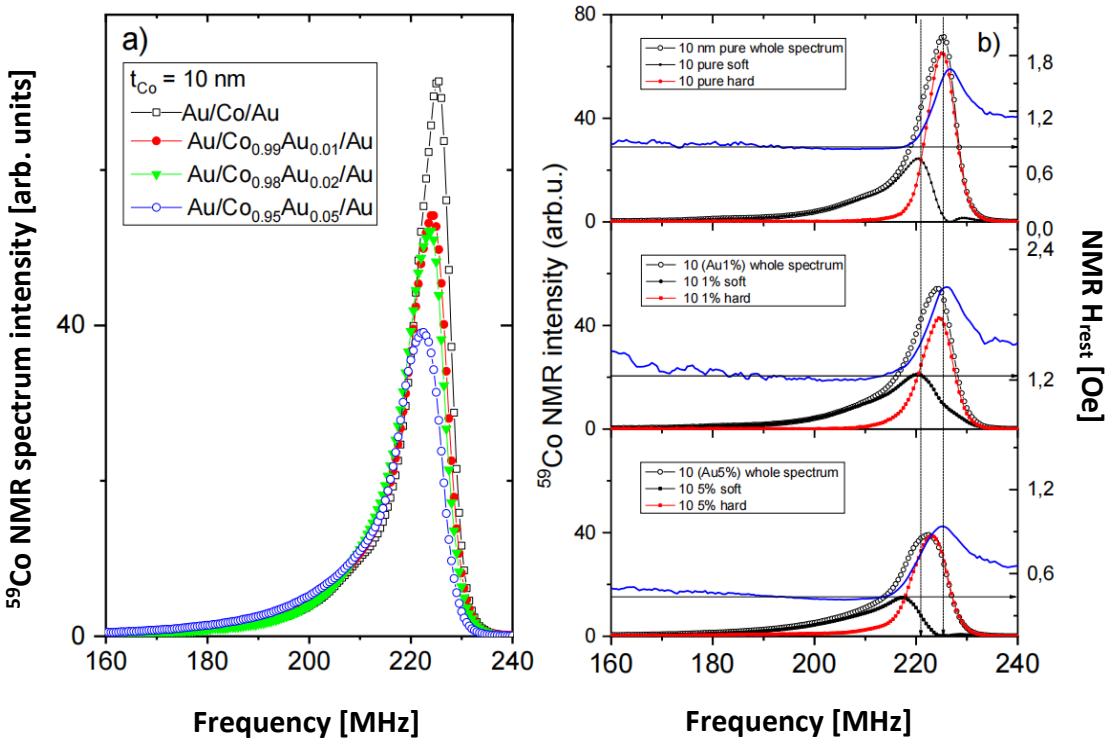

Fig. 3.1.1.6 (a) ^{59}Co NMR spectra registered from the Au/$Co_{1-x}Au_x$/Au (x = 0, 0.01, 0.02, 0.05) layers. (b) ^{59}Co NMR spectra of Au/$Co_{1-x}Au_x$/Au (x = 0, 0.01, 0.05) layers decomposed into magnetically soft (black points) and hard (red points) components. Blue lines represent acquired H_{rest} values.

As expected, judging by the lack of the structural transformation of 10 nm thick Co layers, the H_{rest} registered for these layers keeps the properties characteristic for the pure Co layer as shown in fig. 3.1.1.6 (b) (blue lines). The corresponding spectra decomposition into "soft" and "hard" components are illustrated in the Fig. 3.1.1.6 (b). It shows that while the total intensity is reduced, the relative population of both components is not significantly altered. Evidently, while 10 nm thick Co films maintain their original ABAB sequence of stacking of densely packed monoatomic layers specific to the hcp phase, the interatomic distances become larger which is reflected in the reduced hyperfine field H_{HF} experienced by ^{59}Co nuclei. In addition, a volume of the magnetic Co decreases systematically with the increasing nominal Au concentration in the layers. The same reduction applies to 20 nm and 30 nm thick layers.

Taken together, the results seem to suggest that when growing the Co layer by co-deposition of Co and Au, a small amount of Au dopant (around 1%) can be present in a Co film. However, direct evidence for the presence of Au in the film in the form of a regular satellite structure in the NMR spectrum associated with the replacement of Co NN by Au was only observed when the crystallographic structure of the layer contained the fcc-Co phase. This situation was observed for the growth of the Co layer on the V buffer, where the layer was characterized by a multi-phase crystal structure already in the case of undoped Co, or in the case of a layer on the Au buffer layer at a sufficiently large Co thickness. The experimental results show that for 10 and 20 nm thick Co layers the hcp-Co structure is stable enough, and the presence of Au is not detectable as the satellite structure in NMR spectrum. However, the crystallographic structure of the layer, while still hcp, deteriorates, as indicated by ^{59}Co NMR results. Hcp structure of the Co layer codeposited with Au becomes unstable around the thickness of 30 nm, and only this partial transformation to the fcc Co structure reveals the presence of Au impurity in the layer. This observation clearly proofs that Au must be also present in the thinner layers. This is because the final thickness of the layer it is not predetermined during the growth. Therefore if Au is present in the 30 nm multiphase layer it is also present in the body of 20 and 10 nm thick films with hcp structure. Most likely, the maintenance of a partial coherence with the Au substrate and the presence of Au impurity introduces such a deformation in the network of the hcp structure that its influence on the local field on Co nuclei is comparable or greater than the replacement of one magnetic neighbor with a non-magnetic Au. The presence of a "soft" component, in addition to a "hard" characteristic for the undistorted hcp-Co structure, in the NMR spectra for layers with a thickness below 30 nm, may support this hypothesis. Only structural relaxation and transformation to the multiphase fcc/hcp state directly reveal the presence of Au in the layer.

However, that raises the question on the origin and on the structure of the “soft” component present in the spectra for the undoped Co layers. A closer look at the comparison of the spectra of both 30 nm Au/Co/Au layers (pure and co-deposited with Au) in Fig. 3.1.1.7, especially at the frequency areas characteristic for fcc-Co and 1-st satellite the in the Au/$Co_{0.99}Au_{0.01}$(30 nm)/Au sample, allows for a certain conclusions to be drawn about the origin of the fcc-Co phase in the Au/$Co_{0.99}Au_{0.01}$(30 nm)/Au sample. The intensity of the ^{59}Co NMR spectrum at these frequencies is also clearly

present in the case of a pure sample, in which this region of the spectrum represents strongly defected and magnetically soft areas of the sample (fig. 3.1.1.3), enclosing highly defected hcp-Co phase, grain boundaries and probable Co:Au interface areas. Note, that the frequency range and the spectrum shape of the "soft hcp" component in the spectrum from the nominally pure 30 nm Co layer is somewhat similar to the spectrum from the fcc Co, including the satellite structure due to Au impurities, in the spectrum for $Co_{0.99}Au_{0.01}$ alloy. This is evidenced in fig. 3.1.1.7 where the spectra from the two films are shown in the respective frequency scale shifted by 5,5 MHz, in order to enhance the similarity between the spectrum shape.

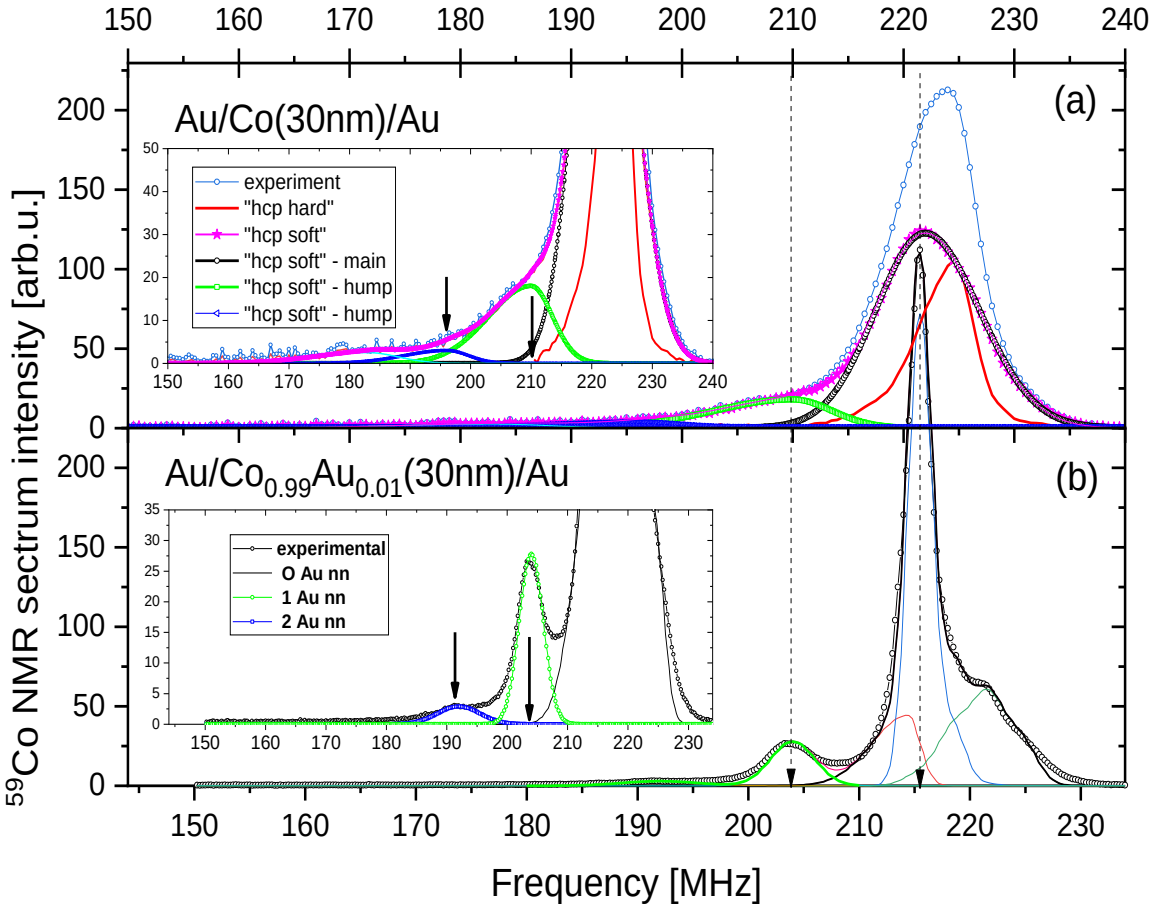

Fig. 3.1.1.7 ^{59}Co NMR spectra registered from the a) reference Au/Co(30nm)/Au layer and the b) Au/$Co_{0.99}Au_{0.01}$(30nm)/Au layer. Note the 5,5 MHz shift between the frequency range for the upper (a) and the lower (b) panels. The insets show the satellite structure of the spectrum from Au/$Co_{0.99}Au_{0.01}$(30nm)/Au layer (lower) and the drastic rise of the low intensity tail of the "soft hcp" component for Au/Co(30nm)/Au. The

arrows indicate the frequency positions of the satellites due to Au in fcc Co in $Au/Co_{0.99}Au_{0.01}/Au$ system and due to Au in "soft hcp" phase in Au/Co/Au system.

The frequency spacing between the main line and the satellites in the fcc Co structure is the same as the spacing between the main line and the intensity bump in the tail of the "soft hcp" line (see the arrows in fig. 3.1.1.7 indicating the frequency positions of the respective lines). In fact, the spectrum from the "soft hcp" component looks similarly to the spectrum from the fcc phase but broadened and shifted up in the frequency scale by 5,5 MHz. This leads to a hypothesis that the magnetically "soft" component is due to the Au admixture present in the hcp-Co layer, despite the fact that the layer was intentionally grown as the chemically pure Co film. Au atoms have bigger atomic radius and when replacing Co, even at a very low concentration, they would introduce a long range structural distortion around its position, thus lowering the ^{59}Co NMR frequency from 226 MHz to around 220 MHz. At the same time Co atoms having Au as the NN would have experienced the reduced H_{HF} giving rise to the intensity bump around 208 MHz. In this scenario the magnetically "soft" hcp component of the layer would be a precursor of the fcc Co phase with the Au admixture on the level of 1 at %, that is observed in the 30 nm thick Co layer when Co was co-deposited with Au. But what is the reason for the presence of Au in the nominally pure Co film? The highly probable scenario is that during the growth of Co film Au atoms migrate from the Au buffer to the grain boundary regions helping to accommodate the large lattice mismatch at Au(111)/Co(0001) interface. As pointed out by Fruchart [FRU03], considering Co/Au(111) system there are several results suggesting that "the grain boundaries might consist of Au atoms that are extracted from the substrate". To support this interpretation Fruchart et al. quote results like the core-level photoemission electron spectroscopy [MAR97], the lifting of the Au reconstruction during the Co dots lateral growth that releases 4 % atomic layer of Au [MAR99], or the wetting of several-atomic layer-thick Co films with Au atoms upon extremely moderate annealing [SPE95]. The results from ^{59}Co NMR study fully agree with this interpretation.

3.1.2 $Co_{1-x}Mo_x$ thin films

This subchapter is based on results acquired by the author of this dissertation from the ^{59}Co NMR study of $Co_{1-x}Mo_x$ alloys which have been published in [NAW19] in 2019.

The ^{59}Co NMR spectra recorded for the $V/Co_{1-x}Mo_x/V$ (x = 0, 0.01, 0.04, 0.1) thin films are presented in fig 3.1.2.1. Spectra decomposition showing the changing satellite structure with the increasing concentration of the Mo impurity is presented on fig. 3.1.2.2.

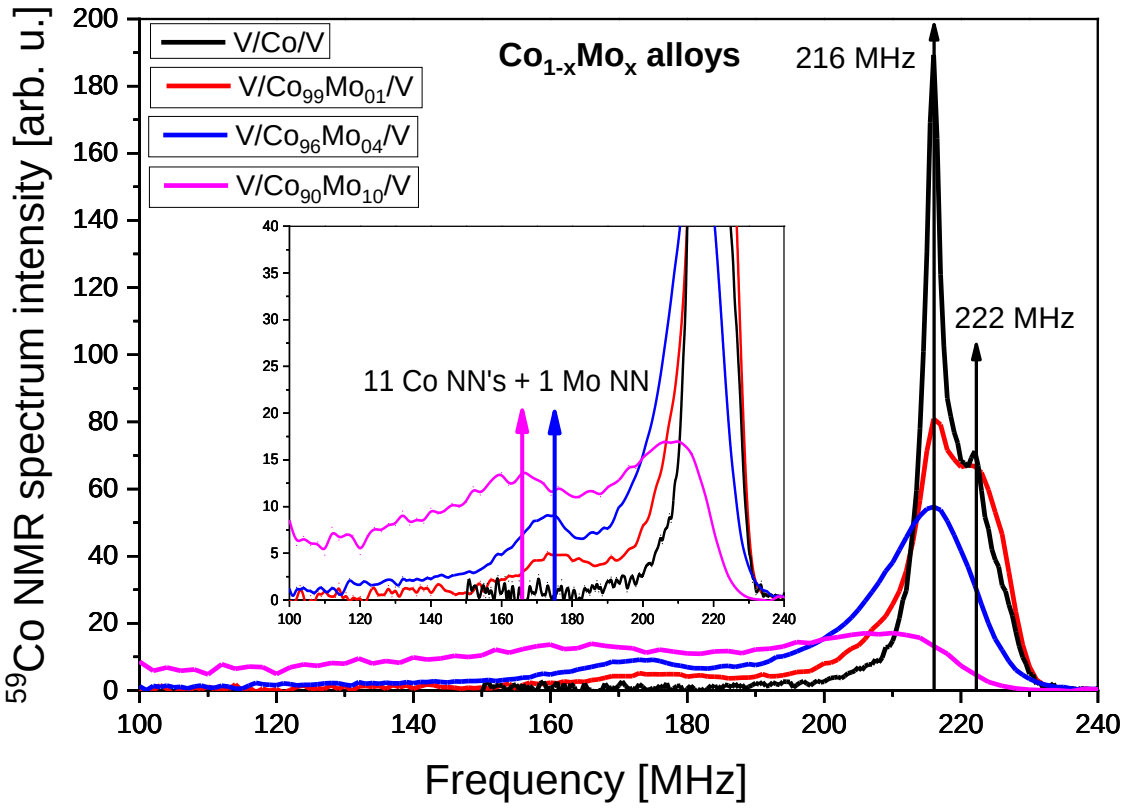

Fig. 3.1.2.1 ^{59}Co NMR spectra corresponding to the $V/Co_{1-x}Mo_x/V$ alloys with Mo impurity concentrations x = 0, 0.01, 0.04, 0.1 (inset – 5x magnification), recorded at 4.2 K.

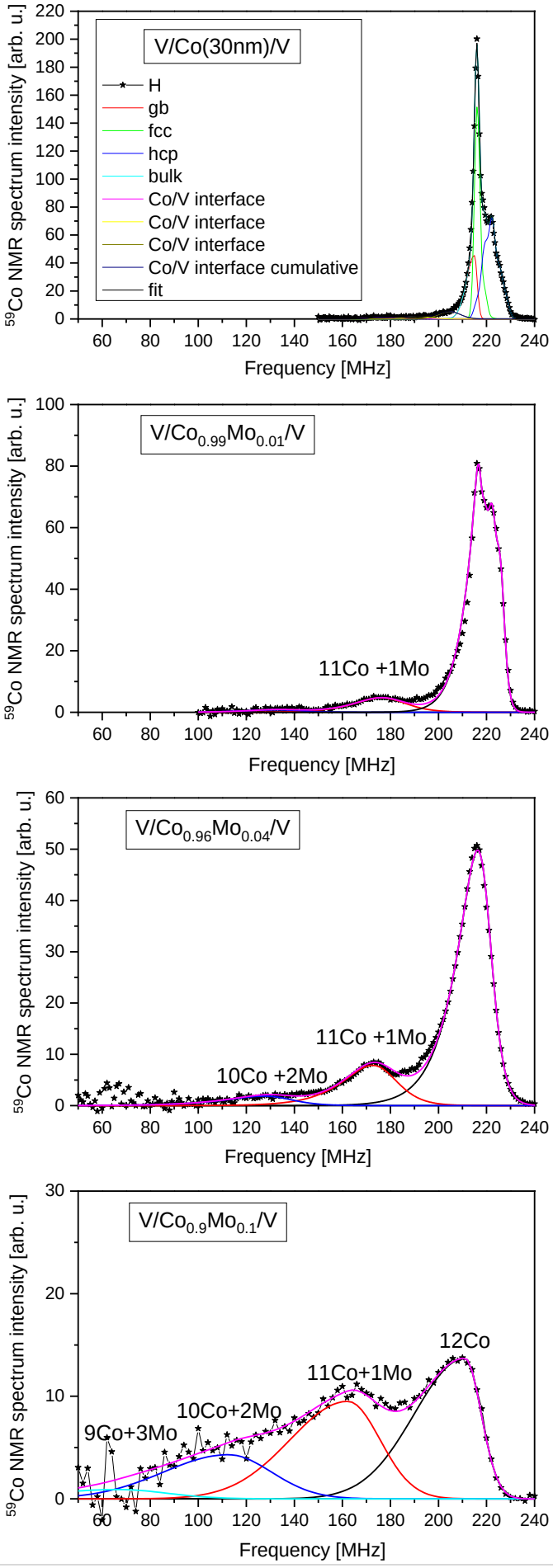

Fig. 3.1.2.2 ^{59}Co NMR spectra in $V/Co_{1-x}Mo_x/V$ thin films registered at 4.2 K, for Mo content x = 0, 0.01, 0.04 and 0.1. The decomposition shows the satellite structure corresponding to Co with the nearest neighbor configurations composed of (12-n) Co and n Mo atoms.

Due to a Mo doping the shape of the spectra undergo a significant modification revealing changes in the H_{HF} distribution. First change is the evidential progressive decrease of the spectrum intensity in the high-frequency part of the spectrum (> 210 MHz) corresponding to the well-defined crystalline Co environments in the fcc-Co and hcp-Co phases. Second new feature is the emergence of a satellite structure in the lower frequencies of the NMR spectrum corresponding to Co with the nearest neighbor configurations composed of (12-n) Co and n Mo atoms. For the $V/Co_{0.99}Mo_{0.01}/V$ film a single broad satellite line around 176 MHz is observed in the spectrum. Further growth of Mo concentration results in a structure consisting of two visible satellite lines as can be seen in the ^{59}Co NMR spectra recorded for $V/Co_{0.96}Mo_{0.04}/V$ and $V/Co_{0.90}Mo_{0.1}/V$ layers. The frequency spacing $\Delta\nu$ between the main line and the subsequent satellite lines is immense (over 43 MHz) and is not constant like in various Co-based alloy systems studied in the past [MEN93], [MAL98]. Moreover a progressive shift of the entire spectrum towards lower frequencies is visible with increasing Mo concentration (see fig. 3.1.2.1). The above relation points to a very strong dependence of ^{59}Co resonance frequency on the local Mo concentration, i.e. a number of Mo NNs, as well as on the average concentration of Mo in Co film. Based on the detailed analysis it is predicted that Co becomes nonmagnetic when surrounded by 3-4 Mo NNs for the concentration as low as 20-30% [NAW19]. All of these features indicate a strong global influence of Mo dopant on Co structure and magnetic properties which is in agreement with the literature [WAW17].

There is still another aspect of Mo doping which has to be discussed. Closer analysis of the ^{59}Co NMR spectra from fig. 3.1.2.1 and fig. 3.1.2.2 shows that both the undoped layer and the one with 1% Mo admixture are multiphase with clearly visible fcc- and hcp-Co environments. However it is impossible to distinguish the corresponding structure in the satellites. Moreover for layers with higher Mo concentration ($V/Co_{0.96}Mo_{0.04}/V$ and $V/Co_{0.90}Mo_{0.1}/V$) the hcp and fcc components of the main line evolve into one broad peak asymmetric towards lower frequencies (with similar shape as the satellites). This hints that Mo atoms do not show any visible preference to enter a particular Co crystallographic phase in the studied thin film alloys. If it were so, then (taking into account two phase composition of the discussed alloys) three different satellite structures could have been expected with the intensity ratio 2:1:1.

In hcp-Co the H_{HF} is anisotropic and it has been shown by ^{59}Co NMR studies in hexagonal Co:Cu and Co:Mn alloys [MAL98] that the frequency of the satellites depends on the position of an alien NN in the matrix. Two different satellite frequencies have been observed experimentally and related with the two possible structural configurations: an alien atom replacing one of six Co NN in the hexagonal plane of the central atom; and one of the three Co NN located in the two planes located below/above this plane. Similar double satellite frequency could be expected in hcp-Co:Mo alloy. As for the cubic fcc-Co, the H_{HF} is isotropic and most likely remains such when modified by the Mo NN. Taking all of this into account, in discussed $Co_{1-x}Mo_x$ alloys one satellite would originate from the fcc-Co:Mo and two from hcp-Co:Mo, each one consisting of the satellite sequences corresponding to n = 0, 1, 2… Mo NNs with a specific location in the NN structure. However, ^{59}Co NMR spectra for $Co_{0.96}Mo_{0.04}$ and $Co_{0.90}Mo_{0.1}$ layers presented in fig. 3.1.2.1 show only one very broad satellite structure which can be explained in two ways. First one is that all three satellites are present but their frequency spacing is very similar and they merge into one broad satellite structure. Second possibility is that this is a result of blurring of the H_{HF} differences between fcc-Co and hcp-Co phases due to the crystal lattice distortion which is caused by the large lattice mismatch between Co and Mo. Moreover, a very large frequency spacing between the satellites and the position of the main line suggest that the impact of Mo NN is not limited to the first neighbor shell but it extends to the second shell. Assuming the influence of Mo atom located in the second coordination shell on the H_{HF} at the nucleus of the central Co atom, the asymmetry of the main line (and to less extent of the satellite lines) can be explained by this effect. However the most probable explanation of the progressive modification of the of the main peak representing pure Co environments in the $Co_{1-x}Mo_x$ layers showed in fig. 3.1.2.1 is that all listed effects are present and contribute consecutively to the observed asymmetric broadening.

To sum up, the observed satellite structure in the ^{59}Co NMR spectra can be, without a doubt, assigned to Co atoms having one (in case of the first satellite) or two (in the case of the second satellite) Mo atoms as NNs. The observed effect of alloying Mo into Co on magnetic properties is stronger than that obtained by Shan [SHA93]. The observed strong effect (highly dependant on Mo concentration [NAW19]) of Mo alien atoms on H_{HF} of Co extends beyond the first coordination shell.

3.2 Epitaxial thin Co (3nm) films grown on various type of buffer (Au or Mo) and capping layer (Au or Mo)

This chapter is based on the ^{59}NMR results obtained by the author of this dissertation, which were published in [WAW17].

Systems where Co is deposited on Mo (110) or Au (111) buffers gained recently attention in terms of their potential use in various spintronic devices. It was shown, that properly designed heterostructures consisting of ferromagnetic Co and non-magnetic Au may have a strong perpendicular magnetic anisotropy (PMA) [GLA14]. The potential of such systems is large, especially that these materials can be important elements of MTJ's which was shown already by Carcia and Zeper [CAR90]. Heterostructures of the Co/Au, Co/Pt, Co/Pd type, characterized by a large perpendicular magnetic anisotropy were also used in the design of MTJ's where the resistivity depends on spin alignment of the two magnetic electrodes separated by an insulating layer [CHA16]. Moreover, Kisielewski et. al showed also that that the PMA in the Co films deposited on an Au buffer is extremely sensitive to the cap layer [KIS02] and for this reason there is a strong need to study and understand the influence of the Au interface on the Co thin films.

At the same time Co/Mo system is considered to be a promising candidate for high-density magnetic recording media and for potential applications in magnetic sensors due to its high magnetic anisotropy energy, magnetization saturation (M_S), and low coercivity (H_C). More importantly, a recent extensive study has been initiated towards using Co/Mo/Co three-layer irradiated by Ga [WAW17n] and lighter ions such as Ne or Ar [WAW18] for fabrication of a double-layer magnonic crystals, demonstrating periodical modulation of magnetization and the interlayer coupling strength in a scale of several dozen nanometers. The body centred cubic structure of Mo is appropriate for growth of Co thin film due to its high surface energy and low inter-diffusion resulting in a reasonably chemically sharp Co/Mo interface. It was recently shown that in the Co layer deposited on the Mo buffer a well-developed two-fold in-plane magnetic anisotropy occurs [WAW17] which is a result of the growth of Co on the Mo (110) buffer. Moreover, in the Mo thickness range between 0,5 and 1,0 nm the

interlayer coupling of magnetization is antiparallel. It has been shown that ion beam irradiation changes the interlayer coupling character and causes a gradual suppression of the ferromagnetic properties.

In this chapter are presented the results of ^{59}Co NMR study of epitaxial Co thin films with different types of buffer and capping layer (Mo and Au). These samples were investigated in order to acquire the knowledge about the actual impact of the upper and lower interface on the structural and magnetic properties of the Co layer, depending on the nature of the metal forming the second layer.

Fig. 3.2.1 depicts ^{59}Co NMR spectra registered for Co thin films in four different configurations of capping or buffer layer - Mo/Co/Mo, Au/Co/Au, Au/Co/Mo and Mo/Co/Au. The positions of main peaks are in 222 - 229 MHz frequency range which is far above the frequency of face centered cubic Co (in bulk fcc-Co the NMR frequency extrapolated to 0 K is 217,6 MHz [POR61]) and is characteristic for hexagonal Co. For this thickness the uniaxial anisotropy is overcome by the shape anisotropy and in-plane magnetization orientation is expected. Therefore hyperfine field anisotropy should not be a factor determining the NMR frequency of hcp-Co. Every deviation from ideal structure influences the H_{HF} and therefore shifts the NMR resonance frequency. The actual Co NMR resonance frequency in such thin layers (d_{Co} = 3nm) depends highly on the type of a buffer and a capping layer and hence it depends from a combination of several factors such as occurrence of additional strains, dislocations or local enhancement of magnetic moment of Co atoms (which was theoretically predicted for very thin Co layers grown on Au buffer [WAL12]). Spectra analysis performed using fitting procedure [BUB00] and presented in fig. 3.2.1 shows a dominant contribution from the hcp-Co environments with the minor contribution from the fcc-phase as well as from Co atoms located at the grain boundaries. Spectra recorded for Au/Co/Mo and Mo/Co/Au also have a minor contribution from the defected fcc-Co phase which derives primarily from the accumulation of fcc stacking faults in the hcp-Co phase.

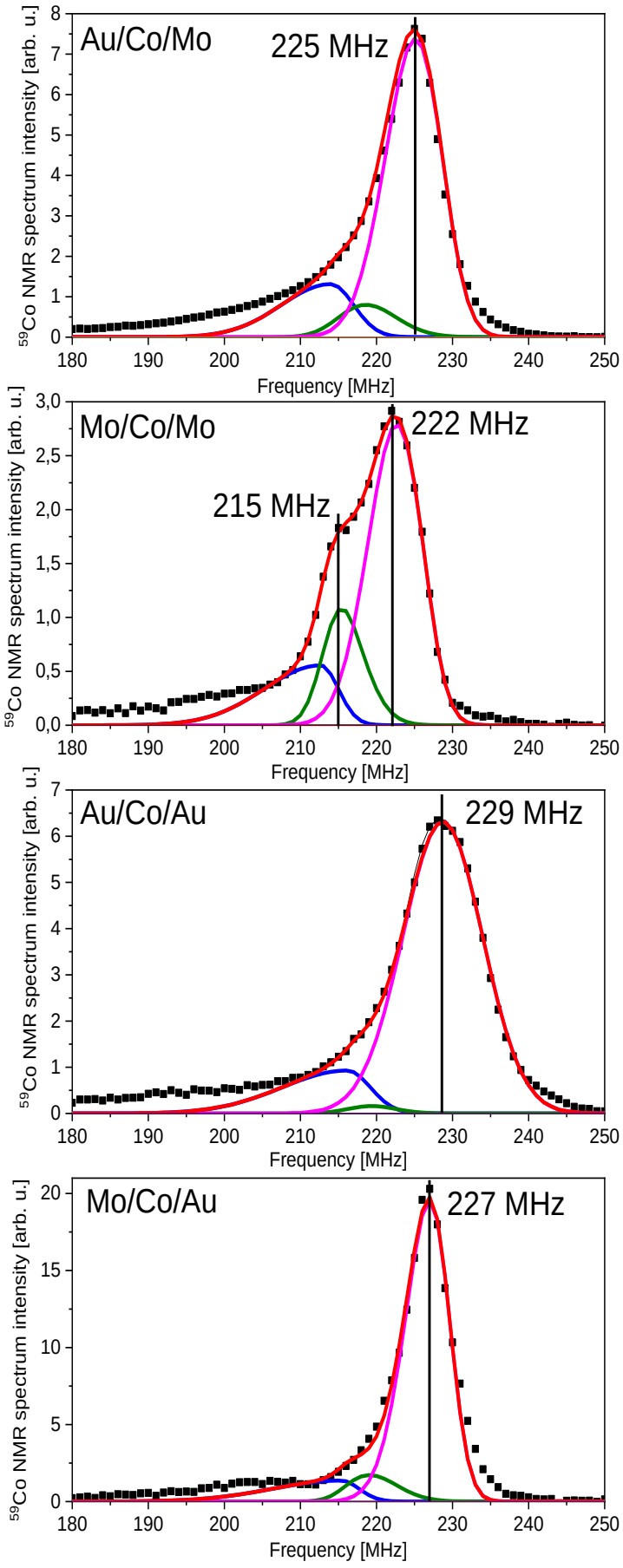

Fig. 3.2.1 ^{59}Co NMR spectra obtained for Mo/Co/Mo, Au/Co/Au, Au/Co/Mo and Mo/Co/Au samples. Black dots represent experimental data, magenta line represents hcp-Co phase, green fcc-Co and blue are the grain boundaries.

The structure of Co layer in Au/Co/Au thin film is rather homogeneous and lacks the fcc-Co phase. At the same time, the component originating from the grain boundaries is not very much exposed in relation to the whole spectrum. However, the NMR resonance frequency is shifted towards higher frequencies (229 MHz). This effect is associated with growth of Co on Au(111) buffer and very thin layer thickness (d_{Co} = 3 nm). A similar effect was observed for the Au/Co(d ≤ 3nm)/Au heterostructures described in chapter 3.3 and its possible origin is discussed in more detail in chapter 3.3.1.

In the case of Mo/Co/Mo thin film, the structure of Co layer is clearly multiphase and consists of the located at 222 MHz which represents the heavily defected hcp-Co phase with a large amount of fcc stacking faults in hcp-Co phase, fcc-Co hump located at 215,5 MHz, and large amount of grain boundaries located at ~210 MHz. However, the amount of fcc-Co phase is still minor in comparison to the hcp-Co. Despite the fact, that Co structure grows irregularly and defected on Mo buffer, which is especially visible in NMR spectrum from Mo/Co/Mo sample in the large contribution from fcc-Co phase and stacking faults, this effect is not so noticeable in Mo/Co/Au thin film in which hcp-Co resonance frequency is close to bulk Co (227 MHz). Moreover, the Co layer in Au/Co/Au and Mo/Co/Au samples seems to have better and more homogeneous crystalline structure (very low contribution from the defected fcc-Co part and moderate contribution stacking faults in contrast to Mo/Co/Mo and Au/Co/Mo thin films). This phenomenon may be explained by the introduction of strain by the Au capping layer which forces deep ordering of the crystalline structure of the Co layer.

In conclusion, in the case of samples grown on an Au buffer, a better crystal structure of Co can be noticed (and this effect is most strongly observed in the case of Au/Co/Au thin film). On the other hand, growth of Co on the Mo buffer or the addition of the Co/Mo interface in general causes the degradation of the Co crystal structure and generation of large amount of fcc-type in hcp phase (as well as within the grain boundaries) stacking faults resulting in (with a sufficiently large accumulation) the formation of the fcc-Co phase. This in turn leads to the lowering of the resonance frequency to 222 MHz in the case of Mo/Co/Mo sample. The use of Au as a capping layer has a positive effect on the structure of the Co layer, making it more uniform and well-defined.

3.3 Epitaxial Au/Co(1,5 - 10 nm)/Au heterostructures

In the past years there have been numerous publications which gave information regarding growth, structural and magnetic properties of Au/Co/Au systems (e.g. epitaxial growth of Au/Co/Au layers studied by TEM [ARD97], [SCH92]; epitaxial growth of Co films on Au(111) studied by STM [VOI91] and GISAXS [LER08]; growth of Co/Au multilayers studied by TEM and HREM [KEH00] as a function of Co layer thickness; ultra-thin Au/Co(d_{Co} = 0 – 7 nm)/Au trilayers layers studied with a combination of in situ electron diffraction, AFM and x-ray scattering [KUM07], Au/Co/Au heterostructures with varying Co layer thickness [KUR07], [GLA14]). Role of Co/Au interface in Au/ Co/Au/MgO/Au heterostructures was investigated by Gladczuk et. all. [GLA14] and Haag et. al. [HAA16] which reported how important is a structure of a Co/Au interface in terms of the structural and magnetic properties of the Co film. However there are yet unsolved or only partly solved issues in the case of thin and ultra-thin Au/Co/Au heterostructures, like the actual role of the Au/Co interfaces and Co layer thickness on the magnetic and structural properties of these systems. Such systems are extremely interesting to study because of the interface effects arising due to the interface sharpness, roughness or strain induced to their crystallographic structure which is caused by the mean lattice mismatch (14%) between Co and Au [ARD97]. Moreover, interface defects can act as pinning centers for domain walls, which modify mechanisms of magnetization reversal.

Occasional NMR experiments on systems containing Co/Au(111) interface were performed, however the case of the Co/Au interface and the dependence of structural properties from d_{Co} weren't investigated there [CES89], [BUB00]. Moreover the growth method and conditions were different than for the samples presented in this dissertation (great importance of growth characteristics was shown by Kingetsu and Sakai [KIN93]).

The following chapter presents ^{59}Co nuclear magnetic resonance study of the epitaxial Au/Co(0001)(d_{Co}=1,5-10 nm)/Au(111) heterostructures which reveal that above a certain Co layer thickness d_{Co} = 2,5 nm a visible structural transition to a relaxed hexagonal structure takes place in the entire volume of the Co film. Moreover, hexagonal Co layers with d_{Co} < 3 nm make atomically sharp interface to Au(111)

substrate in major part of the interface. A number of studies on similar Au/Co/Au heterostructures with varying Co layer thickness have already been performed, however with a usage of different techniques [KUR07] [GLA14]. Therefore ^{59}Co NMR study would be a perfect complement to the already existing investigations, bringing (due to its short-range character) additional unique information regarding the growth, structure, phases and magnetic properties of the Co layer.

As mentioned in the earlier part of this chapter (3.2), properly designed Au/Co/Au heterostructures may demonstrate a strong perpendicular magnetic anisotropy [GLA14]. This effect is investigated by many groups and in different types of systems which reported that the magnitude of the PMA in very thin films is strongly influenced by such factors as: their internal structure, thickness, type and quality of the interface (interaction of the atoms at the interface and strains induced by the lattice mismatch between the two layers). However the most important role was ascribed mainly to structural and hybridization effects at the interface. Ab initio electronic band calculations [WAN94] [UJF96] imply that the interface anisotropy originates from the hybridization of the 3d Co and 5d Au orbitals. It influences the electronic bands from Co *d* orbitals that are in the plane of the surface or being perpendicular to it. Differences between the spin-orbit energies for spin parallel and perpendicular to the surface significantly affects the magnetic anisotropy. In the Au/Co/Au heterostructures are present two Au/Co interfaces (up and bottom) which are grown in different conditions. This strongly influences the electronic interaction of Co and Au surface atoms due to the fact that arrangement of the nearest neighbors is not uniform along the interface. [HAM01].

3.3.1 Experimental results

The NMR spectra from the Au/Co/Au samples are presented in fig. 3.3.1.1. Concerning the structural characterization, acquired ^{59}Co NMR spectra demonstrate that Co films mainly consist of a hcp-Co phase which is consistent with the literature data (previous experiments like X-ray diffraction or EXAFS indicate that Co grown on Au(111) buffer have a hcp structure for films thicker than 4 ML [MAR99], [BEL99]).

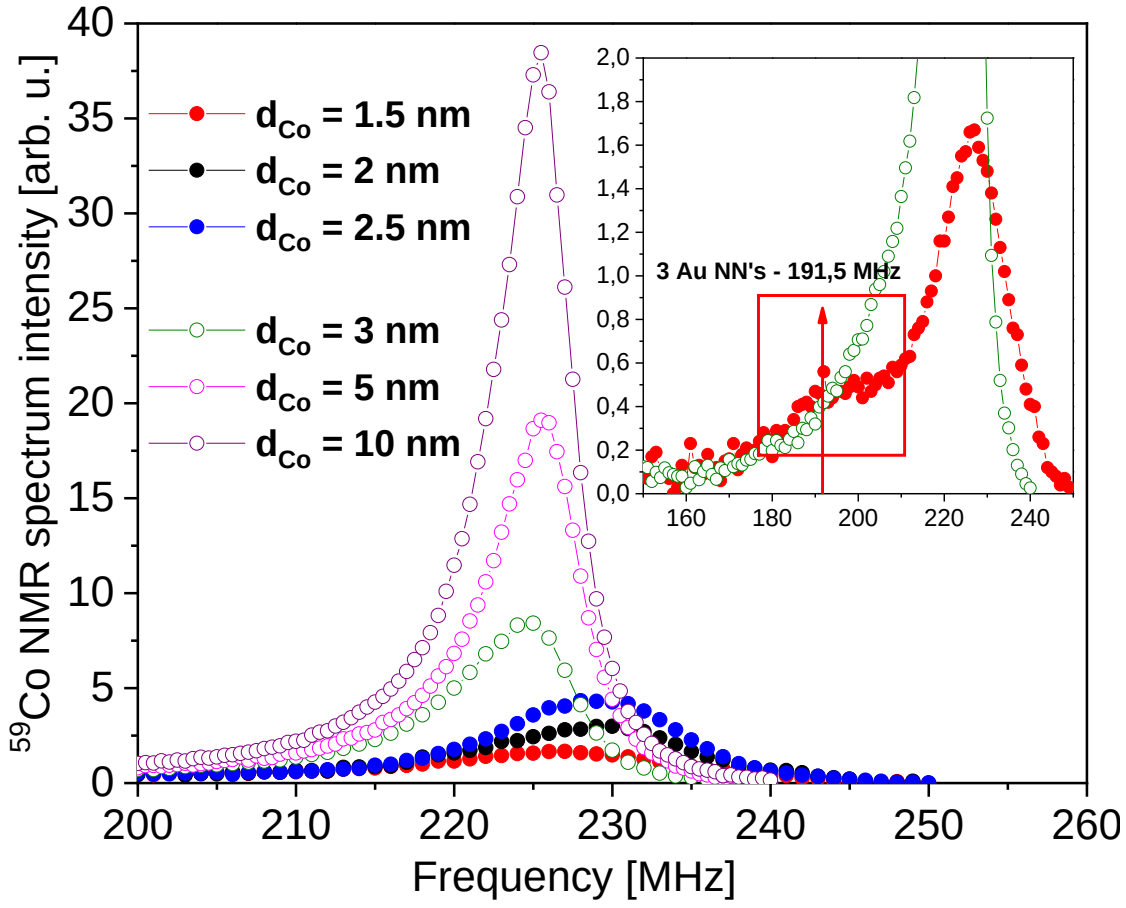

Fig. 3.3.1.1 ^{59}Co NMR spectra recorded at 4.2 K, corresponding to the samples with d_{Co} = 1,5 – 10 nm. For layers with $d_{Co} \geq 3$ nm a structural transition to a relaxed hexagonal structure takes place in the entire volume of the Co film which manifests itself in shift of the NMR frequency towards lower values and (inset) rise of the NMR spectra intensity at 190 - 210 NMR frequency range.

Each spectrum can be divided into two parts: the one originating from crystalline metallic Co, which manifests itself by a broad clearly visible peak in higher frequencies, and the other one originating from the defected or regular hcp-Co structure having nonmagnetic Au NN (interfaces with the Au buffer and capping layer) and defects such as grain boundaries (which may be defined as interface between two grains or crystallites where Co areas are defected, but still it is a ferromagnetic and metallic Co which gives a contribution to the spectrum [CER01, JED04]) which is visible as a long tail extending to the lower frequencies of the spectra. For samples with 3 nm and higher Co thicknesses the NMR line which corresponds to a crystalline hcp-Co is situated at 225,5 MHz. However for samples with $d_{Co} < 3$ nm, Co atoms located inside a bulk of the layer reveal a higher resonance frequency (229 MHz) than that reported for a bulk sample with magnetization in the hexagonal plane. As for the interfacial part of the spectra (< 200 MHz), a characteristic permanent structural fragment can be distinguished which is a reflection of Co atoms which have nonmagnetic NN in their closest surrounding (fig. 3.3.1.1. - inset). Each alien non-magnetic NN shifts down corresponding Co NMR frequency [PAN01], [PAN01n]. Areas characteristic for sharp interface can be distinguished, which is visible in the bump observed at 191,5 MHz in the NMR spectra (for the Co layers with thicknesses ranging from 1,5 nm to 2,5 nm) which most likely originates from the Co atoms in hcp (ABA stacking) in configuration with 9 Co NN (6 in the same plane and 3 in the upper plane) and 3 Au NN (in the lower plane) - fig. 3.3.1.2.

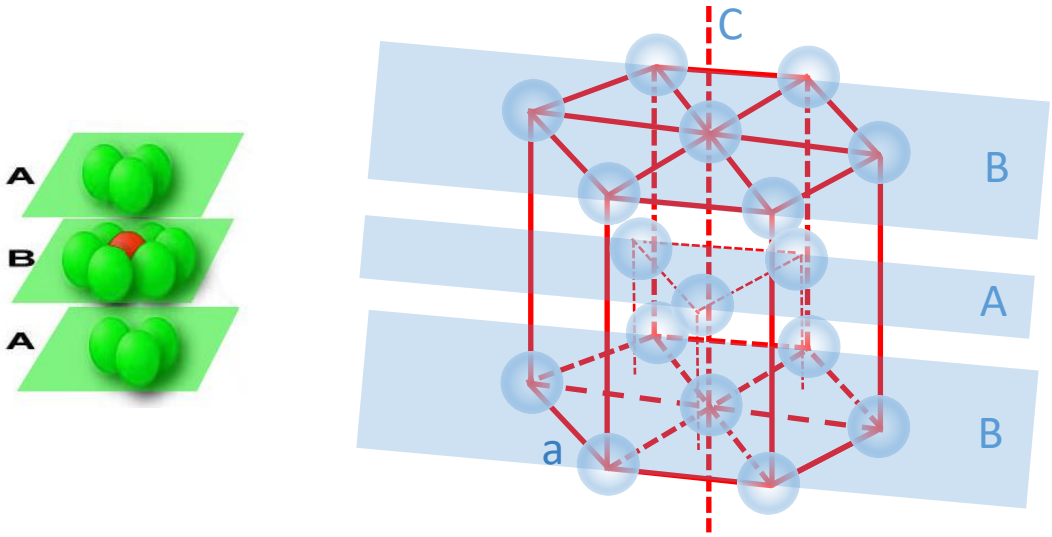

Fig. 3.3.1.2 Due to the fact, that examined Co thin films are epitaxially grown, a sequence of 3 planes can determine the frequency in NMR spectrum.

Assuming that the 191,5 MHz hump reflects hcp-Co in configuration with 9 Co NN and 3 Au NN, and that the frequency spacing $\Delta\nu$ between main hcp-Co line in Au/Co(d_{Co}<3 nm)/Au spectra and subsequent satellites originating from Co with 1, 2 and 3 Au NNs is nearly additive, then the frequency spacing $\Delta\nu$ can be estimated at ~ 12,5 MHz. The value by which one Au NN reduces the H_{HF} around probed ^{59}Co nuclei is obtained from the relation $2\pi\upsilon = \gamma H_{HF}$ ($\gamma/2\pi$ = 10,054 MHz/T) [ALP94], and therefore $\Delta H_{HF} = \Delta\nu/\gamma$ = 12,5 MHz/10,054(MHz/T) = 1,24 T. This value is very similar to the one obtained from 30 nm thick $Co_{0.99}Au_{0.01}$ alloys in which appearance of the satellite structure was associated mainly to the presence of Au in the fcc-Co phase ($\Delta\nu$ = 12,5 MHz).

Recorded ^{59}Co NMR spectra from examined Au/Co/Au heterostructures show unobserved earlier structural transition which takes place in the entire volume of the Co film after increasing the thickness of layer from 2,5 nm to 3 nm (see fig. 3.3.1.1). This modification of the structure includes two main features. First one is a frequency shift of the Co crystalline bulk part to the lower frequencies. An explanation for this phenomenon may be the fact that to a certain layer thickness, Co grows epitaxially on Au(111) in form of polygonal 2 ML high islands which grow laterally with increasing coverage, as was observed by Voigtländer et. al. via STM [VOI91]. It does not form an uniform layer hence, although the magnetization is in the plane, there is most probably

present a demagnetizing field acting on an independent Co islands (similarly as observed in the the case of formed $Ag_{1-x}Co_x$ nanoclusters in annealed $Ag_{1-x}Co_x$ thin films [JED04]) the contribution of which is opposite to the direction of magnetization causing the NMR resonance frequency shift to the higher values. Once a continuous layer is formed at a certain layer thickness (2,5 nm $\leq d_{Co} \leq$ 3 nm [VOI91]) this contribution will disappear and the NMR resonance frequency will take near bulk-like values which is in fully consistent with results presented in this chapter as shown in Fig. 3.3.1.1.

Second feature of the structural rearrangement seen in the NMR spectra recorded for discussed Au/Co/Au heterostructures is an increase of the intensity at 190 – 215 MHz frequencies. This cannot be explained only by lowering of the frequency of the „bulk" part of the spectrum. Various publications ([ARD97], [KUM07], [WAL12]) report that first Co layers at the Co/Au(buffer) interface suffer large isotropic in-plane tensile strains extending over the whole volume of the film which are a result of the 14% Co/Au mean lattice mismatch [DUP90]. The strain is strongest at the first and second Co layer and then it relaxes gradually with Co layer thickness. Rising NMR intensity in the low-frequency part of the NMR spectra is a reflection of the appearance of greater amount of Co atoms having 1 and 2 nonmagnetic Au NN . It can be understood, that at a critical Co layer thickness (2,5 nm < d_{Co} < 3 nm) energetically more favorable becomes partial breaking of the continuity of the Co layer with the buffer and emergence of misfit dislocations. Generation of dislocations at the Co/Au bottom interface as a mechanism of strain release was reported already by Ardhuin [ARD97] and Kumah [KUM07]. The strain at the bottom interface is released not only by dislocations, but also by an incorporation of Au atoms into stressed Co layers (mainly into generated dislocations), especially in the grain boundaries. Such mechanism was proposed by Cagnon et. all. [CAG01]. This mechanism is consistent with ^{59}Co NMR results presented in this chapter and explains the rise of the NMR intensity in the 190-215 frequency range.

The structural transition in the sample is also visible in the restoring fields H_{rest} which were recorded during the ^{59}Co NMR study (fig. 3.3.1.3). Averaged values of H_{rest} are presented in table 3.3.1.1. The Panissod protocol [PAN01n] is used to retrieve the value of the H_{rest} acting on electronic magnetization giving rise to resonance at a given frequency. In thin films one of the reasons which may lead to the H_{rest} increase is a

noticeable amount of defects which pin down the magnetization. Second reason for this matter can be non-uniform/discontinuous crystalline structure of the studied layer - NMR work focusing on Co/Cu multilayers with different d_{Co} [JED98] imply a significant role of the layer structure. The anisotropy of discontinuous Co in form of small grains is larger than that of the continuous layer which is seen in rising H_{rest} for very thin Co layers.

Table 3.3.1.1 Presented averaged values of H_{rest} in the dependence of the rising Co layer thickness clearly indicate higher magnetic stiffness in the case of layers with $d_{Co} < 2,5$ nm than in the case of layers with $d_{Co} > 2,5$ nm. The $d_{Co} = 2,5$ nm layer thickness can be considered as the borderline thickness at which the overall structural transformation of the Co layer occurs.

d_{Co} [nm]	Averaged H_{rest} [Oe]
1,5	393
2	364
2,5	212
3	60
5	49
10	55

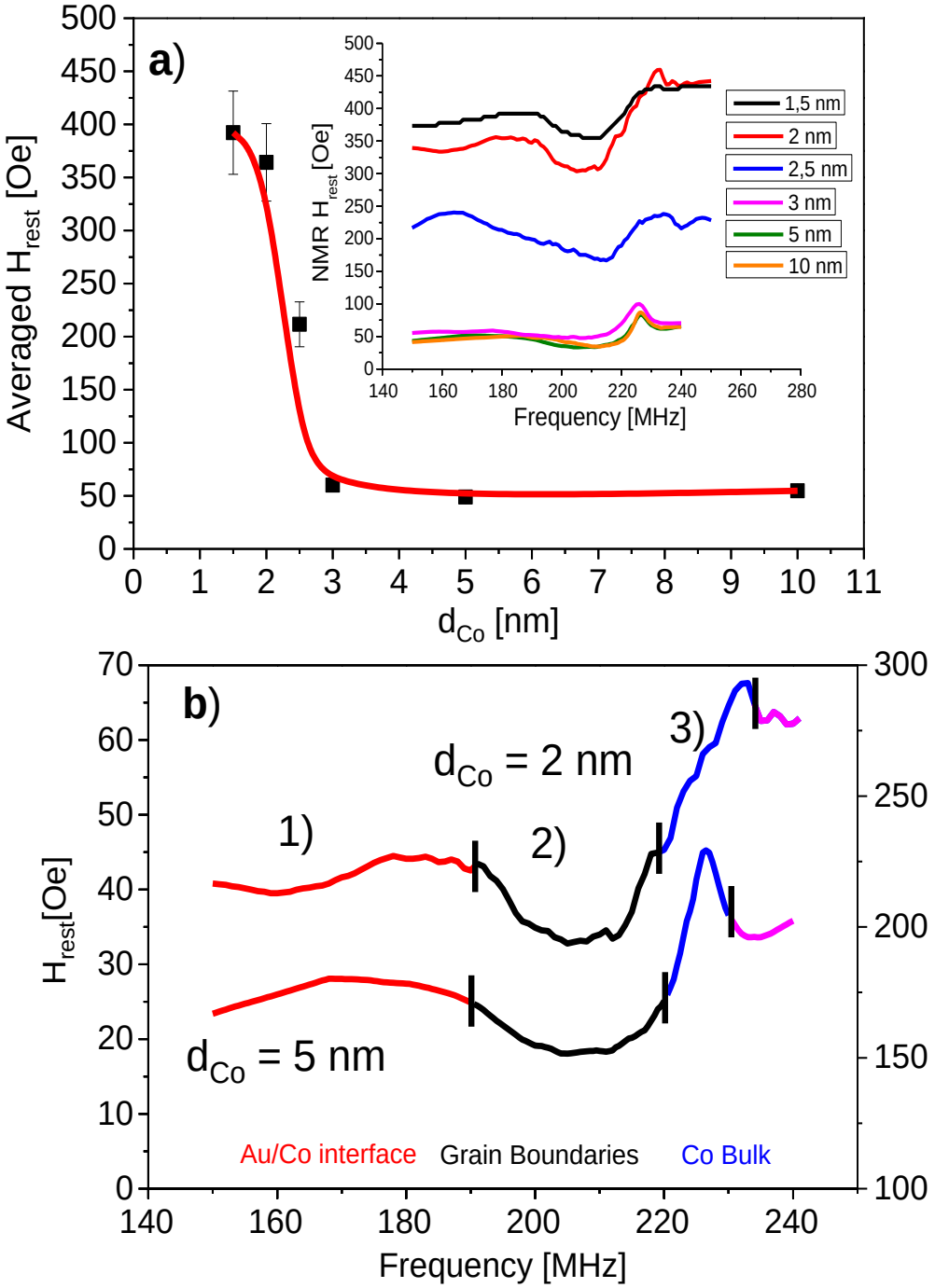

Fig. 3.3.1.3 a) Averaged restoring field as a function of Co layer thickness. Samples with 1,5 – 2,5 nm d_{Co} are distinctly magnetically harder than thicker samples, (inset - dependence of the H_{rest} on the NMR frequency for all samples); b) Dependence of the restoring field on the NMR frequency samples shows, that studied samples are magnetically inhomogeneous. It can be clearly distinguished, that "bulk part" 3) is significantly harder than the Co/Au interfaces 1) (mainly due to hcp-Co structure which is anisotropic) whereas grain boundary areas 2) are magnetically softest – inset shows

H_{rest} for all examined samples. It can be seen that strained samples with 2,5 nm > $d_{Co} \geq$ 1,5 nm have generally a significantly larger values of H_{rest} when comparing to the Co samples with d_{Co} > 2,5 nm. This again suggests an appearance of a structural change in the samples at the point near d_{Co} = 2,5 nm.

It can be noticed from fig. 3.3.1.3 b) that frequencies corresponding to areas of bulk Co are being rather magnetically harder (have higher H_{rest} with maximum near the NMR frequencies of the bulk hcp Co) than Co/Au interface regions (~150-200 MHz) which can suggest, that strains in the Co/Au interface induced by the lattice mismatch have a small influence on H_{rest} and are rather lowering the local magnetic stiffness. At the same time H_{rest} reaches minimum values in the grain boundary regions and small grains (~200-210 MHz) which can be understood, that these areas are having lowered magnetic anisotropy and are magnetically softer than bulk Co and interface areas. Overally enhanced H_{rest} values for thinner samples originate, with a high degree of probability, from discontinuous character of the Co layer. In mentioned earlier work [VOI91] which focuses on the STM examinations of the grown Co ultra-thin films was shown that, in the case of samples with very low thicknesses (d_{Co} < 2,5 nm) the structure maintains its discontinuous granular character. However upon the d_{Co} around 12 ML (~2,4 nm) a granular structure disappears and surface develops to a 10 - 30 nm size terraces. This is reflected in presented here NMR results for samples with 2,5 nm ≥ $d_{Co} \geq$ 1,5 nm in which rise in the H_{rest} values is caused by the discontinuities of the crystalline structure which can be considered as pinning centers of the magnetization. Upon a certain layer thickness (2,5 nm ≥ $d_{Co} \geq$ 1,5 nm) the structure of the sample improves in depth which is obviously reflected in the reduction of H_{rest} values for thicker samples $d_{Co} \geq$ 3 nm.

3.3.2 Modeling of the interfaces

In order to achieve more information from the NMR spectra about the structure of the Co samples, especially in the interface areas, spectra simulations were carried out which were based on a model describing an interface between two chemically different materials (fig. 3.3.2.1).

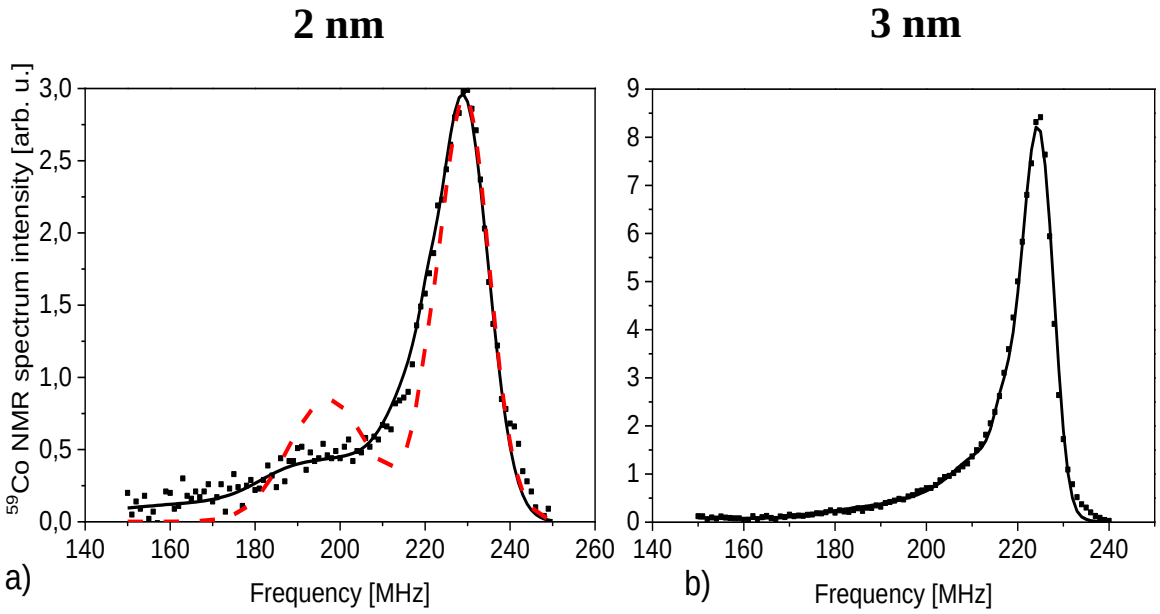

Fig. 3.3.2.1 a) NMR spectrum of 2 nm Co sample fitted with a model describing concentration profile of alien atoms in the Co interfacial layers. Dashed red line represents case where one of the interfaces is sharp in the whole plane and the other one is mixed; straight black line represents the case of asymmetric mixed interfaces; dots represent experimental data. b) NMR spectrum of 3 nm Co sample fitted with the same model as for the 2 nm sample for the case of asymmetric mixed interfaces.

The model assumes that the Co layer structure can be considered as a stack of single monoatomic layers with a dense packing structure arranged in the direction perpendicular to the layer. Consequently it is taken under consideration that each Co atom in hcp(0001) and fcc(111) structure has got 12 NN located at 3 adjacent atomic planes (3 above, 3 below and 6 in the middle like presented in fig. 3.3.1.2). In each of this planes Co atom considered as a central to his 12 NN can have either only Co NN, or

can have a dopant of alien atoms of particular concentration and probability of the occurrence of particular nearest neighbor configuration consisting of 12-n Co atoms and n alien atoms can be described by the binominal law. Those atoms are influencing the H_{HF} and thus cause a change of the ^{59}Co NMR frequency. Assuming fcc (111) stacking (ABC) (or hcp (0001) stacking (ABA)) the probability of finding Co atoms which are surrounded by N nearest-neighbor of the X-type (e.g. Au, Cu or Ni) atoms, in the *ith* atomic layer is given by:

$$P_i(N) = \sum \Phi(n_{i-1};3, p_{i-1}) * \Phi(n_i;6, p_i) * \Phi(n_{i+1};3, p_{i+1})$$

(3.3.2.1)

with the binomial distribution function defined as:

$$\Phi(n; z, p) = \frac{z!}{n!(z-n)!} p^n (1-p)^{z-n}$$

(3.3.2.2)

where p_j is the concentration of X atoms and n_j is the number of nearest neighbor X atoms in the jth atomic layer and the summation is taken for all sets satisfying $N = \sum_{j=i-1}^{j=i+1} n_j$

Line intensity from Co atoms located in the ith atomic layer:

$$S = A * \sum_i (1-p_i) * P_i(N) \qquad \textbf{(3.3.2.3)}$$

The model assumes an existence of pure Co bulk like layer, which is accounted for by an additional line at the frequency and of the intensity corresponding to the layer thickness and its structure (fcc or hcp), and subsequent layers which are considered to be „interface“. In these „interface" layers are present areas of pure Co and Au/Co alloy-like areas with certain Au concentrations. Simulations of the up and down interfaces with the assumption, that in one of the interfaces was a sharp chemical transition

between pure Co layer and pure Au layer in whole plane didn't actually reproduce the experimental data (fig. 3.3.2.1 a) – dashed line). The intensity in the region around 190 MHz frequency in the simulated spectrum was noticeably bigger in comparison to the experimental points which was an argument that such model doesn't work properly. On the other hand, spectral fitting with the assumption that in the samples are two non-identical asymmetrical interfaces, and one interface is mixed while the second one consists of regions where are remains of the sharp interface which are being separated by mixed regions where Co atoms have a varied numbers of Au nearest neighbors, allows to accurately reproduce the experimental data (fig. 3.3.2.1. a) – straight line). This lets to draw a conclusion, that in the Co/Au interface pure Co areas coexist with much bigger ones of cobalt embedded in Au rich, disordered (alloy-like) regions. Averaging over the whole interface area it resembles (and may be treated in this way) a mixed three dimensional Co/Au interface layer with partial fragments of sharp interface and mixed fragments where Co atoms have Au NNs in plane, and can be simulated in this way (fig. 3.3.2.2). Again, this cannot be regarded as a chemically mixed interface, but rather as a very rough and discontinuous Co interface.

In the case of Au/Co/Au thin films with Co layer thicknesses ranging from 1,5 nm to 2,5 nm (based on the conclusions obtained from STM studies on epitaxially grown Co ultra-thin films on Au(111) buffer [VOI91]) there are present most probably two asymmetric interfaces (which results from best matching fitting parameters): the lower one Au/Co 1 ML thick which consists of areas with sharp interface (70%) and areas of half-mixed ($Co_{0.5}Au_{0.5}$) interface (30%) and the upper one which is mixed interface of 2 ML thickness where in first ML (closer to last pure Co layer) is a 15% concentration of Au atoms ($Co_{0.85}Au_{0.15}$) and second ML (closer to last pure Au layer) is a 30% concentration of Au atoms ($Co_{0.70}Au_{0.30}$) - fig. 3.3.2.3. However, samples with $d_{Co} \geq 3$ nm behave in a different way. There is a noticeable shift of the intensity towards lower frequencies which may indicate relaxation happening throughout the system. Another observable thing is rise in the intensity, especially in the 190-205 MHz area, which is most probably caused by three factors: shift in the intensity to the lower frequencies, higher amount of grain boundary regions and change in the interface region, more precisely, migration of Au atoms the Au buffer to the grain boundary regions helping to accommodate the large lattice mismatch at Au(111)/Co(0001) interface, which was postulated in the case of Au/$Co_{1-x}Au_x$/Au thin films discussed in chapter 3.1.1.

Because of this fact, simulations of the interfaces in samples with Co layer thicker than 2,5 nm had to be modified (fig. 3.3.2.4). The mixed Co/Au areas in the lower interface had to be enlarged in the fit. The lower Au/Co interface is 1 ML thick which consists of areas with sharp interface (50% of the total area in th layer) and areas of $Co_{50}Au_{50}$ two dimensional random alloy (50% of the total area in the layer). The upper one (1 ML thick) is mixed in the whole layer where Au alien atoms or vacancies are taking about 57% of the layer area which suggests that upper interface in thicker samples is somewhat more flattened/less mixed. Received data fits very accurately reproduce the experimental data.

The decomposition of ^{59}Co NMR spectra recorded for Co thin films in Au/Co(2nm)/Au and Au/Co(3 nm)/Au systems, with a distinction between up and down interfaces, are presented in fig. 3.3.2.3 and fig. 3.3.2.4 respectively.

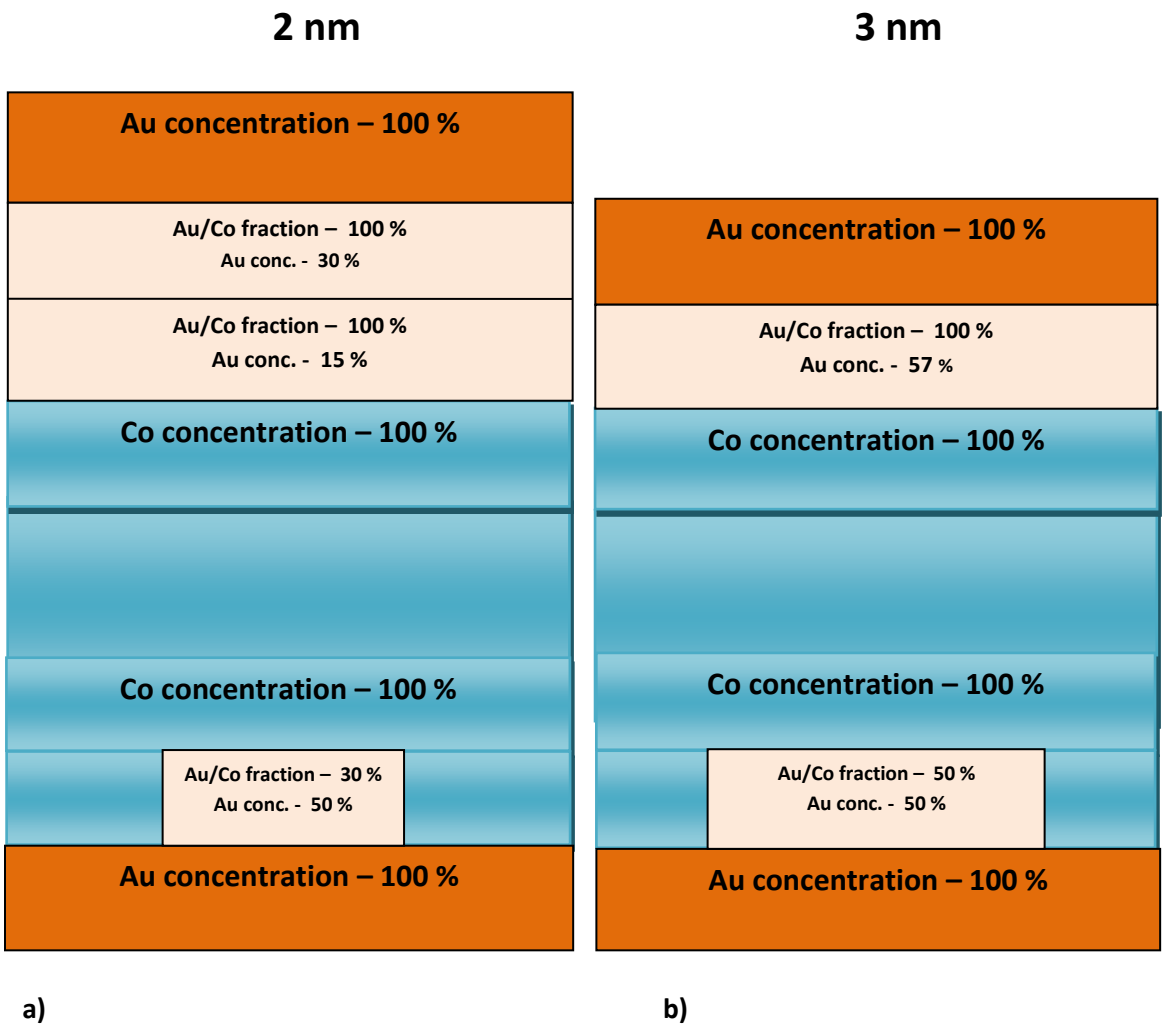

Fig. 3.3.2.2 A schematic of upper and lower interfaces with the concentrations of Au and Co atoms for a) 2 nm thick sample and b) 3 nm thick sample. This is only an averaging over the whole interface. In fact, the interface surface consists of a 1 ML pure Co steps (and in the case of the upper interface of 2 nm Au/Co/Au sample - 2 ML) distributed throughout the interface and which are separated by areas of Co atoms having Au NN.

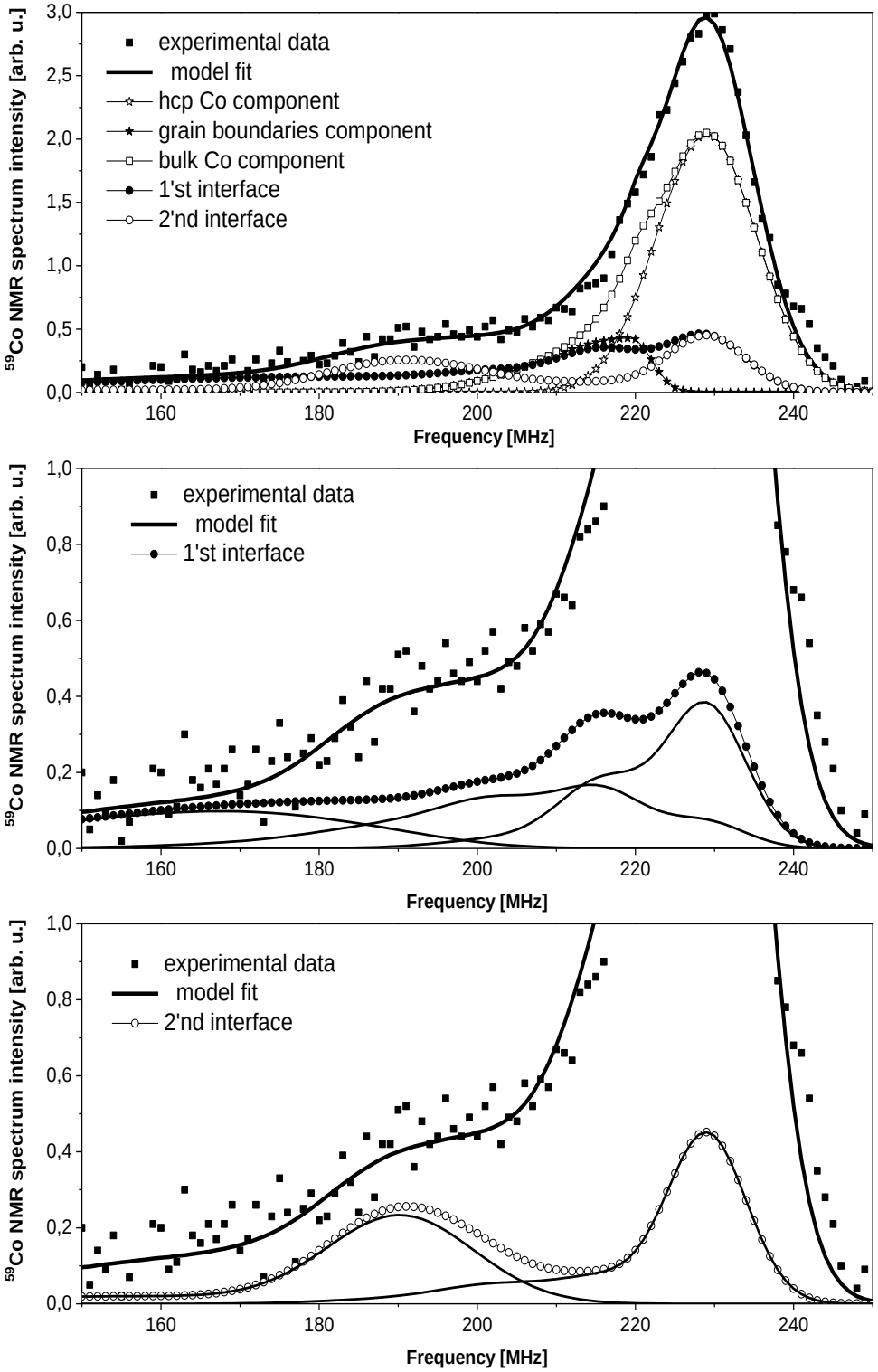

Fig. 3.3.2.3 (up) The deconvolution of ^{59}Co NMR spectra recorded for Au/Co(2 nm)/Au thin film into components representing "bulk" hcp-Co part of the sample, grain boundaries and asymmetric Co/Au interfaces; (in the middle) Au/Co interface between Au substrate and Co layer contribution where are shown: contribution from the last bulk pure Co layer and from interface layer consisting of pure Co patches (70% of the layer area - sharp Au/Co interface) and patches build of $Co_{50}Au_{50}$ two dimensional random

alloy (30% of the layer area); (in the bottom) Co/Au interface between Co layer and Au capping layer showing the contribution from the last bulk pure Co ML and the mixed 2 ML interface build from two dimensional $Co_{85}Au_{15}$ random alloys.

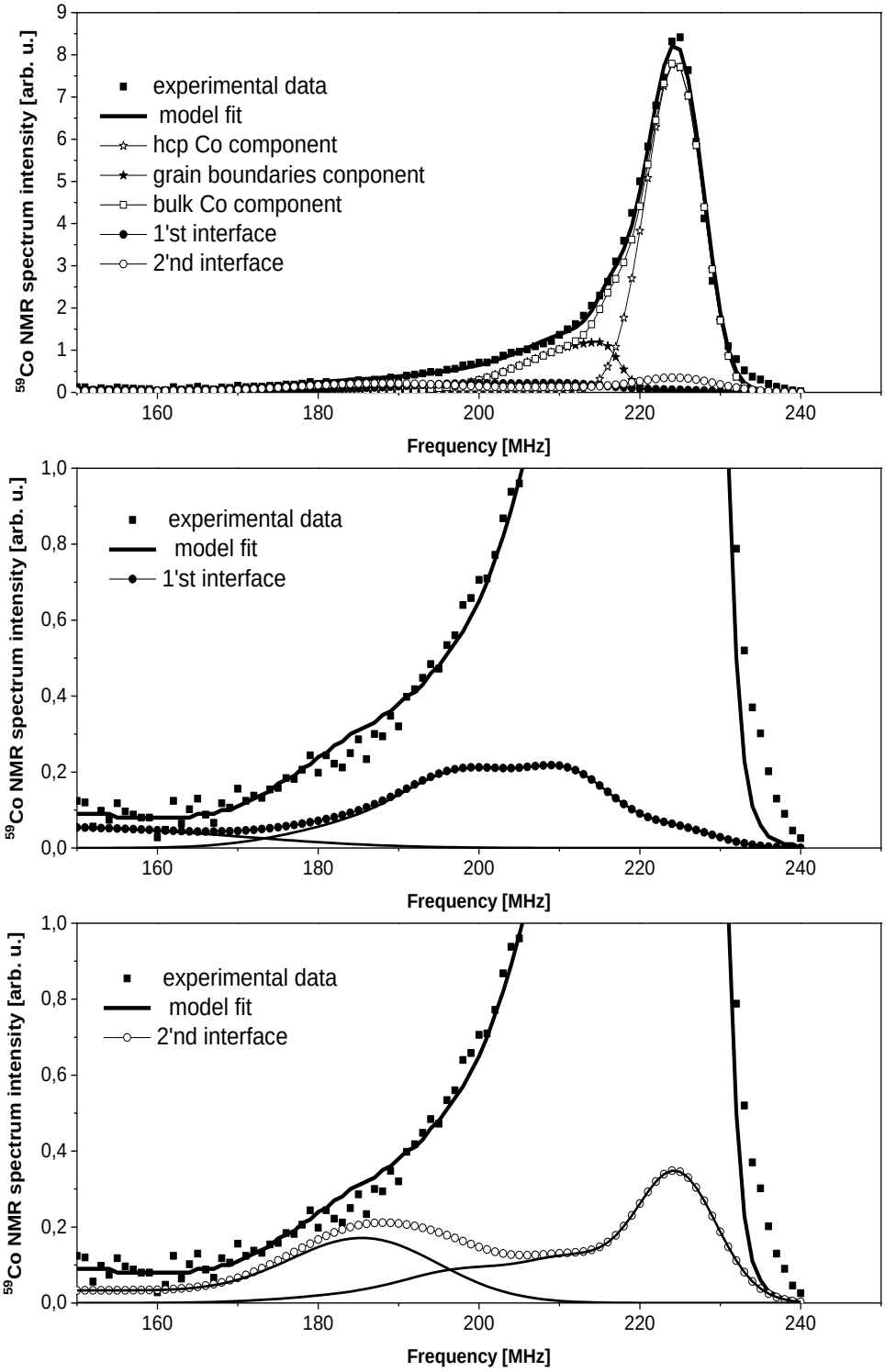

Fig. 3.3.2.4 (up) The deconvolution of ^{59}Co NMR spectra recorded for Au/Co(3 nm)/Au thin film into components representing "bulk" hcp-Co part of the sample, grain

boundaries and asymmetric Co/Au interfaces; (in the middle) Au/Co interface between Au substrate and Co thin film contribution where are shown: contribution from the last bulk pure Co monolayer and from interface layer consisting of pure Co patches (50% of the layer area) and patches build of $Co_{50}Au_{50}$ two dimensional random alloy (50% of the layer area - sharp Au/Co interface); (in the bottom) Co/Au interface between Co and Au capping layer showing the contribution from the last bulk pure Co monolayer and the mixed interface layer build from two dimensional $Co_{43}Au_{57}$ random alloy.

Data acquired from the spectra simulations also indicate, that rising intensity in low-frequency part of the spectra for Co samples thicker than 2,5 nm is caused not only by the shift in the intensity, but also by the increasing amount of grain boundaries (fig. 3.3.2.5).

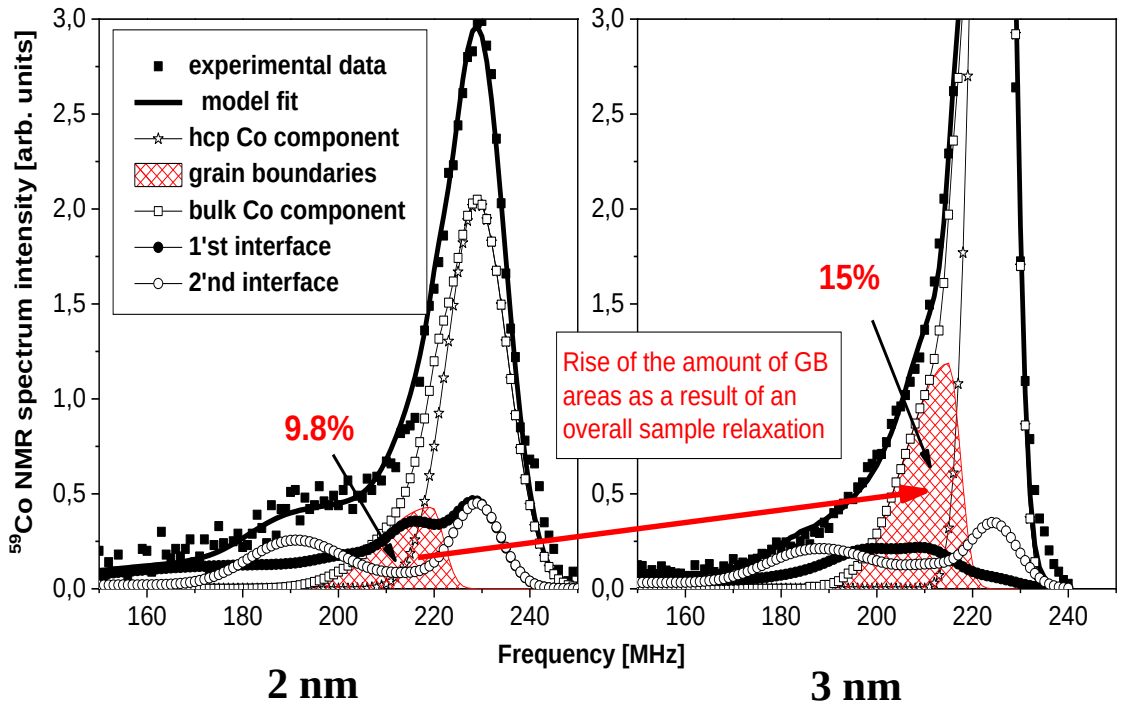

Fig. 3.3.2.5 NMR spectra of 2 nm (left) and 3 nm (right) thick Co samples fitted with a model describing profile of concentration of alien atoms in the Co interface layers. The black-white striped area illustrates the component corresponding for the grain boundaries

In the case of 3 nm thick Co sample the component corresponding to grain boundaries takes about 15% of the whole spectra intensity while in the case of 2 nm thick sample it takes only 9,8% of the whole spectra intensity. This may be explained by the fact, that after certain Co thickness, the Co areas are starting to relax and merge into bigger terraces of about 2 ML height. Observable discontinuous area becomes quasi-continuous and “empty” areas are being filled with Au atoms.

3.4 Oxygen implanted polycrystalline Co(30nm) thin films

The last part of the chapter regarding the NMR results on Co thin films I have devoted to the NMR measurements on polycrystalline Co thin films implanted with oxygen ions in order to create CoO antiferromagnetic compound (AF) and to induce the exchange bias effect. Thin films with EB are currently frequently studied due to their wide technological applications [NOG99], [NOG05], [PAR99]. Exchange bias effect is used in spintronic devices, such as magnetic read heads of hard disk drives [NOG99], [NOG05] or magneto-resistive memories (MRAM) [PAR99]. Because of this fact it plays an important role in modern computer technology. Nowadays, one of best known EB systems consists of ferromagnetic cobalt and antiferromagnetic cobalt oxide created through Co surface oxidation. However, since surface oxidation is a self-limiting process, it results in an oxide thickness of only a few nm, which forms a single interface between Co and CoO [GRU00]. But recently, an oxygen ion implantation was introduced as an alternative technique to form CoO embedded in entire volume of ferromagnetic material [DEM10] (e.g. in the interior of a thin ferromagnetic film). It has been shown that implantation of oxygen ions into thin Co films locally induces the formation of antiferromagnetic cobalt oxides giving rise to exchange bias phenomena. Whereas ion irradiation has been previously used to structurally and magnetically modify magnetic materials at the nanoscale [FAS08], this approach yields a new application for ion implantation. In contrast to Co/CoO bilayers, which exhibit a single planar AFM/FM interface, it has been expected that oxygen ion implantation would result in multiple AFM/FM interfaces (i.e. more granular-like) distributed throughout the most of the volume of the layer [DEM11] which in turn would lead to an enhanced exchange bias properties for a given thickness of the Co layer [DEM11, DEM12] and to critical changes in properties, such as the magnetic reversal mechanism [DEM10]. Moreover, it has been shown that, using a single-energy ion implantation approach, a uniform oxygen distribution profile in the Co layer can be acquired [MEN13] thus leading to further enhancement of exchange bias properties in comparison to AFM/FM bilayers or oxygen-implanted FM layers with Gaussian-like inhomogeneous oxygen depth distribution (improved loop homogeneity, enhanced exchange-coupling magnitude, increased blocking temperature). Due to the fact, that EB effect is being

induced with oxygen ion implantation it is adequate to ask a question about the behavior of such granular systems under thermal-activation effects. This was another of the problems in which I managed to gain insight into during my work under this PhD thesis. Menéndes et. al. [MEN14] has suggested that oxygen ions spread mainly throughout the Co sample in the grain boundaries, tend to diffuse to the Co/Au interface areas due to the annealing treatment. This would be caused by thermal activation effects which lead to pronounced separation of Co and oxygen and, consequently, migration of oxygen.

Since characteristic properties of oxygen-implanted Co systems may significantly differ from those of superficially oxidised Co/CoO bilayers, it was the aim of my work to investigate it. In this chapter I present a detailed NMR analysis of the role of implantation process, as well of the role of annealing treatment in the EB properties of oxygen-implanted Co thin films with a uniform oxygen-depth profile. The purpose of this study is to understand, by means of NMR, the actual impact of oxygen ion implantation on Co polycrystalline ferromagnetic thin films (its role in modifying the structural and magnetic properties) and to verify the actual influence of annealing treatment on magnetic and structural properties of already implanted Au/Co/Au samples.

3.4.1 Exchange bias effect

This section will briefly present the phenomenological description of the exchange bias (EB) effect. EB effect was first observed W. H. Meiklejohn and C. P. Bean in 1956 in surface-oxidized Co particles which were accidentally cooled in a magnetic field far below Néel temperature T_N of CoO [MEI56]. They observed shift and broadening of the hysteresis loop with respect to the one obtained after cooling without magnetic field. At first, this phenomenon was called *unidirectional anisotropy*. However, in order to underline the origin from the interfacial exchange interaction between a ferromagnetic (FM) and antiferromagnetic (AFM) material (uncompensated spins AFM at the interface [GöK01]) which results in a preferential direction for the ferromagnetic spins, nowadays it is named *exchange anisotropy*. When the first monolayer of the AFM aligns with the FM and the subsequent monolayers of the AFM order antiparallel with each other we are dealing with uncompensated interface fig. 3.4.1.1. a). However, antiparallel spin alignment within a monolayer characterizes compensated interface at which the effect of spins pinning the FM layer is canceled giving rise to a net zero H_{EB} fig. 3.4.1.1. b). Occurrence of a compensated or uncompensated interface depends on the characteristic AFM and the crystalline directions. For example, CoO exhibits a compensated interface for epitaxial [100] and [110] layers and an uncompensated interface structure for epitaxial [111] and polycrystalline [111] layers.

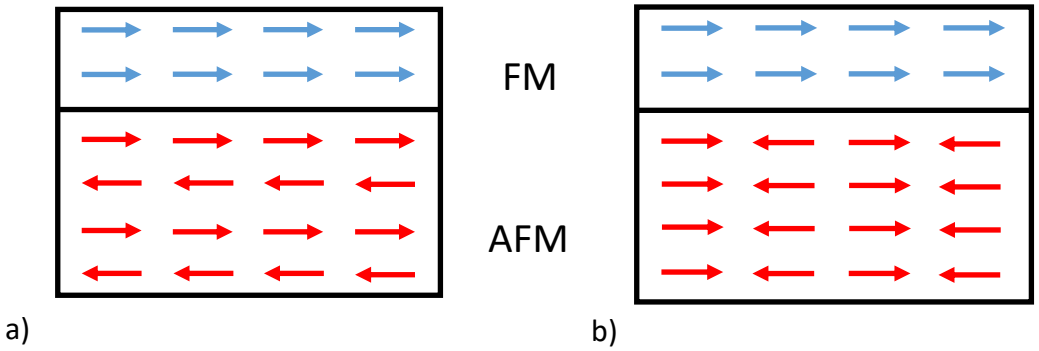

Fig. 3.4.1.1 Schematic representation of a) an uncompensated FM/AFM interface and (b) a compensated FM/AFM interface.

Various theoretical models have been proposed over the years, trying to explain certain aspects of this phenomenon [NOG05, NOG99, RAD07, MAL88, BER99, STA00, KIW01], however none of them fully describes the complicated nature of this effect. Meiklejohn and Bean proposed an intuitive model explaining FM/AFM coupling and resulting exchange bias effect. This model is schematically shown in Fig. 3.4.1.2.

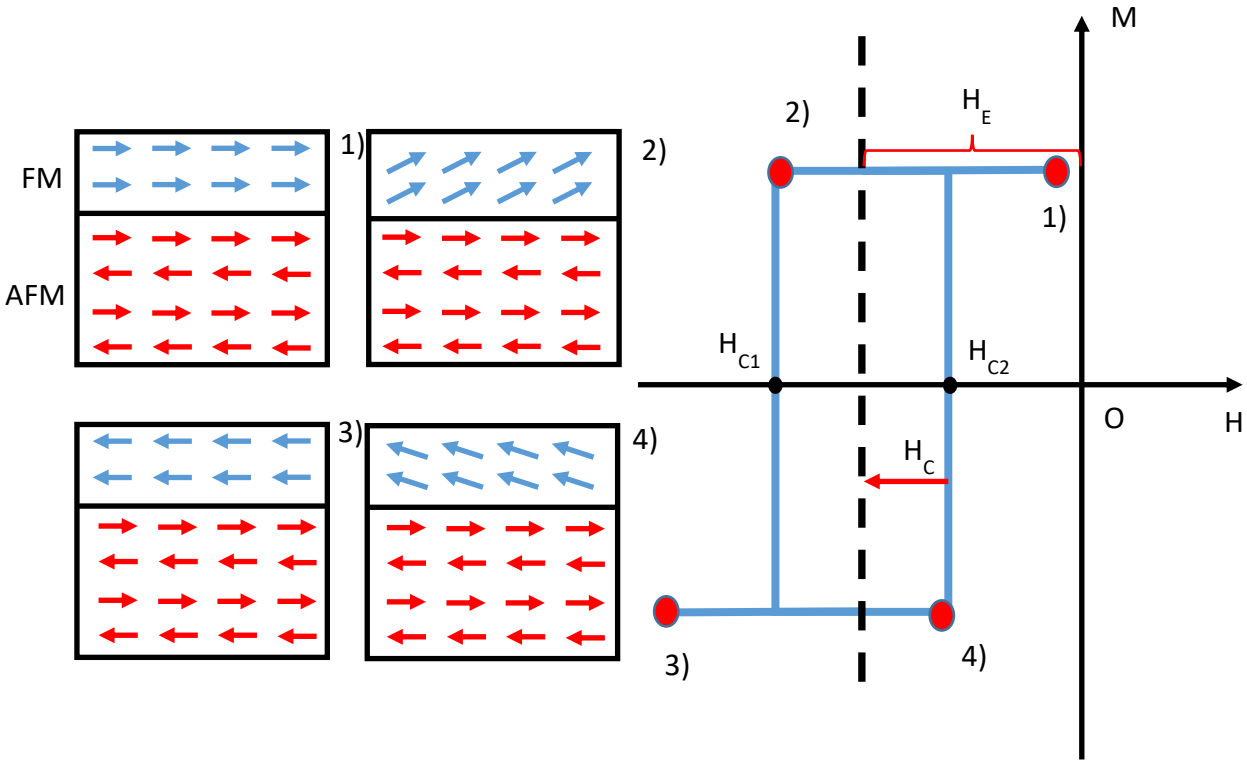

Fig. 3.4.1.2 Schematic representation of the intuitive model for EB proposed by Meiklejohn and Bean. 1) When the system is cooled below Néel temperature T_N in an external magnetic field, in an uncompensated FM/AFM interface, a ferromagnetic coupling originates at the interface between the FM and the first monolayer of the AFM. 2) Reversal of the external magnetic field causes the reorientation of FM spins. At the same time the AFM spins will not reorient due to the strong AFM anisotropy. However, because of the coupling at the interface they will exert a torque on the FM spins. 3) Due to the the torque on the FM spins, a higher magnetic field has to be applied in order to overcome the FM/AFM coupling and to saturate the spins in the direction opposite to the FC direction, which thus results in the shift of the hysteresis loop towards negative fields. 4) Reversal of the magnetic field back to the initial field direction causes the FM spins to rotate with the aid of the internal field of the FM-AFM coupling. The FM spins will then align with the external magnetic field at lower fields.

Two effects characteristic for EB, shift and a broadening of the hysteresis loop of the FM, can be expressed with two quantities, the *exchange bias shift* and the *coercivity*:

$$H_E = \frac{1}{2}(H_{C2} + H_{C1})$$

$$H_C = \frac{1}{2}(H_{C2} - H_{C1}) \qquad \textbf{(3.4.1.1)}$$

where H_{C1} and H_{C2} are the coercive fields of the descending and ascending branches of the hysteresis loop, respectively. H_E is zero in the absence of EB and H_C increases after the induction of EB. The shift of the hysteresis loop is in the opposite direction to the external field direction according to model proposed by Meiklejohn and Bean (however, EB shifts in the direction of the external magnetic field have been observed in FeF_2/Fe bilayers [NOG96]).

3.4.2 Experimental results

Figure 3.4.2.1 a) shows the NMR spectrum recorded for the non-implanted Au/Co(30nm)/Au thin film. It consists of two main components: the one originating from the bulk pure Co areas seen in the spectrum as high-frequency peaks reflecting fcc and hcp crystalline Co phases and stacking faults (> 210 MHz), and a low-frequency part (< 210 MHz) originating from the Co areas with highly distorted lattice symmetry, Co atoms having nonmagnetic NN and grain boundary areas. In order to obtain a quantitative information about the phase content the deconvolution of the ^{59}Co NMR spectrum from an as-deposited non-implanted Au/Co(30nm)/Au thin film has been performed. The illustrated individual spectral components correspond to the structural elements of the layer (fig. 3.4.2.1 a). Blue line reflects the fcc-Co phase (217 MHz) and red highly defected hcp-Co phase (223 MHz). The green line reflects the signal originating from Co atoms located at the grain boundaries. The signal originating from the Co/Au interfaces (< 210 MHz) was fitted by an additional Gauss lines (magenta line) which represent Co atoms in configurations in which one two or three Co NN are replaced by nonmagnetic Au NN.

Figure 3.4.2.1 b) shows the NMR spectra recorded for the oxygen implanted Au/Co/Au thin films (implantation fluence ranging from 0 to 35×10^{16} ions/cm^2). The NMR measurements show that the ion implanted samples exhibit significantly modified structural features. The metallic ferromagnetic Co undergoes a significant structural transformation revealed by several ^{59}Co NMR spectrum modifications. The first modification is the progressive decrease of the spectrum intensity in the high-frequency part of the spectrum (above 216 MHz), corresponding to the well-defined crystalline Co areas. Second modification is the enlargement of the low-frequency part of the NMR spectra, especially at the grain boundaries, extending to lower frequencies. Detailed NMR analysis of these structural features resulting from oxygen implantation will be discussed in the latter part of this chapter.

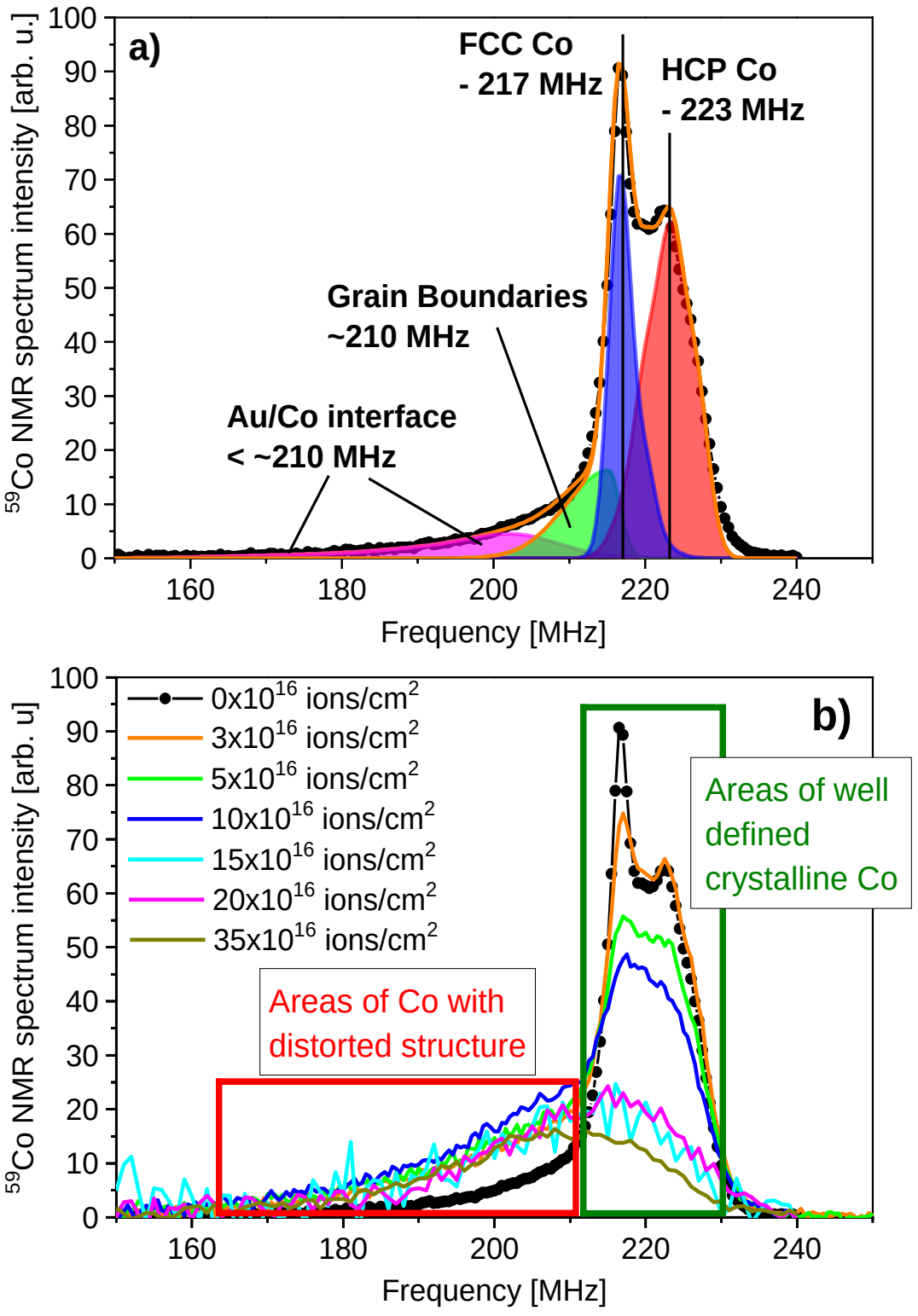

Fig. 3.4.2.1 (a) ^{59}Co NMR spectrum recorded for non-implanted Au/Co/Au sample (black dots correspond to the experimental data, red line represents hcp-Co phase, blue – fcc-Co phase, green – grain boundaries and magenta - Co/Au interface area). (b) ^{59}Co NMR spectra, recorded at 4.2 K, corresponding to the non-implanted sample and

samples implanted with oxygen ions at 3×10^{16}, 5×10^{16}, 1×10^{17}, 2×10^{17} and 3.5×10^{17} ions/cm^2.

The loss of the signal from the crystalline ferromagnetic metallic Co can be linked to two factors. One is of chemical character and it is the formation of Co_xO_y phase which is antiferromagnetic insulator in 4.2 K. Transformation from the ferromagnetic metallic Co to Co^{2+} ionic state characteristic for CoO compound changes the ^{59}Co resonance frequency due to the different electronic state. The second factor responsible for the depletion of the crystalline Co signal is a structural modification in the spots where highly energetic oxygen ions had collisions with Co target nuclei leading to a modified structure extending from a grain-boundary-like regions in ferromagnetic metallic Co to an non crystalline amorphous-like Co structure with strongly damped ferromagnetic properties and progressively lowered ^{59}Co resonance frequency. This transformation is evidenced from an increase of the spectra intensity centred around 210 MHz and extending down to 150 MHz. However, to this spectral range also some contributions from chemical intermixing diminishing ^{59}Co hyperfine field and leading to a lower resonance frequency can be anticipated: an injection of Au atoms from the capping layer into the volume part of the Co sample due to collision with oxygen ions, leading to the enlargement of the upper Co/Au interface area or replacement of Co magnetic nearest neighbors with weakly bound oxygen ions or even atomic voids.

In order to verify which mechanism is responsible for the observed structural changes, additional ^{59}Co NMR studies were carried out in analogous Co samples not capped with Au overlayer but with oxidized Co surface. The ^{59}Co NMR study have shown that, regarding the loss of crystalline order, samples without Au capping behave similarly to those with Au capping layer which unambiguously allowed to verify that Au capping does not play any significant role in the appearance of the low-frequency ^{59}Co NMR signal (Fig. 3.4.2.2). The contribution to the low frequency part of the spectrum from Co:Au mixing caused by oxygen implantation is negligible and structural damage of Co dominates in the low-frequency signal below 210 MHz.

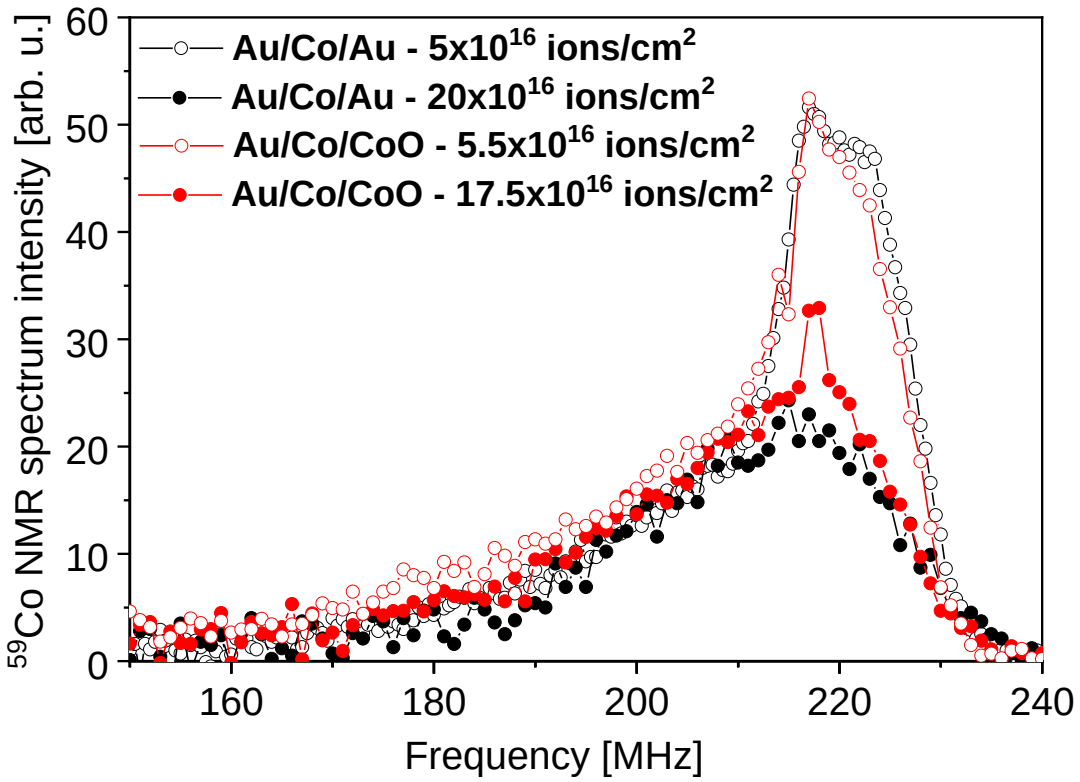

Fig. 3.4.2.2 Comparison of oxygen implanted Au/Co/Au and Au/Co/CoO samples.

Figure 3.4.2.3 presents the structural evolution of thin Au/Co/Au layers with an increasing dose of implanted oxygen ions. Performed ^{59}Co NMR spectra decomposition clearly demonstrate that the relative content of the hcp-Co and fcc-Co phases in the samples remains nearly constant with the increasing implantation fluence. From this it can be concluded that ion implantation in this case does not lead to an allotropic fcc → hcp phase transformation. In addition, as a result of the ion implantation process, an enlarged low-frequency component of the NMR spectrum appears (visible in fig. 3.4.2.3 as a blue area below the frequency of 210 MHz). The low-frequency component arises already at the lowest fluence but the shape of it is established at 5x10^{16} ions/cm^2 fluence and remains almost unaltered at higher implantation fluences (fig. 3.4.2.4).

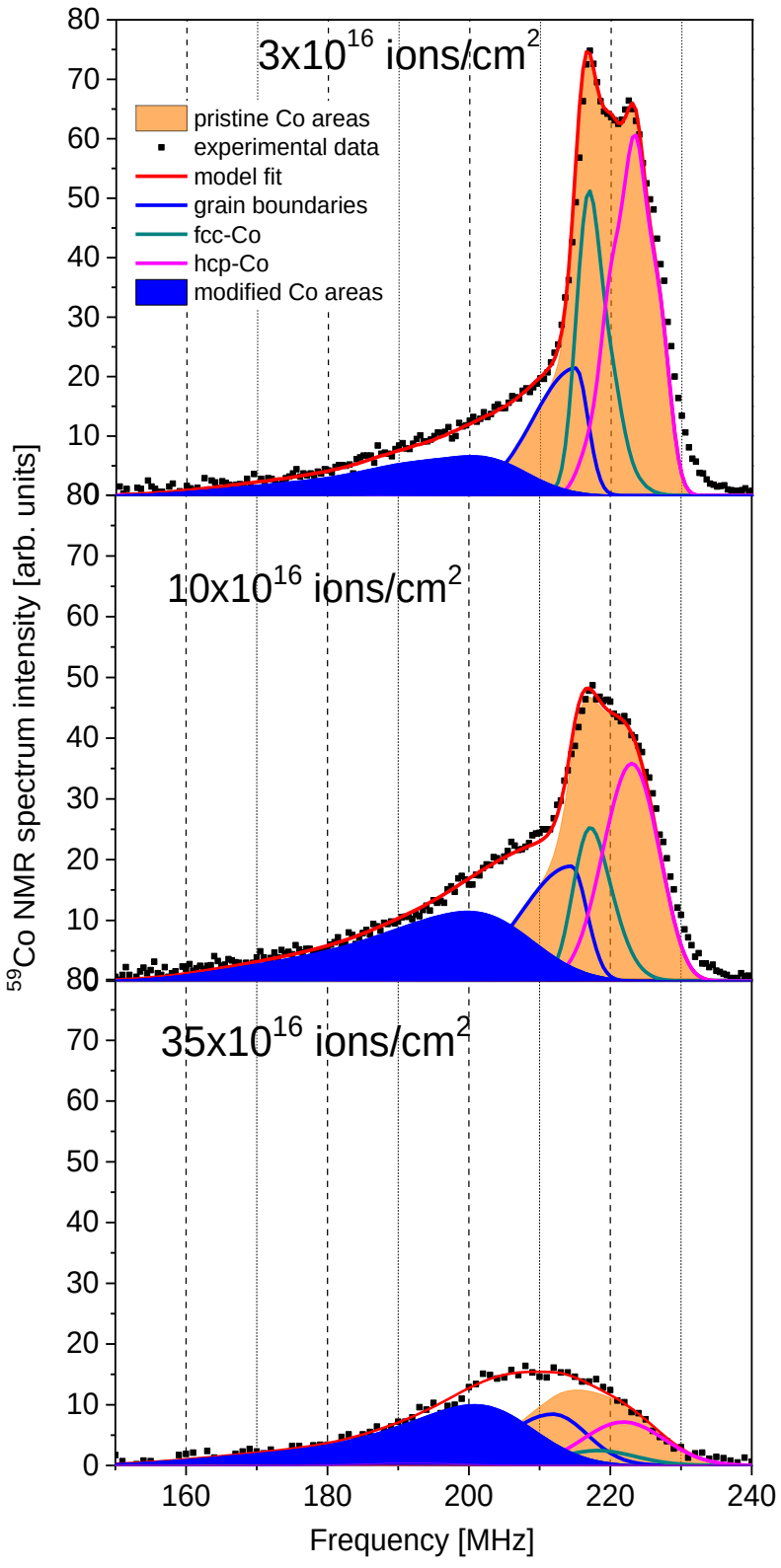

Fig. 3.4.2.3 Evolution of an Au/Co/Au system depending on the dose of implanted oxygen. Orange part represents crystalline, metallic parts of Co layer. Blue part represents areas of Co layer modified by oxygen implantation.

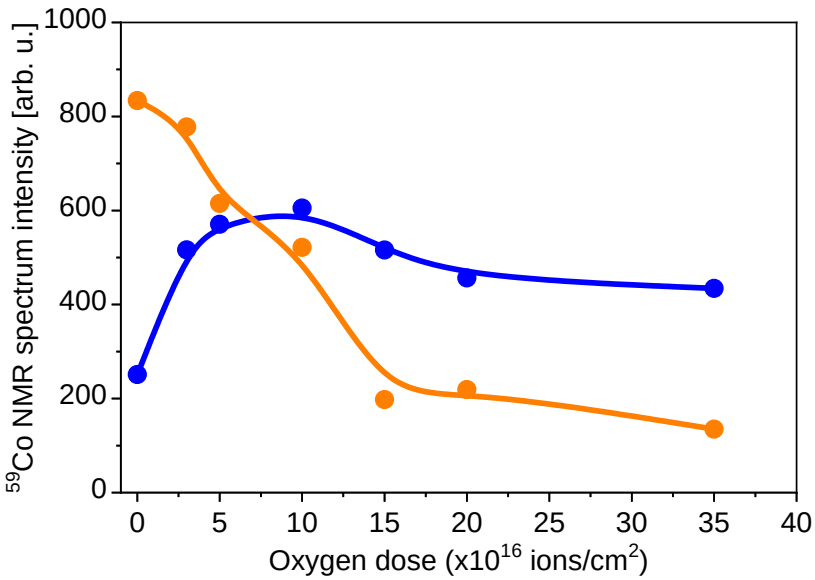

Fig. 3.4.2.4 Intensity dependence of the "bulk" part of the Co layer and areas, modified by implantation, on oxygen dose. Blue dots are representing regions with distorted structure modified by oxygen ion implantation (like grain boundaries, vacancies, Co/Au interfaces); orange dots represent pristine sample areas (crystalline metallic fcc-Co and hcp-Co and grain boundaries); lines are introduced to guide the eye.

The low-frequency component has its maximum close to ~210 MHz frequency which is ascribed to the areas of grain boundaries. The enlargement of the signal at these NMR frequencies indicates the appearance of a great number of regions in which Co closest environment is highly defected due to oxygen implantation and their structure reminds the structure of grain boundaries which divide the large monolithic areas of the non-defected Co into smaller ones. However, an increase of spectrum intensity of the low-frequency part extends also to the lower frequencies, which indicates an increase of Co atoms in a position with non-magnetic NNs or reduced number of NNs shifting down resonance frequency of Co. As shown in the earlier part of this chapter, this effect cannot be assigned to the enlargement of the upper Co/Au interface (thrusting of the Au atoms from the capping layer into the volume part of the Co sample by the implanted oxygen ions). A puzzling phenomenon in the case of the studied implanted Au/Co/Au thin films is that despite gradual decrease of the amount of crystalline metallic and structurally well-defined Co (seen as orange area in fig. 3.4.2.3 and orange points in fig. 3.4.2.4), the low-frequency profile behaves rather independently and remains practically unchanged when applying higher doses of

oxygen (see fig. 3.4.2.4). Therefore, the appearance of the low-frequency component cannot be the only reason of the decrease of the signal reflecting the "bulk" crystalline Co part of the layers.

An additional explanation for this phenomenon is the creation of CoO in the sample. Co^{2+} atoms when forming a chemical bond with oxygen have strongly modified electronic structure in comparison to metallic Co and therefore will have a different resonance frequency which was observed by [OKA77]. Direct observation of ^{59}Co NMR signal from Co^{2+} in Co implanted films have not been carried out systematically since ^{59}Co NMR signal from CoO is hardly observable due to AF structure of CoO. However a dedicated ^{59}Co NMR experiment on Au/Co/Au sample implanted with $1x10^{16}$ ions/cm^2 fluence has shown a very broad (330 – 580 MHz frequency range) ^{59}Co NMR signal in 4.2 K temperature centred around 490 MHz (fig. 3.4.2.5) corresponding to Co^{2+} ions in $Co_{1-x}O_x$ like environment indicating formation of Co oxides due to oxygen implantation. This is a direct proof of the assumption above and a second explanation for the disappearance of the high-frequency signal originating from crystalline part of the Co layer. Recoded resonance frequency is not far from the one reported by Okada and Yasuoka in CoO single crystal in 4.2 K (498 MHz) [OKA77].

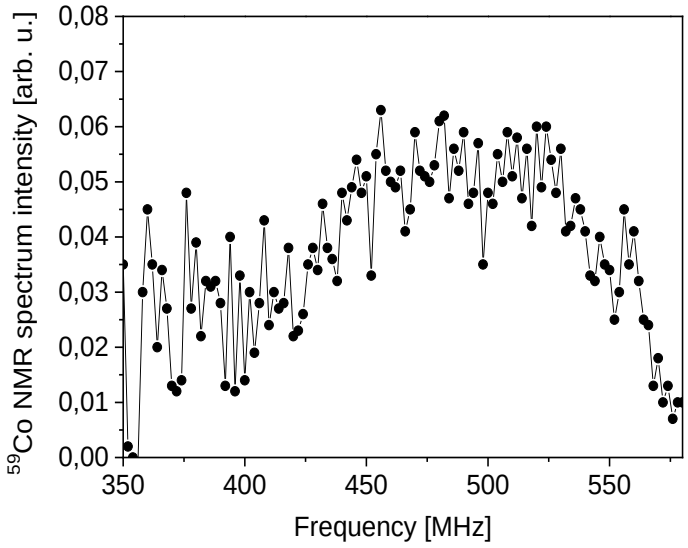

Fig. 3.4.2.5 ^{59}Co NMR spectrum recorded from one of the implanted Au/Co/Au samples ($1x10^{16}$ ions/cm^2 fluence). Signal intensity around 490 MHz is characteristic for Co^{2+} ions in CoO. This confirms a formation of Co oxides (AF in 4.2 K). Black dots are the experimental data and the black lines are just to guide the eye.

Additionally, during a ^{59}Co NMR study of oxygen implanted Au/Co/Au samples also NMR restoring field measurements were performed. The ^{59}Co NMR H_{rest} of the different samples indicates a significant increase of magnetic stiffness at 4.2 K with growing fluence, which confirms a presence of EB caused by AF CoO since this increase of H_{rest} is absent at the temperatures above Néel temperature of CoO (e.g. RT) (Fig. 3.4.2.6).

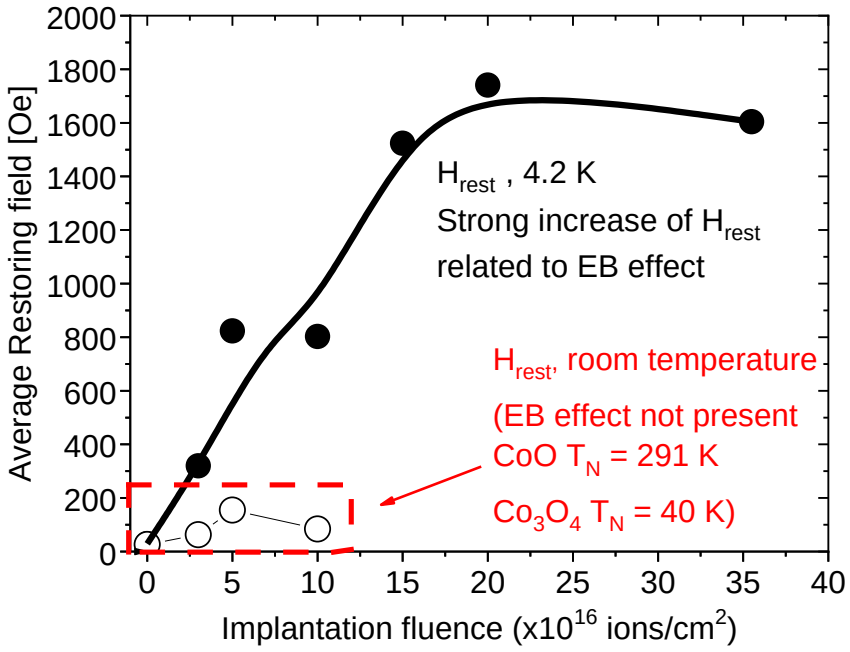

Fig. 3.4.2.6 Formation of CoO is confirmed from a strong increase of H_{rest} in 4.2 K.

In order to verify the hypothesis assuming grain-boundary oxidation mechanism in examined polycrystalline samples, a serie of textured Cu/Co/Au trilayers was prepared which were implanted with similar doses of oxygen ions with similar energies like in the polycrystalline samples. Due to the fact, that textured samples have better crystalline structure than the polycrystalline samples, the amount of grain boundary areas in those samples in significantly lower (8 % of total spectrum intensity). The comparison of ^{59}Co NMR spectra from polycrystalline samples with spectra acquired from textured ones shows (fig. 3.4.2.7) that oxygen implantation of textured layer with similar dose doesn't have exact impact on the structure like in the polycrystalline samples. It can be clearly seen that the spectrum in the frequency range characteristic for grain boundaries

(~210 MHz) undergoes significantly less changes in comparison to polycrystalline sample in which, at similar implantation dose, a rapid increase of the intensity characteristic for Co atoms stacked in the grain boundary areas can be observed. Therefore, a theory of grain-boundary transport of implanted oxygen ions in polycrystalline samples is likely true.

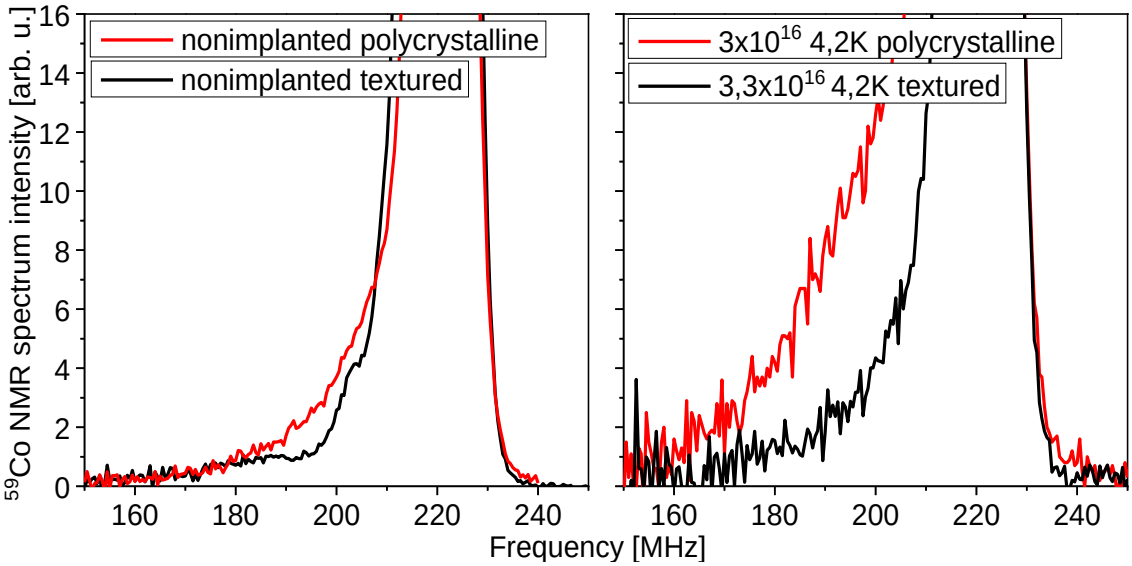

Fig. 3.4.2.7 Comparison of polycrystalline (red lines) and textured (black lines) samples (spectra taken at 4.2 K).

Based on the knowledge obtained from the ^{59}Co NMR study for individual samples, an example pattern of structural changes in the Co layer can be deduced which occurs due to the ion implantation process. Because of the fact that presented in this chapter Au/Co/Au samples are polycrystalline which contain a high amount of grain boundaries (14% of the total ^{59}Co NMR spectrum intensity) implanted oxygen is most likely transported through them where it embeds forming Co_xO_y compounds (Fig. 3.4.2.8 b) as it was reported earlier [DEM11]. With growing implantation fluence the number of grain boundary areas in which CoO is forming is increasing. Already at the lowest fluence the number FM/AFM (Co/CoO) interfaces is rapidly increasing up to the state of near saturation at $10x10^{16}$ ions/cm^2 dose. At larger doses of implanted oxygen the amount of grain boundary areas stay at the almost constant level and at the same time a rapid decrease of well-defined crystalline Co areas (having 12 Co NN) occurs. It

suggests, that the two lowest implantation doses cause the formation of a "skin-like" structure consisting of cobalt oxide formed at the grain boundaries around the Co grains. Subsequently irradiated ions with time only further degrade the already existing morphological condition in the sample. Volume of the Co grains decreases, in contrast to the surface area of Co grains (and thus area Co/CoO interface) which remain quantitatively the same. This in turn suggests changes in Co/CoO interfaces such as the appearance of CoO erosions of Co grains (Fig. 3.4.2.8 c) or oxygen and cobalt oxide inclusions in Co grains, thus increasing the Co/CoO interface to Co grain size ratio. This “erosion” effect occurs in such a way that, despite the crystalline volume of Co decrease, the quantitative volume of the Co/CoO interface areas remains almost unchanged or very slightly decreases and appears in the sample in the same way as shown in fig. 3.4.2.8 c.

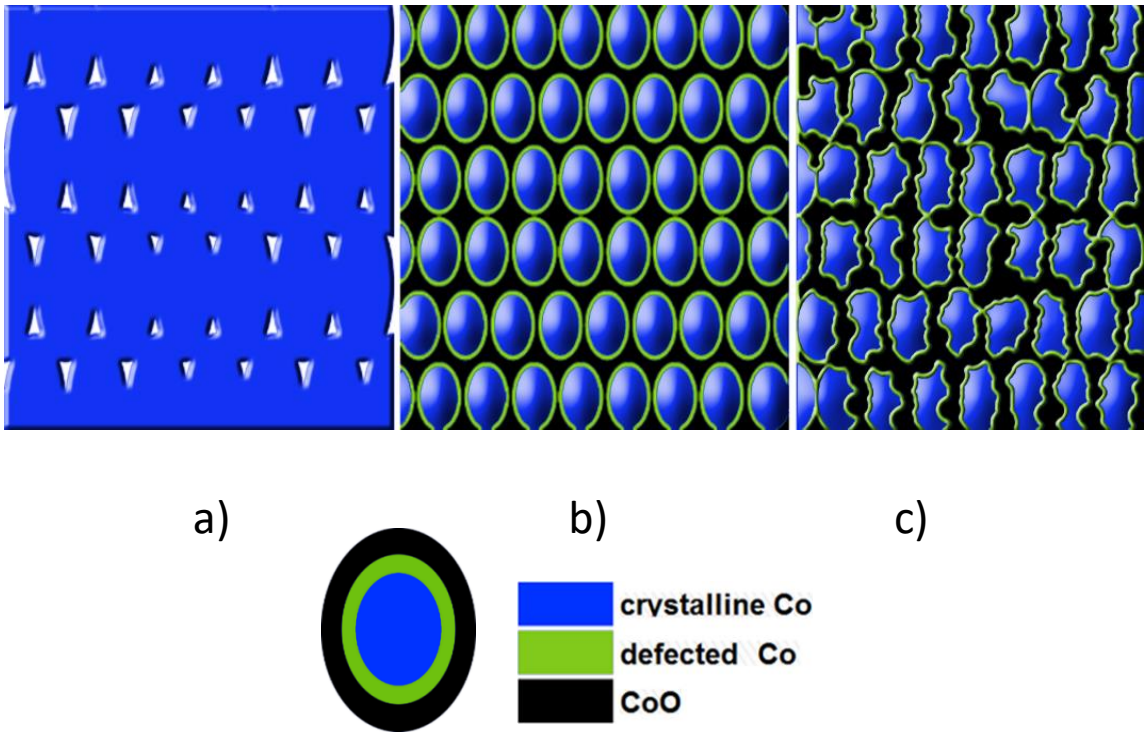

Fig. 3.4.2.8 Schematic representation of Co layer structure changes occurring after oxygen implantation process (a – non-implanted Co structure, b – implanted with small oxygen dose, c – heavily implanted Co structure). Blue areas represent crystalline Co; green areas represent areas of Co defected by oxygen implantation in which Co atoms are neighboring with oxygen, CoO or vacancies; black areas represent areas of formed CoO.

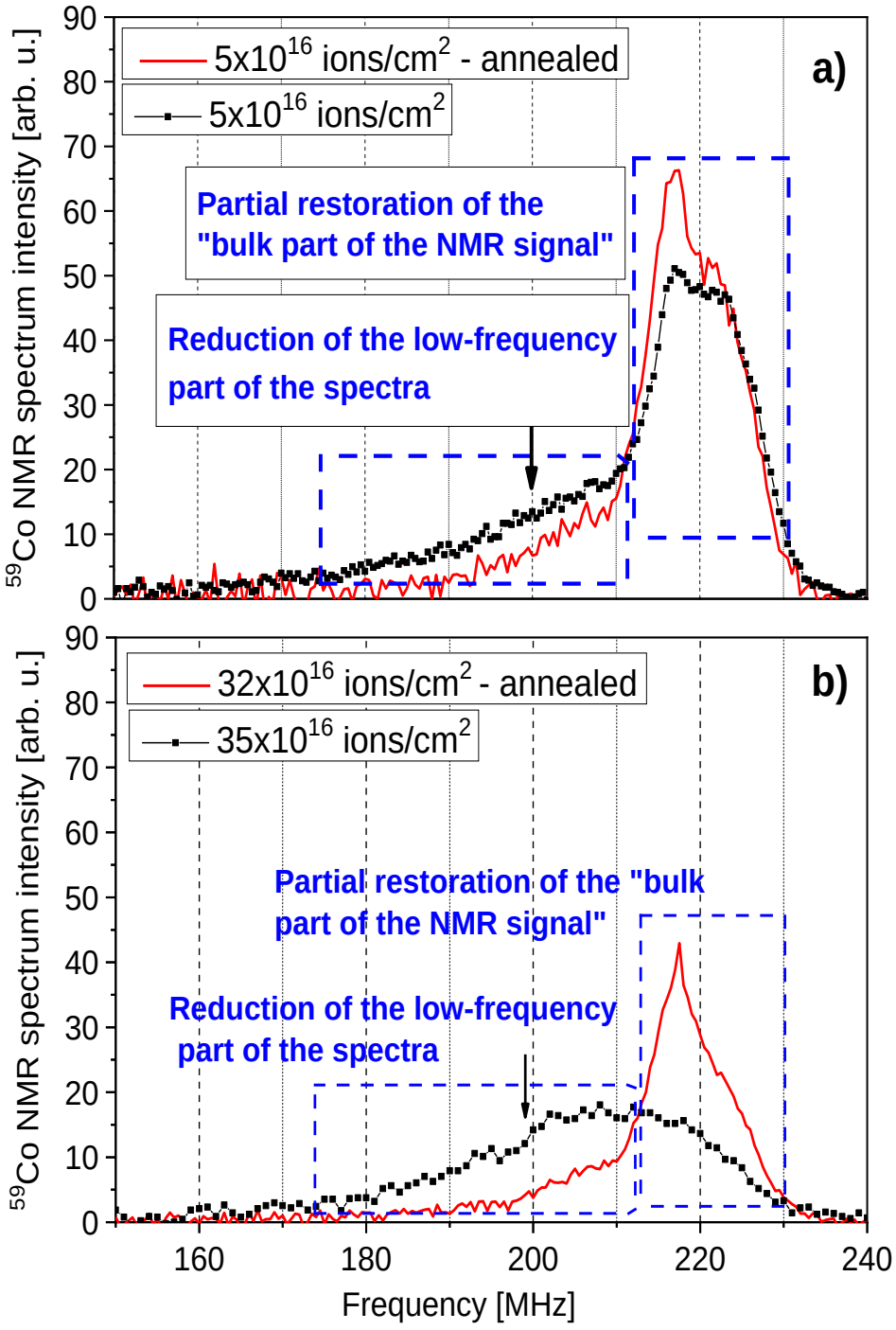

Fig. 3.4.2.9 Comparison of the NMR spectra from annealed and non-annealed series for a) lightly-implanted and b) heavily-implanted Co samples.

The CoO areas inside the grain boundaries are enlarging with the growing implantation fluence (not visible clearly on the NMR spectra in the experiment due to its antiferromagnetic nature) at the expense of the metallic crystalline Co. This is the reason of a strong loss of "bulk Co" signal in the NMR spectrum along with an increase in the intensity (and almost unaltered from a certain oxygen ions dose) of the signal from the destroyed by implantation but still ferromagnetic Co.

In order to acquire a better understanding about the behavior of the FM/AFM implanted Au/Co/Au system, a series of ^{59}Co NMR study of an Au/Co/Au samples implanted with oxygen ions that have undergone the process of annealing have been performed (fig. 3.4.2.9). Menéndez et. al. suggested that oxygen ions spread mainly throughout the Co sample in the grain boundaries tend to diffuse to the Co/Au interface areas due to the annealing treatment [MEN14] which is caused by thermal activation effects leading to a pronounced separation of Co and oxygen and, consequently, oxygen migration. Already at first glance one can see a significant difference between NMR spectra from annealed samples comparing to non-annealed ones. Annealing treatment draws back most of the structural changes which were introduced due to the oxygen implantation. It initiates a partial structural reconstruction of Co layer leading to a significant improvement of crystalline structure which is seen in the restoration of the signal originating from the crystalline ferromagnetic metallic Co (fig. 3.4.2.9). Radical reduction of the intensity in the low-frequency part of the NMR spectra suggests a disappearance of areas of distorted Co structure, areas where Co atoms have oxygen nearest neighbors and areas with Co_xO_y phase. Hence a reduction of FM/AFM interfaces is caused by a probable oxygen migration from the grain boundaries. This is especially seen in the drastic reduction of the measured H_{rest} (magnetic stiffness) of the annealed samples in comparison to oxygen implanted non-annealed ones (Fig. 3.4.2.10) which can be linked to a decreased magnitude of EB effect which follows the oxygen migration and reduction of FM/AFM interfaces.

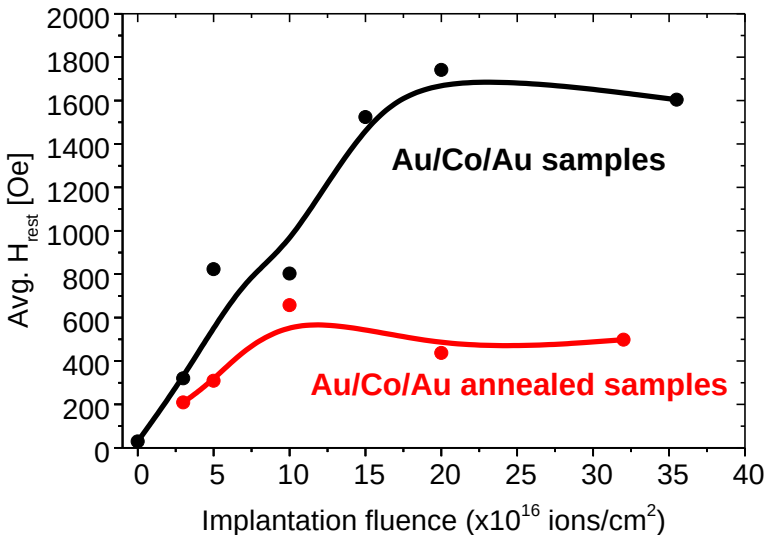

Fig. 3.4.2.10 Change in the magnetic stiffness (restoring field - H_{rest}) due to the annealing treatment (strong reduction of exchange bias effect caused by decrease of FM/AFM interfaces).

The interpretation of actual influence of annealing treatment on oxygen implanted Au/Co/Au samples, based on the NMR experiment and analysis, is following. Annealing treatment at chosen conditions causes a thermal activation of oxygen ions, and hence a diffusion of those ions from grain boundaries in the inner parts of the sample. The oxygen transport happens over grain boundaries and is followed by a partial recrystallization process caused by migrating oxygen ions. In other words oxygen diffusing through grain boundaries causes a local rearrangement of Co atoms to fcc-Co-like or hcp-Co-like structures, seen in the NMR spectra as mentioned earlier changes. Presented data and conclusions drawn from ^{59}Co NMR spectra analysis are fully in line with the results shown in [MEN14].

4

Conclusions

The subject of this dissertation was to study the local magnetic and structural properties of thin and ultra-thin Co films using a ^{59}Co nuclear magnetic resonance technique. The research was divided into several stages, in which thin cobalt layers were studied in various buffer/capping layer configurations and cobalt layer thickness, due to their potential to be used as an element of spin valves in MTJ's [CAR90], and when subjected to O ion implantation with the aim to induce a strong EB effect [DEM10], [MEN13].

However, at the initial stage of research ^{59}Co NMR experiments were performed on $Co_{1-x}Mo_x$ and $Co_{1-x}Au_x$ thin film alloys. These experiments were designed as a base and starting point to further NMR studies of Co thin films. Their purpose was to reveal an actual influence of alien NN (Au and Mo) atoms on hyperfine fields around Co matrix atoms, which would be significantly helpful in analysis and then proper design (especially in tailoring magnetic properties) of spintronic systems based on, or consisting of such materials. For example in the case of $Co_{1-x}Mo_x$ NMR study it is expected that the obtained results will prove useful in explaining the phenomenon of intermixing effects in Co/Mo/Co three-layers system subjected to the ion beam irradiation [WAW17a] which is aimed at fabrication of double-layer magnonic crystals.

^{59}Co NMR study of the $Co_{1-x}Au_x$ alloys has shown that structure of the Co layer depends strongly on the material used as the buffer and on the Co layer thickness. V/$Co_{1-x}Au_x$ (d_{Co}=30nm)/V layers exhibit a multiphase fcc/hcp-Co crystalline structure. However, in the case of Au/$Co_{1-x}Au_x$/Au samples, while the as-deposited Au/Co(d_{Co}=30nm)/Au layer and Au/$Co_{1-x}Au_x$/Au layers with a thickness d_{Co} < 30 nm have only visible hcp-Co crystalline structure, the Au/$Co_{0.90}Au_{0.01}$(d_{Co}=30nm)/Au layer

exhibit a multiphase mixture of hcp-Co and fcc-Co (for the most part) phases (similarly like in samples grown on V buffer) with a clearly marked satellite originating from the Co atoms in the 11 Co + 1 Au NN environment. Presence of Au dopant in the film in the form of a regular satellite structure in the NMR spectrum was only observed directly when the crystallographic structure of the layer contained the fcc phase. It has been estimated, that Au as fcc-Co nearest neighbor lowers its ^{59}Co NMR frequency by around 12 MHz which corresponds to the reduction of the hyperfine field by 1,19 T. Nevertheless, the indirect presence of Au dopant in the case of $Au/Co_{1-x}Au_x(d_{Co}<30nm)/Au$ samples was also detected in the magnetically "soft" strongly defected hcp-Co component of the layer accompanying magnetically "hard" characteristic of the undistorted hcp-Co structure. The "soft" hcp area of the layer is considered as a precursor of the fcc Co phase with the Au admixture on the level of 1 at %, that is observed in the 30 nm thick Co layer when Co was co-deposited with Au. At layer thickness of 30 nm a structural relaxation and transformation to the multiphase fcc/hcp state directly reveal the presence of Au in the layer. Moreover, existence of the magnetically "soft" structural hcp component has been also observed in the as-deposited $Au/Co(d_{Co} < 30nm)/Au$ thin film. Explanation for this phenomenon may be the fact that during the growth of Co film some Au atoms migrate from the Au buffer to the grain boundary regions helping to accommodate the large lattice mismatch at Au(111)/Co(0001) interface (as was pointed out by Fruchart [FRU03]).

The ^{59}Co NMR study of the $Co_{1-x}Mo_x$ alloys revealed that each Mo nearest neighbor overwhelmingly decreases the resonance frequency of Co. The frequency shift is significantly bigger than in the case of Au NN in $Co_{1-x}Au_x$ alloys. Primarily, at very small Mo concentration ($x \approx 0$) each Mo nearest neighbor lowers the ^{59}Co NMR resonance frequency by over 43 MHz, which corresponds to the reduction of hyperfine field by 4,34 T. This particularly means that at the temperature of 4,2 K, the Co atoms become conceivably non-magnetic already with five molybdenum atoms that have penetrated into the nearest neighborhood of the cobalt atom. Obviously this effect increases with Mo concentration due to the additive contribution from Mo in the more distant coordination shell. The extrapolation to Mo concentration higher than the one used in the study predicts that Co atoms become non-magnetic when they are already surrounded by 3 Mo nearest neighbors for the concentrations x = 0,2 - 0,25 [NAW19]. As for the structural properties, no preference has been observed in forming the fcc or

hcp $Co_{1-x}Mo_x$ alloy in the studied concentration range ($0 < x < 0,1$). However, alloying of Mo and Co significantly increases the amount of stacking faults, which stays in agreement with the results of theoretical calculations for binary alloys [ACH17], [ACH18].

In my work I have also studied **epitaxial thin Co (3nm) films grown on various type of buffer (Au or Mo) and capping layer (Au or Mo)**. The idea of the carried out study was to investigate the effect of buffer and capping layer on the structural and magnetic properties of the Co layer. The conclusions drawn from the recorded ^{59}Co NMR spectra of are following: only in the Mo/Co/Mo sample the fcc-Co phase is clearly visible alongside the hcp-Co phase. In light of the results obtained for $Co_{1-x}Mo_x$ alloy samples the presence of the fcc-Co phase in this case can be attributed to the alloying at the double Co/Mo interface and overall structural heterogeneity with large contribution from stacking faults and grain boundaries as a result of growth of Co on Mo substrate. In the case of samples grown on an Au buffer, a better crystal structure of Co can be noticed. The use of Au as a capping introduces additional strain to the Co layer also has a positive effect on the structure of the Co layer, making it more uniform and well-defined, which implies an important role of the Au capping in deep ordering of Co crystalline structure.

The next step resulting from previous measurements was to use ^{59}Co NMR technique to examine structural and magnetic modifications of **epitaxial Au/Co(d_{Co} = 1,5 – 10 nm)/Au heterostructures in the dependence on Co layer thickness.** Obtained results show that each Au nearest neighbor of Co in hcp stacking decreases its NMR frequency by around 12,5 MHz which corresponds to the reduction of hyperfine field by 1,24 T. This frequency shift is very similar to the one caused by 1 Au NN of Co in fcc stacking acquired from the study of $Co_{1-x}Au_x$ alloys (12 MHz). ^{59}Co NMR spectra analysis show that upon a critical layer thickness ($2,5\ nm \leq d_{Co} \leq 3\ nm$) Co layer grows in discontinuous/non uniform manner. Bottom Co/Au interface in samples with $d_{Co} \leq$ 2,5 nm remains atomically sharp in the major part of the contact area. However above this level of d_{Co} a visible structural modification to a continuous/uniform hexagonal structure occurs in the whole volume of the sample. It manifests itself in the shift of the NMR frequency towards lower values and (most of all) in rise of the NMR spectra intensity at 190-210 MHz frequency regions which is caused by the appearance of larger amount of grain boundaries and migration of Au atoms from the Au buffer to the

grain boundary regions helping to accommodate the large lattice mismatch (as was postulated in the case of $Co_{1-x}Au_x$ alloys). Described structural changes upon crossing the critical Co layer thickness alter also their magnetic properties - ^{59}Co NMR restoring fields have revealed a significant decrease of magnetic stiffness at 4.2 K in Co layers with $d_{Co} > 2,5$ nm.

The final stage of research work was **^{59}Co NMR investigation of oxygen implanted Au/Co/Au and Au/Co/CoO thin films** which has shown that while the as-deposited sample consists of a mixture of fcc and hcp-Co phases and stacking faults, implanted samples exhibit different structural features. Although there is no allotropic fcc › hcp phase transformation in polycrystalline samples, the metallic Co undergoes a significant loss of crystalline order. For high fluence implantation, traces of CoO can be envisaged from a new NMR line present at around 490 MHz. ^{59}Co NMR restoring fields indicate a large increase of magnetic stiffness at 4.2 K due to the exchange anisotropy introduced by the presence of antiferromagnetic CoO (i.e. EB). This in turn confirms that oxygen ion implantation is an adequate technique to form AFM CoO in the interior of thin Co layers. The comparison of ^{59}Co NMR analysis of the polycrystalline, textured and annealed polycrystalline oxygen-implanted samples confirms the existence of proposed earlier grain boundary oxidation mechanism [DEM11]. ^{59}Co NMR studies from annealed (573 K) samples have shown radical structural changes indicating a migration of implanted oxygen from the inner part of the Co film due to thermal activation and re-crystallization process assisted by diffusion of oxygen atoms from the inner part of the Co film. This in turn causes reduction of significant amount of FM/AFM interfaces and massive weakening of EB effect which is clearly visible in the average H_{rest} values in 4.2 K comparing to the results acquired before annealing treatment.

5

Literature

1. [ABR61] Abragam A, *"Principles of Nuclear Magnetism"*, *Oxford University Press*, (1961)
2. [ACH17] Achmad T, Fu W, Chen H, Zhang C, Yang Z, *J. Alloys Compd.*, **694**, 1265-1279 (2017)
3. [ACH18] Achmad T, Fu W, Chen H, Zhang C, Yang Z, *J. Alloys Compd.*, **748**, 328-337 (2018)
4. [ALP94] van Alphen E A M, de Velthuis S G E, de Gronckel H A M, Kopinga K, de Jonge W J M, *Phys. rev. B*, **49**, 17336-17341 (1994)
5. [ARD97] Ardhuin H, Snoeck E, Casanove M J, *Journal of Crystal Growth*, **182**, 394-402 (1997)
6. [BEL99] Belkhou R, Marsot N, Magnan H, Le Fèvre P, Barrett N, Guillot C, Chandesris D, *J. Electron Spectrosc. Relat. Phenom.*, **251**, 101-103 (1999)
7. [BER99] Berkowitz A E and Takano K, *J. Magn. Magn. Mater.*, **200**, 552 (1999)
8. [BRU89] Bruno P, Renard J P, *Appl. Phys. A*, **49**, 499 (1989)
9. [BUB00] Bubendorff J L, Mény C, Beaurepaire E, Panissod P, and Bucher J P, *Eur. Phys. J. B*, **17**, 635-643 (2000)
10. [CAG01] Cagnon L, Devolder T, Cortes R, Morrone A, Schmidt J E, Chappert C, and Allongue P, *Phys. Rev. B*, **63**, 104419 (2001)

11. [CAR90] Carcia P and Zeper W, *IEEE Trans. Magn.*, **26**, 1703 (1990)

12. [CER01] Cerisier M, Attenborough K, Jedryka E, Wójcik M, Nadolski S, Van Haesendonck C and Celis J P, *J. Appl. Phys.*, **89**, 7083–7085 (2001)

13. [CES89] Cesari C, Faure J P, Nihoul G, Le Dang K, Veillet P, Renard D, *J. Magn. Magn. Mater.*, **78**, 296-304 (1989)

14. [CHA88] Chappert C, Bruno P, *J. Appl. Phys.*, **64**, 5736 (1988)

15. [CHA07] Chappert C, Fert A, and Van Dau F N, *Nat Mater.*, **6**, 813 (2007)

16. [CHE01] Cherifi S, Boeglin C, Stanescu S, Deville J P, Mocuta C, Magnan H, Le Fèvre P, Ohresser P and Brookes N B, *Phys. Rev. B*, **64**, 184405 (2001)

17. [CRA55] Crangle J, *Philos. Mag.*, **46**, 499 (1955)

18. [DEM10] Demeter J, Meersschaut J, Almeida F, Brems S, Van Haesendonck C, Teichert A, Steitz R, Temst K and Vantomme A, *Appl. Phys. Lett.*, **96,** 132503 (2010)

19. [DEM11] Demeter J, Menéndez E, Temst K and Vantomme A, *J. Appl. Phys.*, **110,** 123902 (2011)

20. [DEM12] Demeter J, Menéndez E, Schrauwen A, Teichert A, Steitz R, Vandezande S, Wildes A R, Vandervorst W, Temst K and Vantomme A, *J. Phys. D: Appl. Phys.*, In-press (2012)

21. [DUP90] Dupas C, Beauvillain P, Chappert C, Renard J P, Trigui F, Veillet P and Vélu E, *J. Appl. Phys.*, **67**, 5680 (1990)

22. [FAS08] Fassbender J and McCord J, *J. Magn. Magn. Mater.*, **320,** 579–596 (2008)

23. [FRU03] Fruchart O, Renaud G, Barbier A, Noblet M, Ulrich O, Deville J-P, Scheurer F, Mane-Mane J, Repain V, Baudot G and Rousset S, *Europhys. Lett.*, **63** (2), 275–281 (2003)

24. [FUK81] Fukushima E and Roeder S B W, *"Experimental Pulse NMR A Nuts and Bolts Approach"*, Addison-Wesley Publishing Company (1981)

25. [GLA09] Gladczuk L, Aleshkevych P, Szymczak R, Dluzewski P, Aleszkiewicz M, Paszkowicz W, Minikayev R and Przyslupski P, *J. Appl. Phys.*, **105**, 063907 (2009)

26. [GLA13] Gladczuk L, Aleszkiewicz M, *Thin Solid Films*, **539**, 372–376 (2013)

27. [GLA14] Gladczuk L, Aleshkevych P, Lasek K and Przyslupski P, *J. Appl. Phys.*, **116**, 233909 (2014)

28. [GOS59] Gossard A C and Portis A M, *Phys. Rev. Lett.*, **3**, 164 (1959)

29. [GöK01] Gökemeijer N J, Penn R L, Veblen D R and Chien C L, *Phys. Rev. B*, **63** 174422 (2001)

30. [GRU00] Gruyters M and Riegel D, *J. Appl. Phys.*, **88**, 6610–6613 (2000)

31. [HAA16] Haag N, Laux M, Stöckl J, Kollamana J, Seidel J, Großmann N, Fetzer R, Kelly L L, Wei Z, Stadtmüller B, Cinchetti M and Aeschlimann M, *New J. Phys.*, **18**, 103054 (2016)

32. [HAH50] Hahn E L, "Spin echoes", *Physical Review*, **80**, 580–594 (1950)

33. [HAM01] Hamrle J, Nývlt M, Višňovský Š, Urban R, Beauvillain P, Mégy R, Ferré J, Polerecký L, and Renard D, *Phys. Rev. B*, **64**, 155405 (2001)

34. [HAN58] Constitution of Binary Alloys, edited by Hansen M, *McGraw-Hill*, p. **471**, New York (1958)

35. [JAY95] Jay J P, *Thesis*, Université Louis Pasteur, Strasbourg (1995)

36. [JAY96] Jay J P, Wójcik M and Panissod P, *Z. Phys. B*, **101**, 471-486 (1996)

37. [JED04] Jedryka E, Wójcik M, Nadolski S, Pattyn H, Verheyden J, Dekoster J and Vantomme A, *J. Appl. Phys.*, **95**, 2770–2775 (2004)

38. [JED98] Jedryka E, Wójcik M, Nadolski S, Kubinski D J, Holloway H, *J. Magn. Magn. Mater.*, **177-187**, 1183-1185 (1998)

39. [JON60] Jones R. V. and Kaminov I P, *Bull. Am. Phys. Soc*., **5**, 175 (1960)

40. [JOM00] Jomni S, Mliki N, Belhi R, Abdelmoula K, Ayadi M, and Nihoul G, *Thin Solid Films*, **186** (2000)

41. [KAW76] Kawakami M, *J. Phys. Soc. Japan*, **40**, 56 (1976)

42. [KEH00] Kehagias T, Komninou Ph, Christides C, Nouet G, Stavroyianni S and Karakostas Th, *Journal of Crystal Growth*, **208**, 401-408 (2000)

43. [KIN93] Kingetsu T and Sakai K, *Phys. Rev. B*, **48**, 4140 (1993)

44. [KIS02] Kisielewski M, Maziewski A, Tekielak M, Wawro A and Baczewski L T, *Phys. Rev. Lett.*, **89**, 087203 (2002)

45. [KIW01] Kiwi M, *J. Magn. Magn. Mater.*, **234**, 584 (2001)

46. [KOB66] Kobayashi S, Asayama K and Itoh J, *J. Phys. Soc. Jpn.*, **21**, 65 (1966)

47. [KUH94] Kuhn W K, He J W and Goodman D W, *J. Phys. Chem.*, **98**, 264 (1994)

48. [KUM07] Kumah D P, Cebollada A, Clavero C, García-Martín J M, Skuza J R, Lukaszew R A and Clarke R, *J. Phys. D: Appl. Phys.*, **40**, 2699–2704 (2007)

49. [KUR07] Kurant Z, Gieniusz R, Maziewski A, Tekielak M, Stefanowicz W, Sveklo I, Zablotskii V, Petroutchik A, Baczewski L T and Wawro A, *J. Magn. Magn. Mater.*, **316**, e511–e514 (2007)

50. [LAZ94] Lazor P, *PhD Thesis*, Uppsala University (1994)

51. [LER08] Leroy F, Renaud G, Létoublon A, Lazzari R, *Phys. Rev. B*, 77 (2008)

52. [MAL88] Malozemoff A P, *J. Appl. Phys.*, **63**, 3874 (1988)

53. [MAL98] Malinowska M, Mény C, Jędryka E and Panissod P, *J. Phys. Condens. Matter*, **10**, 4919-4928 (1998)

54. [MAL99] Malinowska M, Wójcik M, Nadolski S, Jędryka E, Mény C, Panissod P, Knobell M, Viegas A D C and Schmidt J E, *JEEE*, **198-199**, 599-601 (1999)

55. [MAR97] Marsot N, Belkhou R, Scheurer F, Bartenlian B, Barrett N, Delaunay M A and Guillot C, *Surface Science*, **225**, 377-379, (1997)

56. [MAR99] Marsot N, Belkhou R, Magnan H, Le Fèvre P, Guillot C, Chandesris D, *Phys. Rev. B*, **59**, 3135 (1999)

57. [MEI56] Meiklejohn W H and Bean C P, *Phys. Rev.*, **102**, 1413 (1956)

58. [MEN13] Menéndez E, Demeter J, Van Eyken J, Nawrocki P, Jędryka E, Wójcik M, Lopez-Barbera J, Nogués J, Vantomme A, and Temst K, *ACS Applied Materials and Interfaces*, **5**, No. 10, 4320-4327 (2013)

59. [MEN14] Menéndez E, Modarresi H, Dias T, Geshev J, Pereira L M C, Temst K and Vantomme A, *J. Appl. Phys.*, **115**, 13 (2014)

60. [MEN93] Mény C, Jędryka E and Panissod P, *J. Phys., Condens. Matter*, **5**, 1547-1556 (1993)

61. [MEN94] Mény C, *Thesis*, Université Louis Pasteur, Strasbourg (1994)

62. [MIC01] Michel A, Pierron-Bohnes V, Jay J P, Panissod P, Lefebvrer S, Bessie`re M, Fischer H E, and Van Tendeloo G, *Eur. Phys. J. B*, **19**, 225-239 (2001)

63. [MOR12] Morant C, Campo T, Marquez F, Domingo C, Sanz J M, and Elizalde E, *Thin Solid Films*, **520**, 5232 (2012).

64. [NAD95] Nadolski S, Wojcik M, Jedryka E and Nesteruk K, *J. Magn. Magn. Mater.*, **140-144**, 2187 (1995)

65. [NAD03] Nadolski S, *"Szerokopasmowe spektrometry jądrowego echa spinowego. Budowa i zastosowania w badaniach materiałów elektronicznych"*, *Prace Instytutu Technologii Elektronowej* (2003)

66. [NAS74] Nasu S, Yasuoka H, Nakamura Y and Murakami Y, *Acta Metall.*, **22**, 1057 (1974)

67. [NAW19] Nawrocki P, Kanak J, Petruczik A, Wawro A and Wojcik M, *Journal of Alloys and Compounds*, **788** (5), 559-564 (2019)

68. [NIS83] Nishizawa T and Ishida K, *Bull. Alloy Phase Diagrams*, **4**, 387 (1983)

69. [NOG96] Nogués J, Lederman D, Moran T J and Schuller I K, *Phys. Rev. Lett.*, **76**, 4624 (1996)

70. [NOG99] Nogués J and Schuller I K, *J. Magn. Magn. Mater.*, **192**, 203–232 (1999)

71. [NOG05] Nogués J, Sort J, Langlais V, Skumryev V, Suriñach S, Muñoz J S and Baró M D, *Phys. Rep.*, **422**, 65–117 (2005)

72. [OIK03] Oikawa K, Qin G W, Sato M, Kitakami O, Shimada Y, Sato J, Fukamichi K and Ishida K, *Appl. Phys. Lett.*, **83**, 966 (2003)

73. [OKA77] Okada K and Yasuoka H, *J Phys. Soc. Jpn.*, **43**, 34-40 (1977)

74. [OKA85] Okamoto H, Massalski T B, Nishizawa T et al., *Bulletin of Alloy Phase Diagrams*, **6**, 449 (1985)

75. [ONO88] Ono F and Maeta H, *Journal de Physique*, **49**, 63-64 (1988)

76. [PAN96] Panissod P, Jay J P, Mény C, Wójcik M and Jędryka E, *Hyperfine Interactions*, **97**/**98**, 75-98 (1996)

77. [PAN97] Panissod P, Mény C, Wójcik M and Jędryka E, *Materials Research Society Symposium Proceedings*, vol. **475**, Editors: Tobin J, Chambliss D, Kubinski D, Barmak K, Dederichs P, Katayama T, Schuhl A, p. 157 (1997)

78. [PAN01] Panissod P, *Magnetism: Molecules to Materials III: Nanosized Magnetic Materials, NMR of Nanosized Magnetic Systems, Ultrathin Films, and Granular Systems*, Chapter **8**, (2001)

79. [PAN01n] Panissod P, Malinowska M, Jedryka E, Wójcik M, Nadolski S, Knobel M and Schmidt J E, *Phys. Rev.* B, **63**, 014408 (2001)

80. [PAN82] Panissod P, Durand J and Budnick J I, *Nuclear Inst. Meth.*, **199**, 99-114 (1982)

81. [PAR99] Parkin S S P, Roche K P, Samant M G, Rice P M, Beyers R B, Scheuerlein R E, O'Sullivan E J, Brown S L, Bucchigano J, Abraham D W, Yu Lu, Rooks M, Trouilloud P L, Wanner R A, and Gallagher W J, *J. Appl. Phys.*, **85**, 8 (1999)

82. [POR61] Portis A M and Grossard A C, *J. Appl. Phys. Suppl.*, **31**, 205S (1961)

83. [RAD07] Radu F and Zabel H, *Exchange Bias Effect of Ferro-/Antiferromagnetic Heterostructures*, *Springer Tracts Mod. Phys.*, **227**, 97–184 (2007)

84. [RAD65] Rado G T and Suhl H, *Magnetism*, Vol. **2**, Part A, *Academic Press Inc.* (1965)

85. [RIE68] Riedi P C and Scurlock R G, *J. Appl. Phys.*, **39**, 1241(1968)

86. [SCH90] Schneider C M, Bressler P, Schuster P and Kirchner J, *Phys. Rev. Lett.*, **64**, number 9, 1059-1063 (1990)

87. [SCH92] Schmid A K and Kirschner J, *In situ observation of epitaxial growth of Co thin films on Cu(100), Ultramicroscopy*, **42–44,** 483–9 (1992)

88. [SCH99] Schuller I K, Kim S and Leighton C, *J. Magn. Magn. Mater.*, **200**, 571 (1999)

89. [SHA93] Shan Z S, He P, Moore C, Woollam J, and Sellmyer D J, *J. Appl. Phys.*, **73**, 6057 (1993)

90. [SHA79] Shavishvili T M and Kiliptari I G, *Phys. Status Solidi b*, **92**, 39 (1979)

91. [SOR03] Sort J, Suriñach S, Muñoz J S, Baró M D, Wójcik M, Jędryka E, Nadolski S, Sheludko N and Nogués J, *Phys. Rev. B*, **68**, 014421 (2003)

92. [SPE95] Speckmann M, Oepen H P and Ibach H, *Phys. Rev. Lett.*, **75**, 2035 (1995)

93. [STA00] Stamps R L, *J. Phys. D: Appl. Phys.*, **33**, R247 (2000)

94. [STA05] Stankowski J and Hilczer W, *Wstęp do spektroskopii rezonansów magnetycznych, Wydawnictwo Naukowe PWN* (2005)

95. [STE67] Stearns M B, *Phys. Rev.* **162**, 496 (1967)

96. [SZE12] Szewczyk A, Wiśniewski A, Późniak R and Szymczak H, *Magnetyzm i nadprzewodnictwo, Wydawnictwo Naukowe PWN* (2012)

97. [THO00] Thomson T, Riedi P C and Krishnan R, *J. Appl. Phys* **87** (9), 6594 (2000)

98. [TUR69] Turow E A and Pietrow M P, *Jądrowy rezonans magnetyczny w ferromagnetykach i antyferromagnetykach, Państwowe Wydawnictwo Naukowe* (1969)

99. [UJF96] Ujfalussy B, Szunyogh L, Bruno P and Weinberger P, *Phys. Rev. Lett.*, **77**, 1805 (1996)

100. [VAZ08] Vaz C A F, Bland J A C and Lauhoff G, *Rep. Prog. Phys.*, **71**, 056501 (2008)

101. [VOI91] Voigtläder B, Meyer G, and Amer N M, *Phys. Rev. B*, **44** (1991)

102. [WAL12] Walczak A Ślusarski T, Lehmann-Szweykowska A, Kamieniarz G, *Acta Phys. Pol. A*, **121**, 3, 653-659 (2012)

103. [WAN94] Wang D, Wu R and Freeman A J, *J. Magn. Magn. Mater.*, **129**, 237 (1994)

104. [WAT61] Watson R E and Freeman A J, *Phys. Rev.*, **123**, 2027 (1961)

105. [WAW17] Wawro A, Kurant Z, Tekielak M, Nawrocki P, Milińska E, Pietruczik A, Wójcik M, Mazalski P, Kanak J, Ollefs K, Wilhelm F, Rogalev A and Maziewski A, *J. Phys. D Appl. Phys.*, **50 (21)**, 215004 (2017)

106. [WAW17a] Wawro A, Kurant Z, Tekielak M, Jakubowski M, Pietruczik A, Böttger R and Maziewski A, *Appl. Phys. Lett.*, **110**, 252405 (2017)

107. [WAW18] Wawro A, Kurant Z, Jakubowski M, Tekielak M, Pietruczik A, Böttger R and Maziewski A, *Phys. Rev. Appl.*, **9**, 014029 (2018)

108. [WEB] https://www.webelements.com/vanadium/crystal_structure.html

109. [WEB96] Weber W, Bischof A, Allenspach R, Black C H, Fassbender J, May U, Schirmer B, Jungblut R M, Güntherodt G and Hillebrands B, *Phys. Rev. B*, **54**, 4075 (1996)

110. [WOJ97] Wójcik M, Jay J Ph, Panissod P, Jędryka E, Dekoster J and Langouche G, *Z. Phys. B*, **103**, 5 (1997)

111. [YAS71] Yasuoka H, Hoshinouchi S, Nakamura Y, Matsui M and Adachi K, *Phys. Stat. Sol. B*, **46**, K81-84 (1971)

112. [YOO98] Yoo C-S, Söderlind P and Cynn H, *J. Phys.: Condens. Matter*, **10**, L311–L318 (1998)

The Author's academic achievments

List of publications:

1. **P. Nawrocki**, J. Kanak, A. Petruczik, A. Wawro and M. Wójcik - *Epitaxial $Co_{1-x}Mo_x$ thin film alloys studied by ^{59}Co NMR* - Journal of Alloys and Compounds, vol. 788 (5), p. 559-564 (2019)

2. **P. Nawrocki**, J. Kanak, M. Wójcik and T. Stobiecki, *^{59}Co NMR analysis of CoFeB-MgO based magnetic tunnel junctions* - Journal of Alloys and Compounds, vol. 741, p. 775-780 (2018)

3. Wawro, Z. Kurant, M. Tekielak, **P. Nawrocki**, E. Milińska, A. Pietruczik, M. Wójcik, P. Mazalski, , J. Kanak , K. Ollefs, F. Wilhelm, A. Rogalev and A. Maziewski - *Engineering the magnetic anisotropy of an ultrathin Co layer sandwiched between films of Mo or Au* - Journal of Physics D: Applied Physics, Vol. 50 (21), p. 215004 (2017)

4. E. Menéndez, J. Demeter, J.Van Eyken, **P. Nawrocki**, E. Jędryka, M. Wójcik, J. F. Lopez-Barbera, J. Nogués, A. Vantomme, and K. Temst - *Improving the Magnetic Properties of Co−CoO Systems by Designed Oxygen Implantation Profiles* – ACS Applied Materials & Interfaces Vol. 5 (10), p. 4320-4327 (2013), 3/10

5. **P. Nawrocki**, L. Gładczuk and M. Wójcik - *Structural changes of Co thin films on Au buffer with the increasing Co thickness – ^{59}Co NMR studies* – in preparation

6. **P. Nawrocki**, M. Wójcik, E. Jędryka, E. Menéndez, J. Nogués, A. Vantomme, K. Temst - *Influence of O^+ ion implantation on structural and magnetic properties of Co thin films studied by ^{59}Co NMR technique* - in preparation

Conference attendance:

1. **P. Nawrocki**, J.Kanak, M. Wójcik, T.Stobiecki - *^{59}Co NMR analysis of CoFeB-MgO based magnetic tunnel junctions,* 24th International Symposium on Metastable, Amorphous and Nanostructured Materials**,** 18-23 June 2017, Donostia-San Sebastian, Spain – oral presentation

2. **P. Nawrocki**, L. Gładczuk, E. Jędryka and M. Wójcik - *Ultra – thin Au(111)/Co/Au heterostructures - ^{59}Co NMR studies,* Joint European Magnetic Symposia 2016, 21 – 26 August 2016, Glasgow, United Kingdom

3. **P. Nawrocki**, M. Wójcik, E. Jędryka, E. Menéndez, A. Vantomme, K. Temst - *O+ implanted Co thin films – ^{59}Co NMR studies,* E-MRS fall 2015, 15 – 18 September 2015, Warsaw, Poland – oral presentation

4. **P. Nawrocki**, M. Wójcik, E. Jędryka, E. Menéndez, A. Vantomme, K. Temst - *^{59}Co NMR studies of Co based systems with exchange bias effect induced by O ion implantation*, ICMFS Cracow 2015, 12 – 17 July 2015, Cracow, Poland

5. **P. Nawrocki** - *Structural and magnetic properties of ferromagnetic Co ultra-thin films - ^{59}Co NMR studies,* Doctoral symposium Mądralin 2014, 16 - 17 May 2014, Mądralin, Poland - oral presentation

6. **P. Nawrocki**, L. Gładczuk and M. Wójcik - *Au/Co/Au heterostructures studied by ^{59}Co NMR technique*, Physics of Magnetism 2014 (PM'14), 23 – 27 June 2014, Poznan, Poland

7. **P. Nawrocki**, M. Wójcik, E. Jędryka, E. Menéndez, A. Vantomme, K. Temst - *Influence of O ion implantation on the magnetic and structural properties of Co thin films studied by ^{59}Co NMR technique* – XLVIII Zakopane School of Physics, 20-25 May 2013, Zakopane, Poland

8. **P. Nawrocki**, E. Jędryka, M. Wójcik, E. Menéndez, A. Vantomme, K. Temst - *Oxygen implanted Co thin films – ^{59}Co NMR studies,* Short Course on Functional Properties of Matter at the Atomic Scale, 21-25 May 2012, Leuven, Belgium